CONTRACT REPORT NO. 15Q84-00271

CHARACTERIZATION OF THIN FILMS USED AS ELECTRODES IN ELECTROCHEMICAL DEVICES

PHASE II

DSS File No. 03SQ.23440-4-9223

Final Report

for

Energy, Mines and Resources
CANMET
Mineral Sciences Laboratory
555 Booth Street
Ottawa, Ontario
K1A 0G1

Attention: Dr. T.A. Wheat
Dr. J.D. Canaday

Prepared by

M.P. Haley

February 27, 1987

ONTARIO RESEARCH FOUNDATION

SHERIDAN PARK RESEARCH COMMUNITY

MISSISSAUGA, ONTARIO, CANADA L5K 1B3 • (416) 822-4111 • TELEX 06-982311

MICROMEDIA

176 pp

WE, THE ONTARIO RESEARCH FOUNDATION, STIPULATE THAT THIS DOCUMENT IS SUBJECT TO THE FOLLOWING TERMS AND CONDITIONS:

1. ANY PROPOSAL CONTAINED HEREIN WAS PREPARED FOR THE CONSIDERATION OF THE ADDRESSEE ONLY. ITS CONTENTS MAY NOT BE USED BY NOR DISCLOSED TO ANY OTHER PARTY WITHOUT OUR PRIOR WRITTEN CONSENT.
2. ANY TESTING, INSPECTION OR INVESTIGATION PERFORMED BY US WILL BE CONDUCTED IN ACCORDANCE WITH NORMAL PROFESSIONAL STANDARDS. NEITHER WE NOR OUR EMPLOYEES SHALL BE RESPONSIBLE FOR ANY LOSS OR DAMAGE RESULTING DIRECTLY OR INDIRECTLY FROM ANY DEFAULT, ERROR OR OMISSION.
3. ANY REPORT, PROPOSAL OR QUOTATION PREPARED BY US REFERS ONLY TO THE PARTICULAR MATERIAL, INSTRUMENT OR OTHER SUBJECT REFERRED TO IN IT. NO REPRESENTATION IS MADE THAT SIMILAR ARTICLES WILL BE OF LIKE QUALITY.
4. NO REPORT ISSUED BY US SHALL BE PUBLISHED IN WHOLE OR IN PART WITHOUT OUR PRIOR WRITTEN CONSENT.
5. OUR NAME SHALL NOT BE USED IN ANY WAY IN CONNECTION WITH THE SALE, OFFER OR ADVERTISEMENT OF ANY ARTICLE, PROCESS OR SERVICE.
6. WE RESERVE THE RIGHT NOT TO COMMENCE AND/OR CONTINUE ANY WORK UNTIL PAYMENT ARRANGEMENTS SATISFACTORY TO US ARE ESTABLISHED.

Phase II Final Report

SUMMARY

The work described in this Phase II final report examines a variety of physical methods which have been applied to the characterization of thin film morphology. Properties such as pore size, surface roughness, porosity, thickness, surface area, permeability, and pore/particle interface have all been evaluated using conventional and/or novel techniques. The techniques investigated include image analysis, profilometry, permeametry, porosimetry, and gas adsorption.

The results of this study indicate that each technique employed has certain limitations with regard to sensitivity, resolution, and range as well as being somewhat dependent upon materials composition. In addition, the methods used to prepare the films were found to be less than adequate with regard to morphological reproducibility, which led to difficulties in correlating the physical parameters measured by different techniques.

Overall, a few techniques have been identified (i.e. image analysis, profilometry, gas adsorption) which show sufficient merit to warrant further investigation particularly for evaluating the relationship between electrode morphology and electrochemical operational behavior. Recommendations for further method development are also presented together with alternative applications for these thin film characterization techniques.

RESUME

Le travail decrit dans ce rapport final du Phase II examine une variete de methods physiques qui ont ete appliquees a la caracterisation de la morphologie des couches minces. Les proprietes comme la gradeur des pores, la rugosite de la surface, la porosite, l'epaisseur, l'aire de la surface, l'aire de la surface, la permeabilite et l'interface pore/particle ont tous ete evaluees avec des techniques conventionnelles et/ou originaux. Les techniques investiges sont l'analyze d'image, "permeametry", "porosimetry" et l'adsorption de gaz.

Les resultats de cette etude indique que chaque technique employe a certaine limitations quant a la sensitivitie, la resolution et la gamme. Il y a aussi une dependance de la composition des materiaux. En plus, les methods utilisees pour preparer les couches n'etaient pas suffisant quant a la reproductibilite de la morphologie. Ceci a mene a des difficultes dans la correlation des parametres physique mesure par les techniques differentes

Tout de meme quelques techniques ont ete identifiees qui merite une investigation supplementaire, particulierement pour evalues la relation entre la morphologie de l'electrode et sa fonctionnement electrochimique. Des recommendations sont aussi presentees pour des developments additionel des methods de caraterisation et des applications alternative pour les techniques de caracterisation des couches minces.

ACKNOWLEDGEMENTS

The author would like to express his sincere thanks to all of those who assisted in the experimental work, discussion of results, and preparation of this report. Those persons include R.T. Lassau, S. Jackson, B. Smith, A.J. Terry, P.C. Markiewicz, M. Taylor, and K.L. Yan, all of Ontario Research and J.G. Murphy, Technical University of Nova Scotia, R. LeRoy of Electrolyser, and J.D. Canaday and T.A. Wheat, both of CANMET, Ottawa.

TABLE OF CONTENTS

		page
	SUMMARY	i
	ACKNOWLEDGEMENTS	iii
1.	INTRODUCTION	1
2.	BACKGROUND	3
	2.1 Fuel Cell Electrodes	3
	2.2 Electrode Fabrication Techniques	6
	2.2.1 Ink Printing	6
	2.2.2 Plasma Spraying	7
	2.3 Physical Characterization Techniques	9
	2.3.1 Image Analysis	9
	2.3.1.1 Lineal Analysis	11
	2.3.1.2 Line Scan Analysis	12
	2.3.1.3 Diameter Analysis	12
	2.3.1.4 Sample Preparation	15
	2.3.2 Profilometry	16
	2.3.2.1 Profile Filtering	17
	2.3.2.2 Surface Texture Parameters	21
	2.3.3 Permeametry	22
	2.3.3.1 Apparatus	23
	2.3.3.2 Validation of Test Rig	23
	2.3.3.2.1 Millipore Membranes	25
	2.3.3.2.2 Nuclepore Membranes	25
	2.3.4 Mercury Porosimetry	27
	2.3.4.1 Impedance Porosimetry	36
	2.3.5 Gas Adsorption	38
3.	EXPERIMENTAL RESULTS ON THIN FILM MATERIALS	42
	3.1 Platinum Paste Films	42
	3.1.1 Image Analysis of Platinum Paste Films	49
	3.1.2 Profilometry of Platinum Paste Films	52
	3.1.3 Permeametry of Platinum Paste Films	58
	3.1.4 Porosimetry of Platinum Paste	58
	3.1.5 Gas Adsorption of Platinum Paste Films	58

Table of Contents cont'd

	page
3.2 Plasma Sprayed Nickel Films	59
3.2.1 Image Analysis of Ni Plasma Films	63
3.2.1.1 Supported Films	65
3.2.1.2 Unsupported Films	68
3.2.2 Profilometry of Nickel Plasma Films	71
3.2.2.1 Supported Films	71
3.2.2.2 Unsupported Films	73
3.2.2.2.1 Fractal Descriptors	76
3.2.3 Permeametry of Ni Plasma Films	80
3.2.3.1 Plasma Film Reproducibility	80
3.2.3.2 Effect of Plasma Spray Conditions	86
3.2.4 Porosimetry of Ni Plasma Films	86
3.2.4.1 Unsupported Films	89
3.2.4.2 Supported Films	94
3.2.5 Gas Adsorption of Ni Plasma Films	97
3.3 Perovskite Films	100
3.4 Silver Membranes	102
3.4.1 Image Analysis of Ag Membranes	105
3.4.2 Profilometry of Ag Membranes	113
3.4.2.1 Direct Pore Measurements	116
3.4.2.2 Impregnition/Dissolution of Ag Membranes	118
3.4.3 Permeametry of Ag Membranes	123
3.4.4 Porosimetry of Ag Membranes	127
3.4.5 Gas Adsorption of Ag Membranes	127
4. CONCLUSIONS	131
4.1 Individual Techniques	131
4.1.1 Image Analysis	131
4.1.2 Profilometry	132
4.1.3 Permeametry	134
4.1.4 Mercury Porosimetry	134
4.1.5 Gas Adsorption	135
4.2 Correlation of Characterization Techniques	136
4.3 Film Preparation Methods	142

Table of Contents cont'd

	page
5. RECOMMENDATIONS	143
5.1 Evaluation of Candidate Electrode Materials	143
5.1.1 Film Preparation	144
5.1.2 Electrochemical Behavior	144
5.1.3 Electrode Life Studies	145
5.2 Characterization Technique Development	145
5.3 Other Applications	146
APPENDIX A Surfacce Texture Parameters Generated by the Talysurf 6 Profilometer	
APPENDIX B Pascal Program for the Numerical Solution of a Fractal Descriptor based upon a Talysurf 6 Profilometer Output	
APPENDIX C Summary Table of Results of Measurements on Selected Films Using Various Techniques.	

Table of Contents cont'd

TABLES

		page
2.1	Relationships Between Electrode Processes and Physical Properties	5
2.2	Physical Dimensions and Flow Properties for Nuclepore Membrane	29
3.1.1	Morphological Parameters for Platinum Paste A-4338 Derived from Image Analysis	51
3.1.2	Surface Texture vs Curing Temperature for Pt Paste (#6926)	53
3.1.3	Surface Texture Parameters for Platinum Paste Films (Phase Corrected, 0.8 mm, Skidless)	55
3.1.4	Comparison of Screen-Printed and Hand-Painted Pt Paste Films	56
3.2.1	Morphological Properties via Image Analysis for Supported Plasma Sprayed Nickel Films	69
3.2.2	Morphological Properties via Image Analysis for Unsupported Plasma Sprayed Nickel Films	71
3.2.3	Surface Texture Measurements of Supported Nickel Plasma Films	74
3.2.4	Surface Texture Parameters for Unsupported Nickel Plasma Sprayed Coating	75
3.2.5	Comparison of Fractal Descriptors with Surface Texture Parameters for Unsupported Nickel Plasma Sprayed Coatings	79
3.2.6	Gas/Flow Pressure Slopes for Unsupported Nickel Plasma Sprayed Films	82
3.2.7	Comparison of Plasma Spray Cponditions via Film Permeability	88
3.2.8	Mercury Porosimetry Analysis of Unsupported Plasma Sprayed Nickel Films (500A, 6" W.D.)	95
3.2.9	Mercury Porosimetry Analysis of Supported Plasma Sprayed Nickel Film	96
3.2.10	Specific Surface Areas of Plasma Sprayed Nickel Films	99

Table of Contents cont'd

		page
3.4.1	Pore and Particle Diameters for Ag Membranes via Image Analysis	111
3.4.2	% Porosity (Voids) for Ag Membranes via Image Analysis	112
3.4.3	Three Phase Line Length Estimate for Ag Membranes	114
3.4.4	Standard Surface Texture Parameters for Silver Membrane Surfaces	115
3.4.5	Gravimetric/Volumetric Determination of Porosity for Silver Membranes	117
3.4.6	Pore and Particle Diameters for Ag Membranes via Profilometry	119
3.4.7	Surface Texture of Impregnated/Polished/Etched 1.2 um Silver Membrane	121
3.4.8	Gas Flow Rsistance From 0.2 um Silver Membrane	128
3.4.9	Surface Area of Silver Membrane Filters	129
4.1	Relationships Between Characterization Techniques for Silver Membranes	138
4.2	Relationships between Characterization Techniques for Supported Plasma Films	138
4.3	Relationships Between Characterization Techniques for Unsupported Plasma Films	139

Table of Contents cont'd

FIGURES

		page
2.1	Optical Photomicrograph of 5.0 um Silver Membrane Filter Showing Solid Phase (Light) and Porous Phase (Dark) (470X)	10
2.2	Thresholded Image of Detected Porous Phase (470X)	10
2.3	Lineal Analysis of Detected Porous Phase (470X)	13
2.4	Diameter or MCD Analysis of Detected Porous Phase (470X)	13
2.5	Line Scan Logic for Evaluating Features with Inclusions	14
2.6	Diameter Logic for Measuring Feature Dimensions	14
2.7	Three Types of Surface Structure	18
2.8	Mechanical Filtering with a Skid Arrangement	18
2.9	Effect of Graphic Filtering	20
2.10	Filtering Effect for Standard ISO Cut-Off's	20
2.11	Schematic of Permeability Test Rig	24
2.12	Permeability Measurements for Millipore Filters	26
2.13	Permeability Measurements for Nuclepore Filters	28
2.14	Poiseulle Fits of Permeability Data for Nuclepore Filters	30
2.15	Incremental Intrusion Histogram for Si-Al Catalyst Support	32
2.16	Cumulative Intrusion Curve for Si-Al Catalyst Support	33
2.17	Picture of Standard Micromeritics Powder and Solid Penetrometers	34
2.18	Diagramatic of Micromeritics Mercury Intrusion Penetrometers	34
2.19	Intrusion Curve for Blank Run of High Precision Penetrometer	37
3.1.1	SEM Photomicrograph of #6926 Platinum Paste cured at 500°C (approx. 3000X)	44
3.1.2	SEM Photomicrograph of #6926 Platinum Paste cured at 800°C (approx. 3000X)	44

Table of Contents cont'd

		page
3.1.3	SEM Photomicrograph of #6926 Platinum Paste cured at 500°C (approx. 150X)	45
3.1.4	SEM Photomicrograph of #6926 Platinum Paste cured at 800°C (approx. 150X)	45
3.1.5	CANMET SEM Micrograph of #6926 Pt Paste cured at 200°C in Hydrogen (450X)	46
3.1.6	SEM Photomicrograph of A-4338 Platinum Paste cured at 100°C (approx. 6200X)	47
3.1.7	SEM Photomicrograph of A-4338 Platinum Paste cured at 800°C (approx. 5800X)	47
3.1.8	CANMET SEM Micrograph	48
3.1.9	SEM Photomicrograph of Regular Epoxy/Polished Platinum Paste (approx. 7500X)	50
3.1.10	Optical Photomicrograph of Vacuum Impregnated/Polished A-4338 Platinum Paste (approx. 500X)	50
3.1.11	Profilometry Scan for Three Strips of Scree-Printed Paste A-4338	57
3.1.12	Profilometry Scan of Hand-Painted Platinum Paste (A-4338)	57
3.2.1	SEM Photomicrograph of Crposs-Sectioned Ni Plasma Sprayed Coating (I = 500 A, WD = 6") Mag approx. 325X	60
3.2.2	SEM Photomicrograph of Cross Sectined Ni Plasma Sprayed Coating (I = 500 A, WD = 6") Mag approx. 325X	60
3.2.2	SEM Photomicrograph of Cross-Sectioned Ni Plasma Sprayed Coating (I = 500 A, WD = 6") Mag approx. 325X	60
3.2.3	Detailed SEM Photomicrograph of Laminate Structures in Ni Plasma Sprayed Coating (I = 500 A, WD = 6") Mag approx. 3100X	62
3.2.4	Detailed SEM Laminate Structures in Ni Plasma Sprayed Coating (I = 300 A, WD = 10") Mag approx. 6900X	62
3.2.5	SEM Micrograph of Ceramic (Alumina)/Metal (Nickel) Interface with no Bond Coat (Mag approx. 6000X)	64

Table of Contents cont'd

		page
3.2.6	Optical Photomicrograph of Impregnated/Polished Plasma Sprayed Supported Nickel Film for Set 1 (500A, 6") Mag approx. 100X	66
3.2.7	Optical Photomicrograph of Impregnated/Polished Plasma Sprayed Supported Nickel Film for Set 2 (300A, 6") Mag approx. 100X	66
3.2.8	Optical Photomicrograph of Impregnated/Polished Plasma Sprayed Supported Nickel Film for Set 3 (300A, 6") Mag approx. 100X	67
3.2.9	Optical Photomicrograph of Impregnated/Polished Plasma Sprayed Unsupported Nickel Film (1 x double pass @ 500A, 6") Mag - 100X	67
3.2.10	Optical Photomicrograph of Impregnated/Polished Plasma Sprayed Unsupported Nickel Film (2 x double pass @ 500A, 6") Mag - 100X	70
3.2.11	Optical Photomicrograph of Impregnated/Polished Plasma Sprayed Unsupported Nickel Film (3 x double pass @ 500A, 6") Mag - 100X	70
3.2.12	Manual Random Walk Strategy for Computing Fractal Dimension (Profile of Ni Plasma Sprayed Film)	78
3.2.13	Permeability Measurements of Set 1 (Single Pass) Nickel Plasma Sprayed Films	83
3.2.14	Permeability Measurements of Set 2 (Double Pass) Nickel Plasma Sprayed Films	84
3.2.15	Peremeability Measurements of Set 3 (Triple Pass) Nickel Plasma Sprayed Films	85
3.2.16	Comparison of the Permeability of Plasma Films (Powder 404) Sprayed Under Various Conditions	87
3.2.17	Cumulative Intrusion Curve for Unsupported Plasma Sprayed Nickel Film (1 x double pass)	90
3.2.18	Cumulative Intrusion Curve for Unsupported Plasma Sprayed Nickel Film (2 x double pass)	91
3.2.19	Cumulative Intrusion Curve for Unsupported Plasma Sprayed Nickel Film (3 x double pass)	92

Table of Contents cont'd

		page
3.2.20	Mercury Intrusion Curves for Unsupported Nickel Plasma Films	93
3.2.21	Mercury Intrusion Curves for Set 1 Samples (500A, 6" of the Supported Nickel Plasma Sprayed Films	98
3.3.1	SEM micrograph of $Co_{0.6}Ni_{0.3}$ $(316SS)_{0.1}$ O_{3-x} Plasma Coating Surface (500X)	101
3.3.2	SEM Micrograph of $Co_{0.6}Ni_{0.3}$ $(316SS)_{0.1}$ O_{3-x} Plasma Coating Cross Section (200X)	101
3.3.3	SEM Micrograph of $Ni_{0.39}Al_{0.59}Mo_{0.02}$ O_{3-x} Plasma Coating Surface (500X	103
3.3.4	SEM Micrograph of $Ni_{0.39}Al_{0.59}Mo_{0.02}$ O_{3-x} Plasma Coating Cross Section (200X)	103
3.3.5	SEM Micrograph of Plasma Sprayed Perovskite Coating on Nickel Mesh (approx. 65X)	104
3.3.6	SEM Micrograph of Surface Structure for Plasma Sprayed Perovskite Coating (approx. 6500X)	104
3.4.2	SEM Photomicrograph of 5 um Rated Ag Membrane Surface (approx. 300X)	106
3.4.2	SEM Photomicrograph of 5 um Rated Ag Membrane Surface (approx. 3000X)	106
3.4.3	SEM Photomicrograph of Polished 5 um Ag Membrane (approx. 1600X)	107
3.4.4	SEM Photomicrograph of Polished 1.2 um Rated Ag Membrane (approx. 1600X)	107
3.4.5	SEM Photomicrograph of Polished 0.8 um Ag Membrane (approx. 1800X)	108
3.4.6	SEM Photomicrograph of Polished 0.45 um Ag Membrane (approx. 1600X)	108
3.4.7	SEM Photomicrograph of Polished 0.2 um Ag Membrane (approx. 1800X)	109
3.4.8	Profilometry Trace of Etched Silver Membrane	120
3.4.9	Profilometry Trace of Etched Silver Membrane (1.2 um)	122

Table of Contents cont'd

	page
3.4.10 SEM Micrograph of HNO_3 Treated 1.2 um Silver Membrane (approx. 1700X)	124
3.4.11 SEM Micrograph of HNO_3 Treated 1.2 um Silver Membrane (approx. 6800X)	124
3.4.12 Permeability Measurements for Silver Membrane Filters (Helium)	125
3.4.13 Comparison of Permeability for 0.2 um Silver Membrane with Different Gases	126

1. INTRODUCTION

The physical characterization of bulk materials is a well established science employing numerous instrumental techniques to examine such properties as size, density, surface area, porosity and pore size, surface texture, shape, and permeability. When considering thin films (1-100 um), however, the application of these techniques is often limited due to the physical size/volume of the film. Conventional methods of characterization do not generally have the degree of sensitivity required to analyze these materials and new approaches or modifications to existing techniques are usually necessary.

In this program, the need for thin film characterization has been driven by the demand in the electrochemical sciences to better understand the dependence of physical morphology on the operational behavior of porous electrodes. Porous electrodes are widely employed in such electrochemical devices as galvanic cells, coulometers, electrolyzers, chemical sensors and pumps, and fuel cells. The efficiency of these devices can be limited by the physical structure of the electrode. The development of suitable characterization techniques will obviously lead to better control on the morphology of formed electrodes, resulting in a means to evaluate alternative electrode compositions. This would have the potential effect of increasing device efficiency while improving overall viability (i.e. material cost, assembly methods).

Studies conducted at CANMET (1) have examined the important morphological properties of porous electrodes as they relate to a number of physical and chemical processes occurring in solid state fuel cells. In their investigations on protonically conducting electrolytes, workers at CANMET have reviewed a variety of physical parameters (e.g. thickness, density/porosity, pore size, surface area) and suggested that with the proper measurement of these properties, steps could be taken to improve the overall fuel cell performance. The objective of the Phase II program, therefore, has been to

identify, develop, refine, and implement characterization techniques which will quantify the physical structure of porous thin film materials in a reliable and reproducible manner.

The approach taken in this study has been to;

1) prepare a variety of porous films using preparative methods suitable for electrode development in fuel cell applications,

2) employ conventional techniques which can be directly applied to thin film materials (i.e. profilometry),

3) modify existing instrumentation to improve the sensitivity and/or resolution (i.e. mercury porosimetry, gas adsorption),

4) develop new methods for thin film characterization (i.e. image analysis, permeability),

5) attempt to inter-relate these techniques by examining controlled porosity/pore structure materials (i.e. silver membrane filters),

6) employ these techniques to characterize the films prepared in 1).

In addition to developing the expertise necessary to evaluate the physical morphology of thin films, this program has included the examination of some of the variables associated with a number of thin film deposition techniques (e.g. plasma spraying, metal paste printing) and has permitted a preliminary assessment of a few novel approaches for characterizing or describing thin films (e.g. impedance porosimetry, fractal analysis). By applying the information generated as part of this study, further work on the dependence of morphology on electrochemical behavior can now be initiated.

2. BACKGROUND

As an introductory phase to this program, an up-to-date review of the technology for characterizing thin film electrodes was initiated and reported in the ORF Phase I Final Report dated March 16, 1985. This phase I report summarizes both the current literature (including bibliography) and discussions with scientific workers in the field on all aspects of the physical morphology of electrodes including important physical parameters (e.g. pore structure, thickness, tortuosity), as well as electrode fabrication techniques and potential characterization procedures. To avoid repetition, the earlier report will serve as the background information for this Phase II report, which describes the experimental approach. For the sake of completeness, however, a brief review of the important physical parameters of fuel cell electrodes is given.

2.1 Fuel Cell Electrodes

Fuel cell electrodes differ from traditional electrodes used in other types of electrochemical devices, in that they must be; 1) porous to allow for the passage of reactant gases, 2) electrocatalytic to stimulate chemical reactions and charge transfer processes, and, of course, 3) electrically conductive to assist in the collection of generated current. The reaction mechanisms encountered in an operational fuel cell are extremely complex and will vary depending upon not only electrode effects but the electrode/electrolyte composition and the partial pressures of reactant gases. The processes inherent to the system include gaseous diffusion through the electrode, electrocatalytic dissociation, atomic diffusion across/through the electrode, charge transfer at the electrode/electrolyte interface, and surface diffusion at the three-phase (gas/electrode/electrolyte) contact area. Since each of these processes is governed by either a physical or chemical characteristic of the electrode and/or electrolyte, it becomes apparent that one must adequately quantify all parameters in order to isolate a particular reaction step, and thereby determine the overall reaction kinetics.

The electrode reaction (dissociation of reactant gases into ionic species including migration to the electrolyte) consists of five distinct processes all of which have at least one controlling physical parameter which can limit overall performance. Table 2.1 lists these process/parameter relationships as well as a number of techniques which may be employed to define or quantify these parameters.

Molecular gas diffusion through the electrode is perhaps the most cited process and is known to be strongly linked to a concentration polarization effect of the fuel cell. The physical parameters which influence this process are the pore structure, pore tortuosity, and electrode thickness.

Closely linked with the pore structure is the total surface area and catalytically active surface area. Obviously, as the number of small pores increases, the overall surface area also increases. This, however, does not necessarily imply that the efficiency of the electrocatalytic process will be enhanced since the active adsorption sites may differ from the general physical adsorption sites (i.e. chemisorption vs. physical adsorption) or the pores may be sufficiently small to limit gas flow.

The diffusion of atomic species can be limiting for some experimental conditions. Although this process is somewhat specific for the species/electrode material composition as well as environment (i.e. temperature and pressure), the particulate size of the electrode material is expected to play a significant role.

Closely related to the particle size of the electrode materials are the three phase line length and the electrode/electrolyte contact area. These parameters are thought to control the charge transfer process and electrolyte surface diffusion respectively.

If, through the physical characterization of electrode morphology, it is possible to isolate each individual electrode process given in Table 2.1, then it becomes reasonable to compare and evaluate alternative types of electrode materials. Although platinum is still regarded as the ideal

Table 2.1 Relationships Between Electrode Processes and Physical Properties

Electrode Process	Controlling Physical Parameter	Measurement Techniques
Molecular Gas Diffusion	Pore Structure Pore Tortuosity Electrode Thickness	SEM/Image Analysis Mercury Porosimetry Gas Adsorption, Profilometry Gas Permeability
Catalytic Activity	Surface Area Surface Roughness Active Adsorption Sites	Gas Adsorption (BET) SEM, Chemisorption Profilometry
Atomic Diffusion	Particle Size	SEM
Charge Transfer	Three Phase Line Length	SEM
Electrolytic Surface Diffusion	Electrode/Electrolyte Contact Area	SEM

electrode material from an electrocatalytic and current collection point of view, the cost will most likely prohibit it from use in large-scale commercial cells. To pursue other suitable materials it is necessary to understand the effects of electrode morphology. This requires suitable techniques for both producing electrodes of a pre-defined and consistent morphology as well as appropriate methods for the complete characterization of the physical structure of the electrode.

2.2 Electrode Fabrication Techniques

A variety of fabrication techniques currently exist for preparing solid thin film electrodes. Each technique will produce an electrode with unique morphological properties, some of which may be totally random and non-reproducible while others may be uniform and lead to completely consistent morphologies. As stated in the previous section, it is desirable to employ the latter techniques particularly when one is trying to isolate and/or correlate individual morphological properties.

A number of conventional thin film preparative methods have been described in the Phase I report. These include ink printing, sputtering and evaporation, thermal spraying, thermal compression and tape casting. For the purposes of this experimental program, two fabrication techniques were employed; ink printing of platinum pastes (both hand painting and screen printing) and plasma spraying of nickel powders. In both cases, the actual electrochemical nature of the film was not considered. These films were assumed to be representative of the morphology generated by each process and subsequently used to study the interdependence of various properties as well as the overall suitability of the techniques for preparing porous electrodes.

2.2.1 Ink Printing

The formation of thin film electrodes on solid substrates using metallized paste printing is a standard practice in such applications as printed circuit boards, recording tape, static shielding and multi-layer capacitors. In most cases, however, the end-use calls for a completely

conductive or resistive coating of precise size, both of which place certain demands on the application technique as well as on the material. (It should be noted that in this industry, printed coatings or electrodes are generally referred to as thick films.)

Inks are generally formulated for specific results when employed in a prescribed manner. They can be applied by a number of means including screen printing, spraying, dipping, and brushing. Each application technique has certain advantages/disadvantages and the selection of technique should be based on of the end-use requirements. For those films of which the reproducibility and precise orientation are not important, dipping or brushing may be appropriate, however where exact control is needed, screen printing is generally employed.

Even when employing a screen printing technique, great care must be taken to ensure consistent films. Factors which can affect the film properties (including morphology) are composition, screen size and tension, squeegee orientation, duration and pressure as well as ink/paste viscosity.(2) These factors can be extremely critical, especially when one is trying to produce a film of unique pore structure.

Conductive inks are available from a wide variety of sources for a wide variety of applications.(3) In this study, two platinum type inks were chosen for further investigation. These were Engelhard pastes A-4338 and #6926, both of which have been developed for oxygen sensor application and therefore form semi-porous coatings/electrodes.

2.2.2 Plasma Spraying

Plasma spraying is a process of developing coatings of varied compositions by the successive build-up of molten or semi-molten droplets on a solid object. Basically, solid particles in the super-micron range are introduced at high velocity to a plasma which can be controlled in temperature up to 15,000°K(4). During their passage through this plasma, the particles are heated to a fully or semi-molten state whereupon they exit from the

plasma and are impacted on a solid object at a prescribed distance (or into a cooling medium in the case of plasma produced powders) to form a thin layer or coating.

It is well known that the coatings have a sandwich-like structure, the properties of which can be regarded as resulting from the deformation and solidification processes of individual droplets and their interaction on contact.[5] One of these properties of interest, particularly for electrochemical electrode studies, is the porosity or rather pore size distribution.

Pore size and porosity can be greatly affected by a number of variables in the plasma spraying operation. Factors such as initial particle size, particle/powder flow, plasma composition and temperature, working distance (plasma to piece distance), and cooling air all contribute to the overall bulk morphology of the final coating.

Plasma spraying offers the following advantages for preparing electrochemical electrodes,

1) molten droplets can easily conform to irregular surfaces thereby providing a good substrate/coating interface.

2) unique chemical compositions (materials) can be prepared during the plasma production of spray droplets (e.g. a number of powders can be intimately mixed and/or reacted in the plasma)

3) the process is amenable to large scale production at a reasonable cost and rate.

Other factors which must be examined when considering the plasma spray option are the thermal stability of the substrate and compatibility of the substrate and the plasma coating. In the former case, although individual droplets cool rapidly when outside the plasma, there will be some degree of substrate heating when the droplets contact the surface. This could be

critical for electrochemical applications where the electrode/electrolyte interface is so important for ionic diffusion and/or charge transfer. In the latter case, film/substrate compatibility may limit potential applications where effects such as thermal expansion may inhibit bonding or materials suitability may lead to corrosion.

In an effort to study some of these properties, a number of nickel plasma films were prepared and subsequently subject to complete physical characterization using the techniques developed in this program. This will be described, in detail, in this report.

2.3 Physical Characterization Techniques

The evaluation of physical morphology for thin film materials places certain demands on the characterization techniques employed. In most cases, conventional methods which were developed for evaluating bulk materials have certain limitations on sample size (volume). The approach of this study has been to modify and extend the application of standard techniques, such that relevant physical data on thin film materials could be obtained. In many cases, the selected techniques were employed to examine the same morphological parameters from a different perspective. In these situations, attempts to correlate the results should provide some degree of validity for employing these methods.

2.3.1 Image Analysis

Image analysis is a quantitative technique for evaluating the size and/or shape of features in an image. The process involves inputing a video image, which may be from a camera (scanner), SEM, or direct video link, to a computer which can generally store the image. Once the image is stored digitally by the computer, its composition can be broken down into what is known as a grey-level map which assigns a distinct (generally 0-255) grey level to each pixel element (a standard video monitor would have approx. 250,000 pixels). The image can then be "thresholded" to group certain grey-levels together, thereby discriminating between different features of

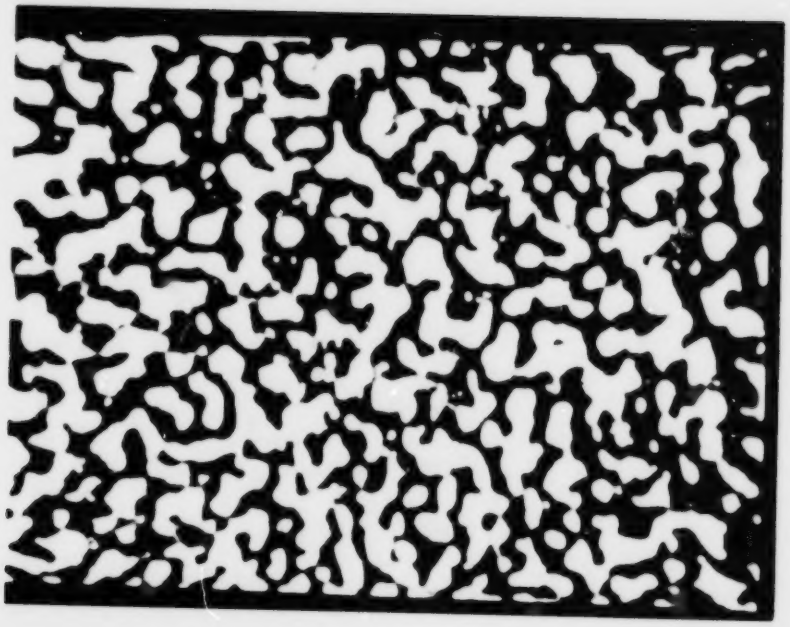

Figure 2.1 Optical Photomicrograph of 5.0 μm Silver Membrane Filter Showing Solid Phase (Light) and Porous Phase (Dark) (470X)

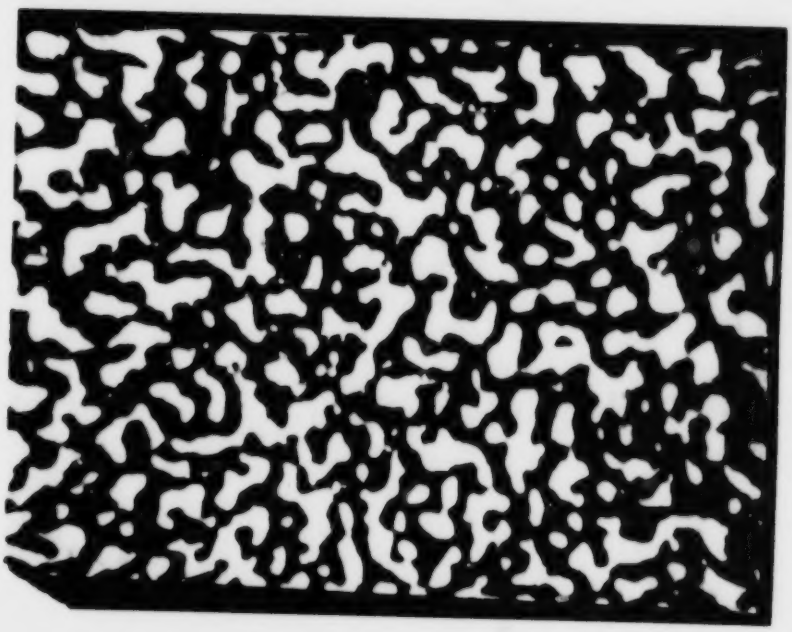

Figure 2.2 Thresholded Image of Detected Porous Phase (470X)

interest. Figure 2.1 shows a photograph of the surface of a polished 5.0 um silver membrane filter. The light particles are the solid silver phase and the dark areas represent the continuous pores. If a threshold is set such that all the darker areas are detected (see Figure 2.2), one can go on to analyze the pore structure of this membrane.

Most modern digital image analyzers currently available also offer various degrees of image processing which can be employed to enhance the image and highlight certain features which are difficult to distinguish otherwise. The image processing capabilities can include erosion/dilation for separating touching features, logical functions for comparing images or adjusting for shading, small feature enhancement to emphasize minute details, filtering to smoothen "rough" edges, and grey-level equalization to improve the contrast of all features.

Once the image has been processed and thresholded for the features of interest, it is possible to perform an analysis which will give quantitative information such as the % area (or porosity), length, width, aspect ratio, orientation, or perimeter. Other parameters or combination of parameters (e.g. shape descriptors, fractals, etc.) can also be obtained by modifying the analysis program.

Ontario Research currently maintains a LeMont Scientific[6] OASYS image analyzing computer which is equipped with a Newvicon tube scanner (camera), 4MB memory (15 image storage), and high resolution (0.001") digitizing tablet (digipad). Analysis software which has been employed in this project to study pore and/or particle dimensions includes a lineal program (chord-length), line scan program, and diameter program (minimum crossing diameter). The operation and application of each of these programs, are discussed in the following sections.

2.3.1.1. Lineal Analysis

This program, also known as cross section chord length or stereological analysis provides a quantitative evaluation of feature width at pre-described

scan lines along either the horizontal or vertical scan direction. Basically, after the features of interest are thresholded, the image is scanned and this technique can measure the chord lengths by recording the number of "on" and "off" points (pixels). By setting the number of scan lines, it is possible to control the number of features or rather the number of chords analyzed. Figure 2.3 shows the chord lengths employed in analyzing the porous film depicted in Figure 2.1.

Data generated from such an analysis can include chord length distribution, average chord length, volume fraction, number of features, edge-to-edge spacing, center to center spacing and surface-to-volume ratio. When applied to the pores and particles of the cross-sectioned films studied in this program, information on the pore/particle diameters as well as the void/solid volume (% porosity) can be obtained.

2.3.1.2 Line Scan Analysis

The line scan analysis program was originally developed for the simultaneous measurement of features containing two or more intensity levels. To do this, the image analyzer keeps track of every line scan (512 horizontal lines) and determines the area and perimeter points of adjacent lines which are thresholded (see Figure 2.5). By storing the perimeter points of all features it is possible to derive such parameters as Ferets diameter (maximum length), width (at right angles to length), and orientation (degrees 0^{o}-360^{o}) of maximum axis as well as perimeter length. Other parameters include % area (% porosity for pore analysis) and shape (width-to-length ratio). For the purpose of this program, area equivalent diameter (the diameter of a circle having the same area as the particle/pore) and area % (porosity) were employed for characterizing film morphology. In most cases however, this analysis can only be applied to non-continuous features since an inter-connected phase will be interpreted as one large feature with many inclusions. For these situations, the lineal or diameter analysis may be more appropriate.

2.3.1.3 Diameter Analysis

The diameter analysis program involves determining the approximate centroid of detected features and then constructing a chord length or diameter

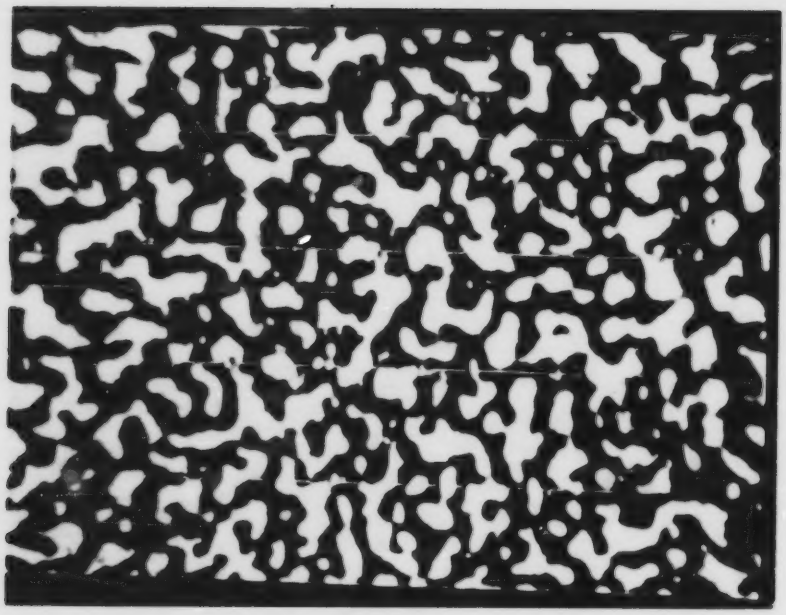

Figure 2.3 Lineal Analysis of Detected Porous Phase (470X)

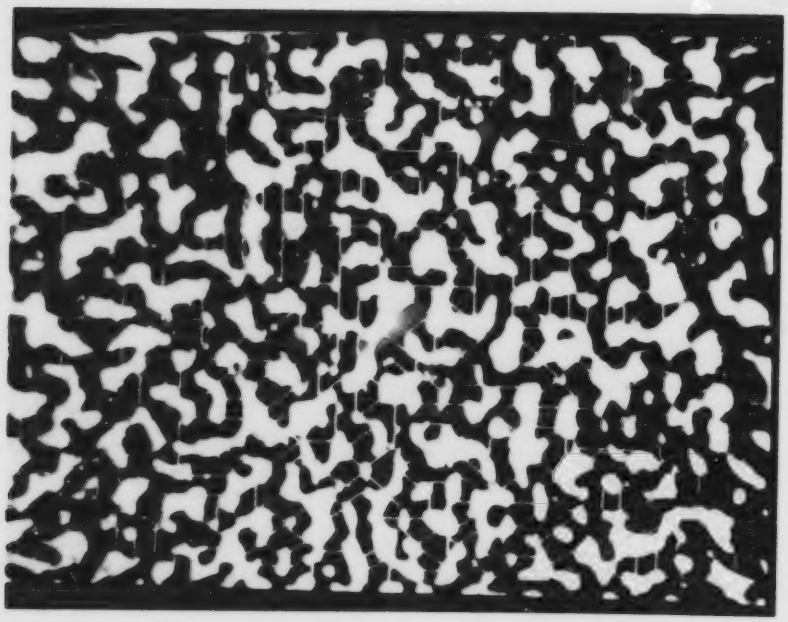

Figure 2.4 Diameter or MCD Analysis of Detected Porous Phase (470X)

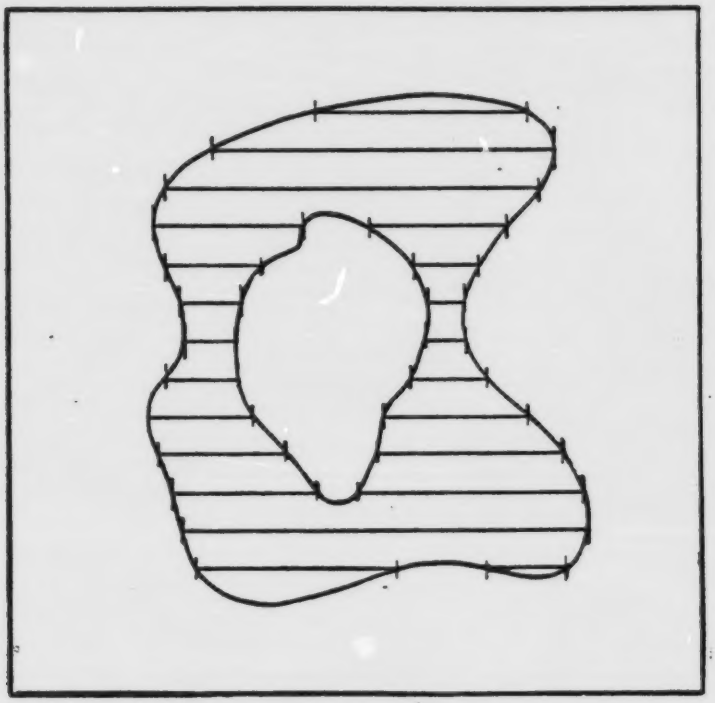

Figure 2.5 Line Scan Logic for Evaluating Features with Inclusions

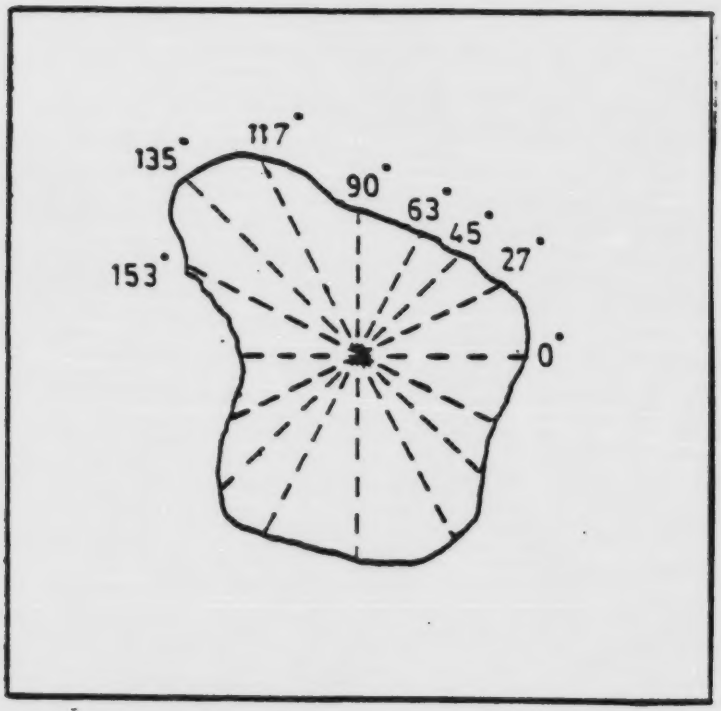

Figure 2.6 Diameter Logic for Measuring Feature Dimensions

length assessment through this point (see Figure 2.6). As a modification to this, the minimum crossing diameter program was developed for work on characterizing porous biomaterials such as coral.(7) By assigning a grid pattern (pixel count) for an image, the starting points for the diameter analysis routine can be determined (those grid points which are contained within the features of interest). The diameter program can then be employed to measure the minimum crossing diameter (MCD) for each point. Figure 2.4 shows a photo of the thresholded pores with a MCD analysis. The MCD results can be averaged to provide mean or median values which may bear some relation to the smallest feature dimension (e.g. pore retentiveness for filters). This parameter was found to correlate well with the pore diameters estimated from visual three-dimensional SEM micrographs for coral samples.(7)

2.3.1.4 Sample Preparation

As stated earlier, the image generated for subsequent analysis can come from a variety of sources, however, it is imperative that the technique employed be selected to provide the maximum degree of contrast between the features of interest and the background. For features which are small in size and have different chemical compositions, SEM examination (particularly backscattered electron (BSE) images) will usually provide sufficient contrast. For materials of varying refractive index or coloration, optical microscopy can often be employed. Either of these approaches can be used directly (e.g. SEM/IA interface, optical microscope/camera) or indirectly through the use of photomicrographs which can be input to the image analyzer through a camera/lens arrangement.

Some problems arise, however, when examining pores or the nature of porous bodies. Since, in fact, there is nothing to measure or observe, distinguishing phase boundaries can be extremely difficult if not impossible. It therefore becomes necessary to impregnate the sample with a material that will permit feature identification. This mounting procedure has become standard practice in metallurgical studies and generally involves filling the voids with a liquid epoxy which sets in the pores.

When the porous features become sufficiently small, it is usually necessary to employ a special low-viscosity mounting medium coupled with vacuum or centrifuge impregnation[7] and/or pressure curing.[8] Set samples can then be cross-sectioned and polished to provide a 2-D picture of the porous nature of the sample. With elaborate computer software and controlled cross-sectional analysis, it is also possible to re-construct 3-D representations from a series of 2-D images.

In this study, porous films were vacuum impregnated and pressure cured with Spurr Low-Viscosity Embedding Media[9] and subsequently cross-sectioned and polished for examination under either the SEM or optical microscope. Quantitative measurements were performed on the 2-D images using the techniques described previously.

2.3.2. Profilometry

Analysis of surface texture has become an important engineering consideration especially when one is examining the interaction between two materials. The measurement of surface texture can be accomplished by a variety of analytical techniques utilizing optical, contact, electrical, and fluid methods.[10] The most widely employed technique, however, is that using the stylus tracking instrument which is generally referred to as profilometry.

Profilometry offers the advantages that it is a simple, proven, and relatively non-destructive means of evaluating differences between bulk materials. In this study, it is hoped that some correlationss can be drawn to relate the surface texture of a porous film to its internal porosity or pore structure as measured by an alternative technique such as permeametry or surface area analysis. This relationship is expected to exist for films that are deposited by a random process, when the exposed surface closely approximates the morphology of underlying layers. If this connection can be established, then profilometry will provide a rapid, potentially "in-process" means of qualifying potential electrode materials.

In quantifying physical surfaces by profilometry it is important to remember that a profilometry trace is a simple scan "snapshot" of the surface on a predetermined line and that the roughness of a surface cannot be adequately described by one parameter. This implies that the measurement of surface roughness is a statistical process in which a number of parameters must be computed. Parameters are therefore best reported as mean values with associated standard deviations for the area of the surface scanned (or number of traces performed).

Ontario Research currently operates a Rank Taylor Hobson Talysurf 6 profilometer[11]. The unit is the top-of-the-line research model and is equipped with the Talydata 2000 computer for calculating over twenty-five surface texture parameters and information on bearing ratios and profile cross-sections. The Talysurf 6 is also capable of operating in a statistical acquisition mode with a variety of stylii (low magnification tip approx. 12 um to high resolution tip approximately 1.5 um diameter). To better understand the measurements given as part of this study, the following sections address some of the more important considerations in conducting and reporting profilometry analyses.

2.3.2.1. Profile Filtering

Any two dimensional surface can be considered to have three types of surface structure; microstructure, which can be referred to as texture or roughness and two macrostructure variables which are termed waviness and form over which roughness is superimposed (see Figure 2.7). To differentiate texture from waviness and form, it is necessary to damp out these secondary effects through the use of filtering.

There are three basic types of filtering commonly used in profilometry; mechanical, graphical, and electrical. The latter technique involves passing the stylus transducer output through a 2-CR (capacitor/resistor) electrical circuit consisting of CR's with identical time constants. Since this approach has not been employed in this study, it will not be considered further.

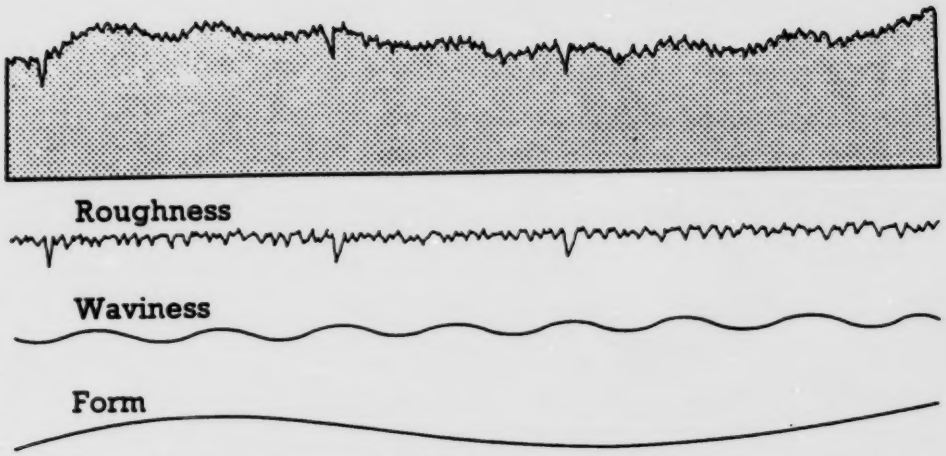

Figure 2.7 Three Types of Surface Structure

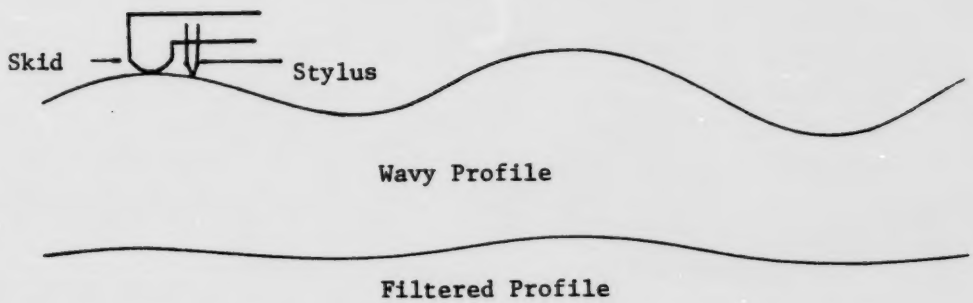

Figure 2.8 Mechanical Filtering with a Skid Arrangement

Mechanical filtering involves the use of a support mechanism known as a skid. Basically the skid supports the stylus arm such that the stylus head is free to follow the movement of the skid over the form or waviness of the surface. Figure 2.8 shows the skid/stylus assembly tracking over a wavy profile. Since the whole assembly is free to move along the peaks and valleys of the form, the stylus movement is dampened. The degree of dampening or filtering is affected by the skid to stylus distance as well as the nature of the surface. Since the skid and the stylus cannot touch the surface at the same point, there is a phase effect which is dependent upon the movement of the skid and stylus as well as the amplitude. For the figure shown, this phase shift tends to 0^{o} since the assembly will move together. However, for profiles where the peak frequency approximates the skid to stylus distance, the resultant phase shift can be 180^{o} and can produce a profile with an amplitude twice its actual value.

Graphical filtering involves correcting for any waviness or form by dividing the total scan length into a series of sampling lengths for which texture parameters are computed independently. Figure 2.9 depicts a surface profile which has both surface texture and a degree of waviness. By segmenting the profile into smaller sampling lengths, L_1, and calculating the center line average (CLA or Ra) for each length, the trace can be replotted as in Fig. 2.10, by joining all the mean lines to form a continuous CLA. This removes the waviness effect from the profile.

Obviously, the selection of sampling length will greatly influence the degree of filtering effected. To standardize profile measurements, therefore, a number of sampling lengths have been established by such organizations as British Standards (BS) and the International Standard Organization (ISO). The five sampling lengths chosen are;

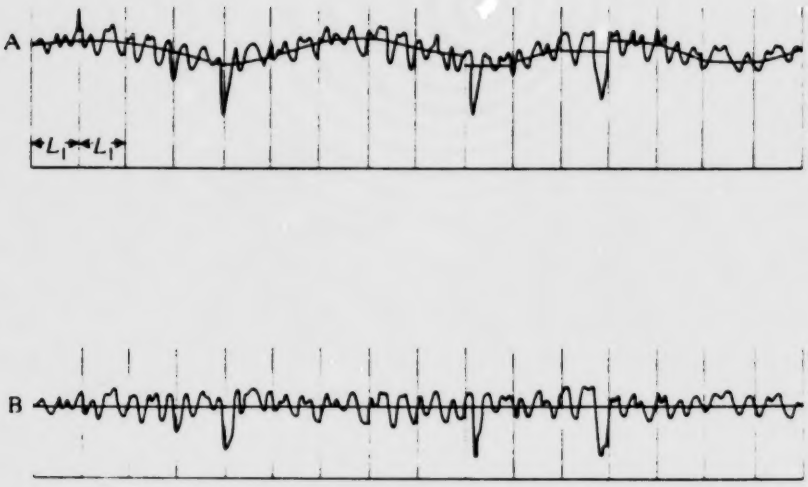

Figure 2.9 Effect of Graphic Filtering

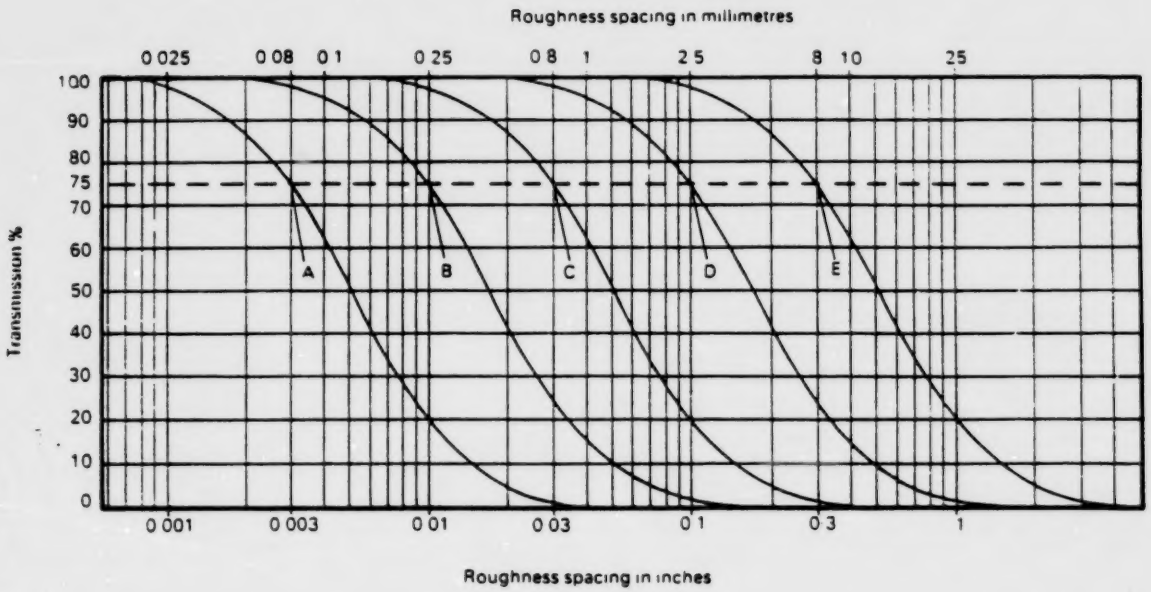

Figure 2.10 Filtering Effect for Standard ISO Cut-Off's

	Cut-off (mm)
A	0.08
B	0.25
C	0.80
D	2.5
E	8.0

The cut off value refers to the value at which 75% of the original profile amplitude is transmitted to the filtered profile. Figure 2.10 shows the filtering effect for each of these sampling lengths.

From the previous considerations on the effects of filtering, it becomes apparent that to compare the surface texture of two or more materials, it is imperative that identical sampling conditions be employed. This constitutes recording both the stylus arrangement (skid or skidless) as well as the filtering mode (cut-off value).

2.3.2.2 Surface Texture Parameters

As mentioned before, the Talysurf 6 system is capable of assessing over 25 standard surface texture parameters which all define some unique properties of the surface. Computed values are generally broken into three classifications; 1) amplitude parameters which are solely dependent upon the vertical displacement of the profile, 2) spacing parameters which are measures of irregularity spacings along the surface, irrespective of the amplitude of the irregularities, and 3) hybrid parameters, which relate to both the amplitude and spacing of surface features.

A listing of the standard surface texture parameters, together with their meaning and method of calculation, is provided in Appendix A.

2.3.3 Permeametry

The application of permeametry or fluid flow studies has long been employed to evaluate relative differences between porous materials. Since permeability measurements are extremely sensitive to small changes in pore geometry, this technique can be applied to the characterization of pore structure in permeable materials. When gases are employed (as opposed to liquids), however, complications can arise due to the laws governing gas flow which vary with the pressures employed and the pore dimensions.

Fluid flow in single capillaries can be classified into four regimes; turbulent, viscous or laminar (Poiseuille), slip flow, and molecular streaming (Knudsen flow). Turbulent flow occurs at high pressures and results in energy losses which produce a non-linear relation between mass flow and pressure. During laminar flow, the mass flow and pressure are directly proportional (linear). As the pressure or capillary size decreases further, there is an increase in mass flow due to slippage at the boundary, and when the mean free path of the gas is approximately ten times the diameter of the capillary, molecular diffusion prevails. In order, therefore, to draw conclusions regarding pore structure without using complex models, it becomes necessary to operate in the viscous or laminar region where simple linear equations relate mass flow, pressure, and pore dimensions.

The relation which governs permeability in this region is given by the Poiseuille equation;

$$Q = \frac{\pi r^4}{8\eta} \cdot \frac{\Delta P}{L} \qquad (1)$$

when Q is the volume of fluid flowing per unit time, r is the radius of the pore, η is the fluid viscosity, ΔP is the pressure differential across the material, and L is the length of the sample (pore).

If a porous medium is treated as a bundle of uniform parallel capillaries, N_o, of radius r, then;

$$Q = \frac{\alpha A N_o r^2}{8\eta} \cdot \frac{\Delta P}{L} \qquad (2)$$

Here A refers to the cross-sectional area of a pore ($A = \pi r^2$) and α is the fractional void area (i.e. percentage of open area across the sample surface). By plotting Q vs ΔP, one should therefore obtain a linear relationship, assuming laminar flow. More complete descriptions of these and other theoretical equations including slip flow and molecular diffusion models may be found elsewhere.(12)

For this program, permeametry is seen as a plausible method for evaluating the reproducibility of preparing porous gas electrode materials of uniform bulk morphology. This technique, however, is somewhat limited in that it is necessary to conduct the analyses on unsupported materials since the presence of any support would seriously influence the observed permeability behavior by either superimposing the flow characteristics of the support on top of that of the films or by altering the pore structure of the film as it is deposited on the support.

2.3.3.1. Apparatus

A simple device was constructed for measuring the pressure drop across a film versus the flow rate of the passing gas. The apparatus is composed of a standard gas cylinder (helium, hydrogen, oxygen) fitted with a pressure regulator capable of reading up to 50 psig in 1 psi increments and a sample holder capable of sealing 25 mm (approx 1") diameter materials (Millipore Gasline Filter Holder). Following the sample holder a Matheson Rotameter #603 was used to measure the flow rate of permeating gas (approximately 0.1 - 10 ℓ/min). Figure 2.11 shows the assembled apparatus.

2.3.3.2. Validation of Test Rig

In an effort to verify the operation of the permeability test rig, a number of studies were initiated using standard membrane filters of known pore retentive ratings.

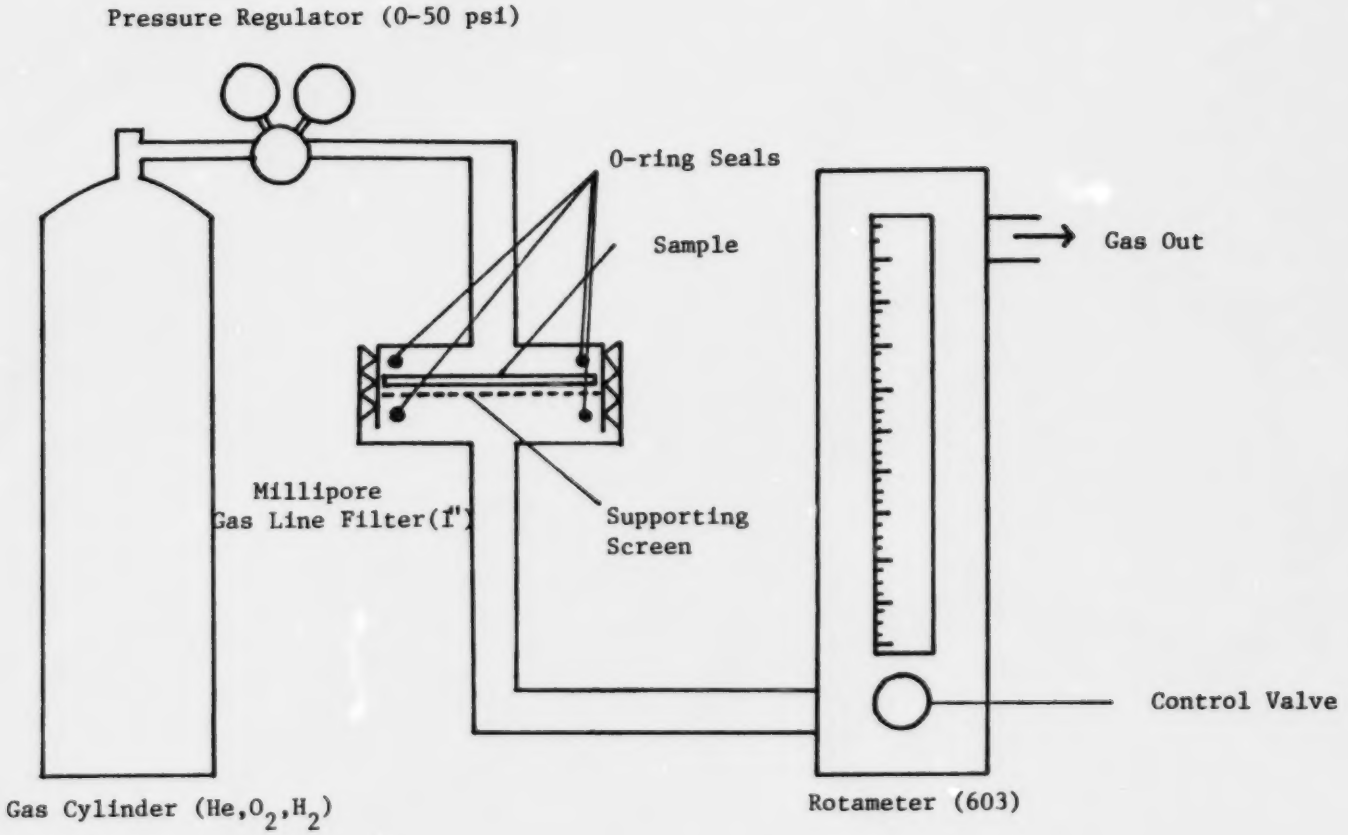

Figure 2.11 Schematic of Permeability Test Rig

2.3.3.2.1 Millipore Membrane Filters

Millipore membrane filters ranging from pore ratings of 5 um to 0.1 um were investigated. Since these materials are comprised of mixed esters of cellulose which provide a very tortuous pore structure, it was originally felt that these membranes would more closely approximate the pores present in plasma sprayed and other films.

Figure 2.12 shows the flow/pressure curves generated for the Millipore filters for pressures from 4-50 psi using the permeability test rig described in Section 2.3.3.1. In addition, a blank run was conducted to establish an upper limit on permeability. For these measurements, only the stainless steel support grid was used in the membrane holder. The rig was subsequently standardized and calibrated before each sample run using these values.

Although the slopes of the curves from Figure 2.12 are relatively linear and vary according to the effective pore diameter, there appears to be little change of significance (in comparison with the blank), until the pore rating drops below 0.8 um. Unfortunately, it is difficult to apply theoretical models to these materials since the pores are extremely tortuous in nature and are rated by only their particle arrestance behavior. Also the total porosity is rather ill defined (ranging from 74-84% for these Millipore membranes) making these permeability measurements semi-quantitative at best.

2.3.3.2.2 Nuclepore Membranes

To better define the effects of pore dimension and porosity on the flow characteristics of porous materials analyzed in this test rig, Nuclepore membrane filters were studied. The Nuclepore membrane is prepared by a nuclear "track-etch" technique which places strict control on the size, density and uniformity of generated pores. The pores also have the advantage of being capillary in nature and relatively straight and non-tortuous ($\pm$ 34°). These materials therefore present the "ideal" case for relating

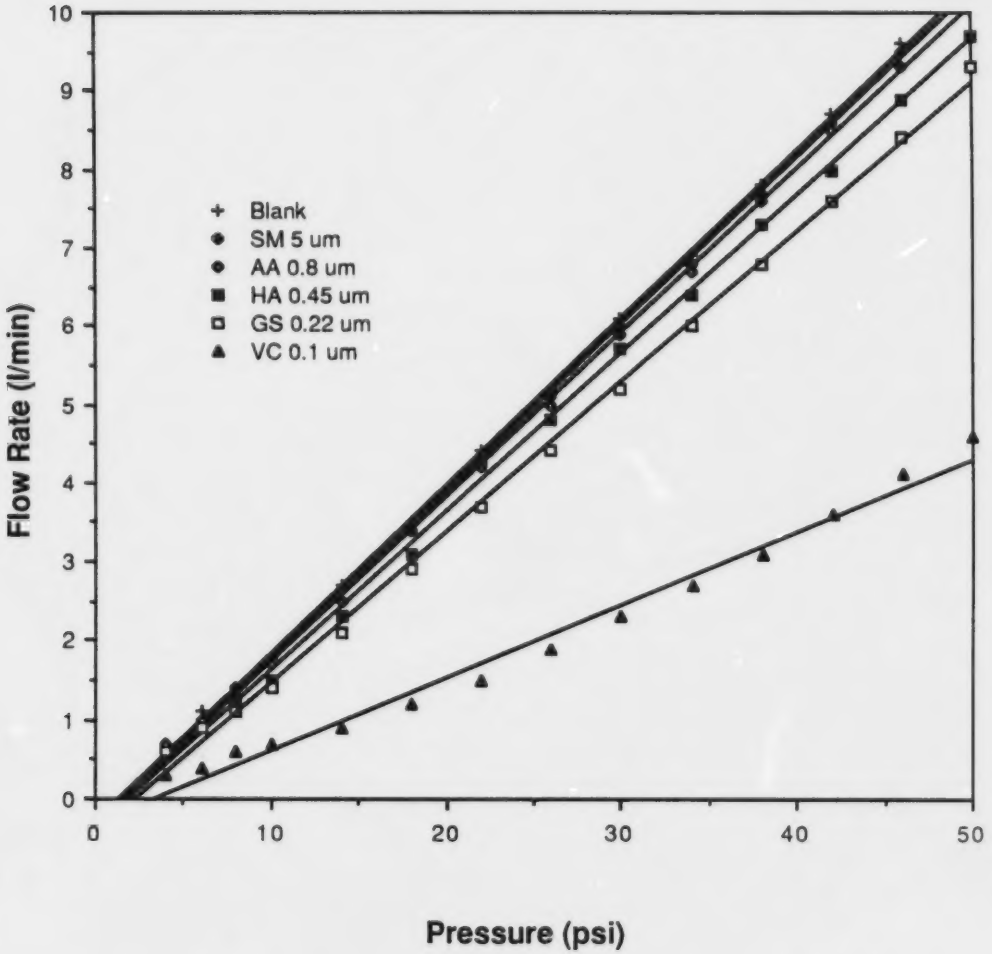

Figure 2.12 Permeability Measurements for Millipore Filters

empirical equations for pore dimension and porosity for flow type measurements and have been employed in the past for proving molecular flow equations.[13]

Figure 2.13 shows the measured flow/pressure curves for Nuclepore membranes ranging from 5 um to 0.05 um. As with the Millipore filters, there does not appear to be an appreciable change in the flow properties until the pore dimension becomes submicron.

To verify that the relationship between mass flow and pore dimension holds, equation (2) was used. From this equation, the slope of a Q vs ΔP plot should be given by;

$$\text{slope (Q vs } \Delta P) = \frac{\alpha A N_o r^2}{8\eta L} \qquad (3)$$

Therefore, a plot of the (slope (Q vs ΔP))/αA versus $N_o r^2/L$ should be a straight line if the flow is in the laminar region.

Table 2.2 gives the measured and calculated values for the Nuclepore filters while Figure 2.14 depicts the plot for (slope(Q vs ΔP))/αA versus $N_o r^2/L$. If one were to omit the data point for the 1.0 m membrane, the fitted curve closely approximates a straight line ($r = 0.99$) which shows that for the pressures employed and the pore dimensions measured, the permeability test rig appears to operate in the laminar region and should therefore be well suited for comparative testing (i.e. relative measurement) of porous materials.

2.3.4 Mercury Porosimetry

The application of mercury porosimetry for evaluating the pore size distribution and total porosity of bulk materials has become a routine analytical technique. The principle is based upon the capillary rise phenomenon whereby an excess pressure is required to cause a non-wetting liquid to climb up a narrow capillary. For cylindrical pores, the pressure P, required to drive mercury into a pore of radius r, is related to the contact angle, θ, between the liquid and solid, and the surface tension of the liquid, γ, by the Washburn equation;[14]

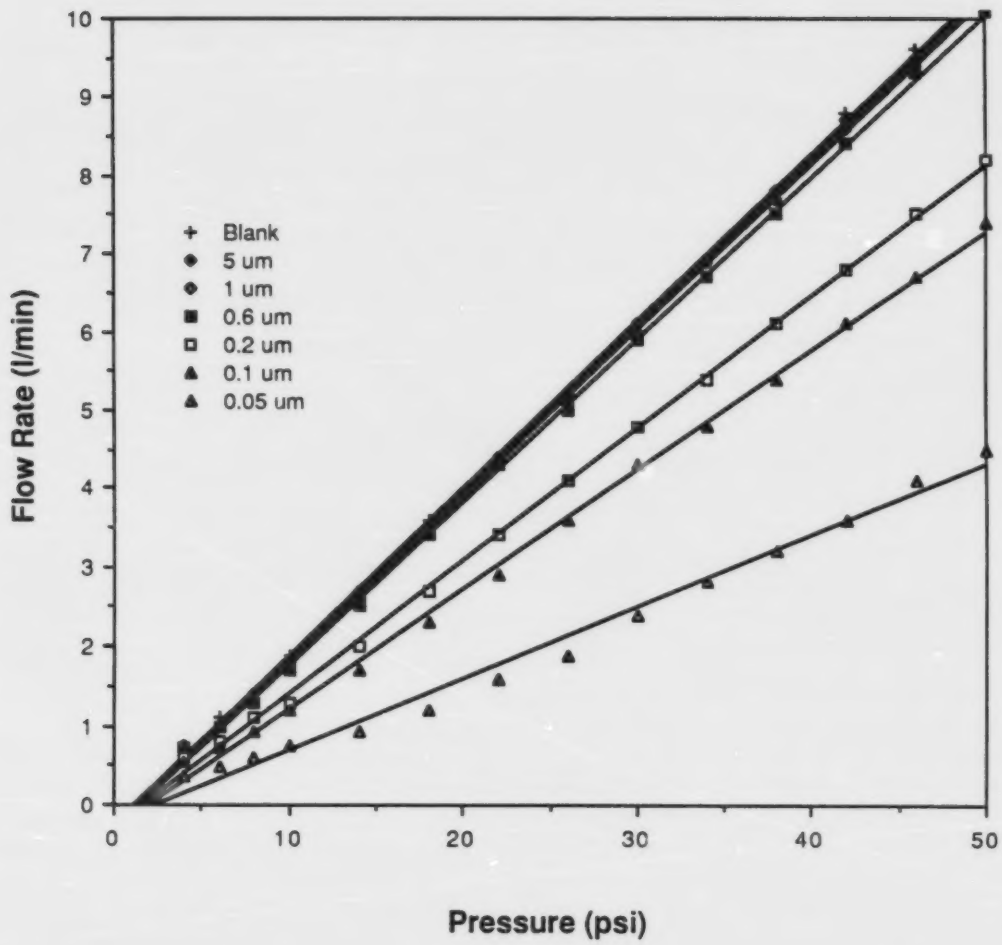

Figure 2.13 Permeability Measurements for Nuclepore Filters

Table 2.2

Physical Dimensions and Flow Properties for Nuclepore Membranes

Pore Diameter (μm)	Pore Density (10^5pores/cm^2)[1]	Membrane Thickness (μm)[1]	αA(fraction open area)	Slope (Q vs Δp)	$\frac{\text{Slope (Q vs } \Delta P)}{\alpha A}$	$r^2No/L(10^5\ \mu m)$
5.0	4	10	0.0785	0.2115	2.693	2.5
1.0	200	10	0.1571	0.2109	1.342	5
0.6	300	10	0.0848	0.2070	2.440	2.7
0.2	3000	10	0.0943	0.1679	1.781	3
0.1	3000	5	0.0236	0.1512	6.418	1.5
0.05	6000	5	0.0118	0.0906	7.691	0.75

1. From Nuclepore Filtration Products Catalog Lab 50 (1980)

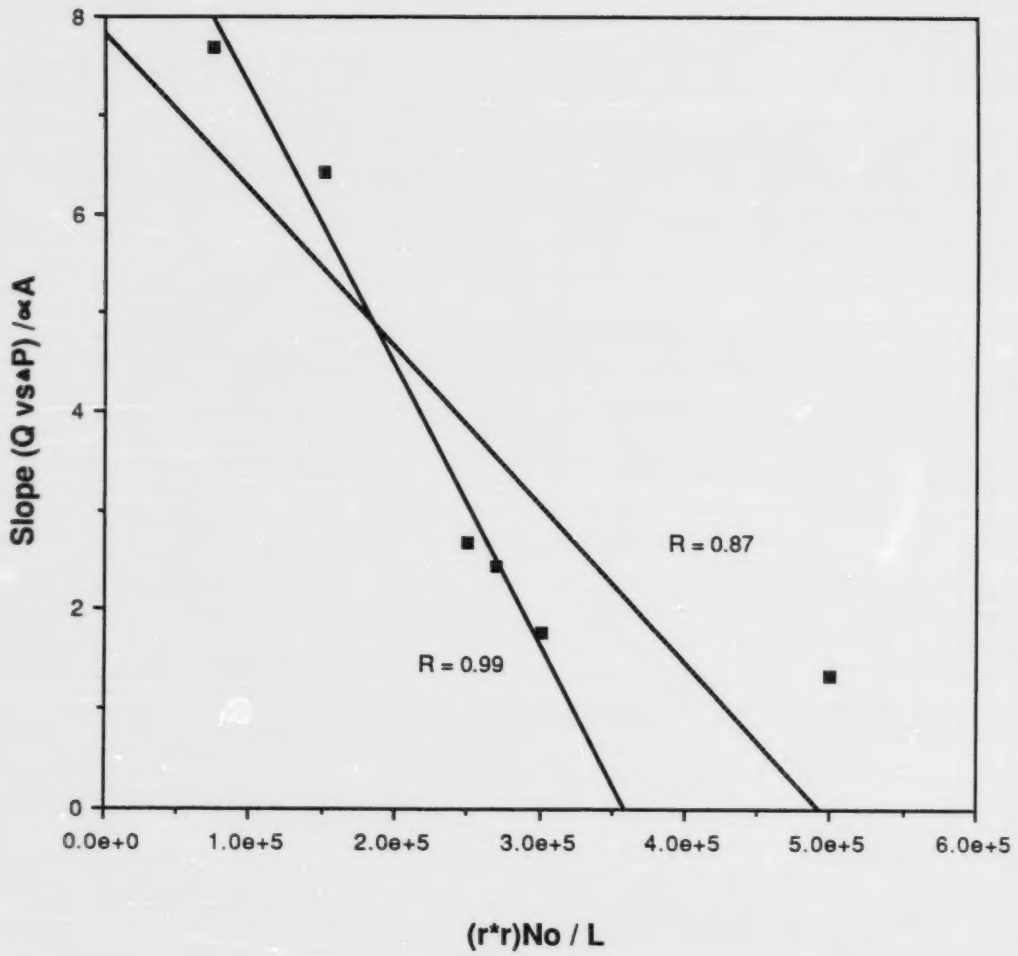

Figure 2.14 Poiseuille Fits of Permeability Data for Nuclepore Filters

$$P = \frac{-2\gamma}{r} \cos\theta \qquad (4)$$

To obtain a complete pore size distribution, the cumulative volume of intruded liquid is measured with increasing pressure which can be related to pore size by equation (4). This corresponds to what is known as an intrusion curve. It is also possible to monitor the volume of liquid expelled by a porous material when the pressure is decreased. The result is termed an extrusion curve. The intrusion and extrusion curves do not necessarily coincide and some type of hysteresis generally exists. Factors such as changing contact angle[15], pore shape[16], and pore potential[17] are all plausible explanations that have been put forward to account for this effect.

Since mercury exhibits a greater contact angle with more materials than any other conveniently usable liquid, it is almost universally employed for the evaluation of pore sizes by the pressure penetration technique. It is also a very suitable liquid for monitoring volume intrusion/extrusion by electrical means since it is a conductive material.

Ontario Research currently employs a Micromeritics Autopore 9200 porosimeter.[18] This unit is capable of operating up to pressures of 60,000 psia, which for mercury on a solid with a contact angle of 130°, corresponds to a smallest intruded pore dimension of 0.003 um or 30A. Figures 2.15 and 2.16 show a typical porosimetry analysis (both incremental and cumulative volumes, respectively) for a standard silica-alumina catalyst support.

In conducting an analysis, a weighed portion of sample is placed inside a penetrometer vessel which is shown pictorially and diagramatically in Figures 2.17 and 2.18. The penetrometer is sealed at one end with the conductive cap and subjected to a vacuum to remove residual air and/or adsorbed species from the porous sample. Without performing this evacuation, air trapped in the pores will be compressed at higher pressures thereby leading to erroneous results.

MICROMERITICS AUTO-PORE 9200 V2.02

ONTARIO RESEARCH FPL
CALIBRATION REFERENCE 820
PNTR NUMBER +13

LP 16:6:53
HP 16:36:5

INCREMENTAL VOLUME (CC/G) VS. PORE DIAMETER
100% = +0.835454E-001

Figure 2.15 Incremental Intrusion Histogram for Si-Al Catalyst Support

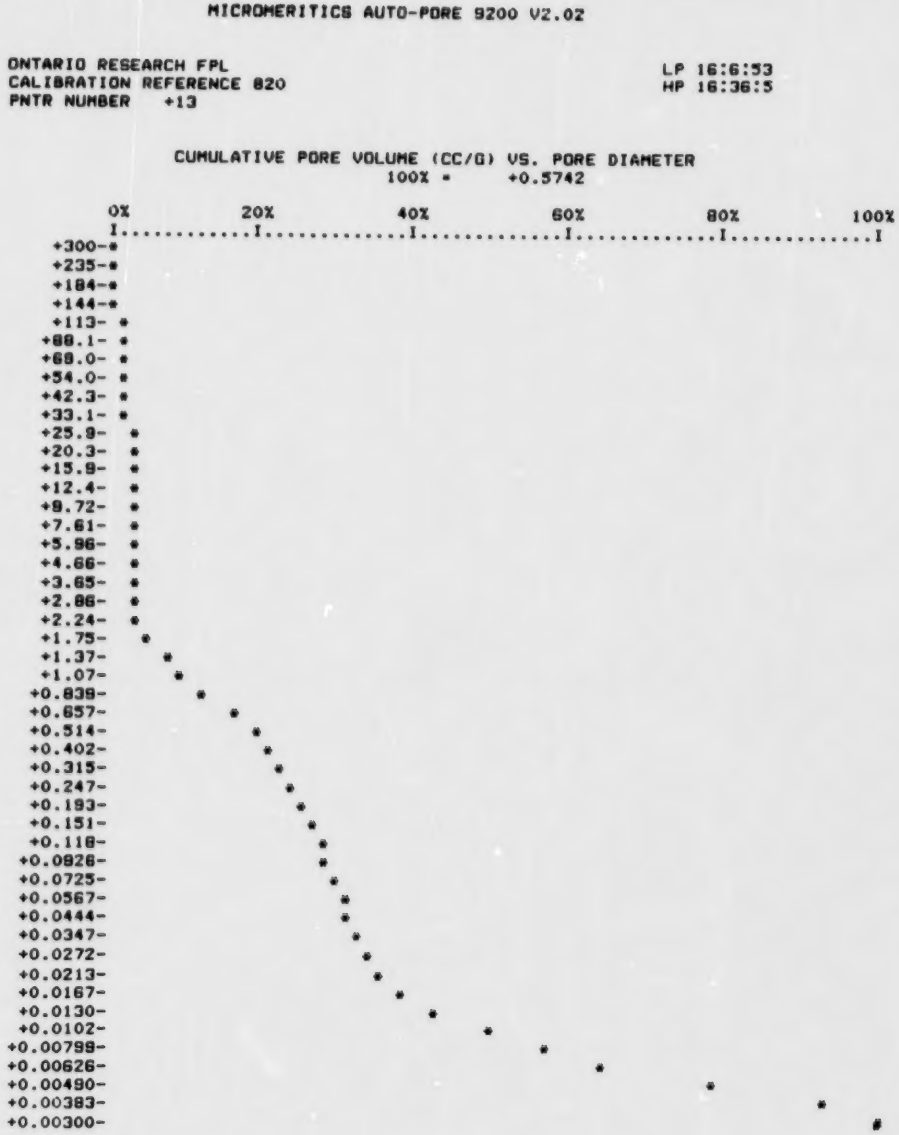

Figure 2.16 Cumulative Intrusion Curve for Si-Al Catalyst Support

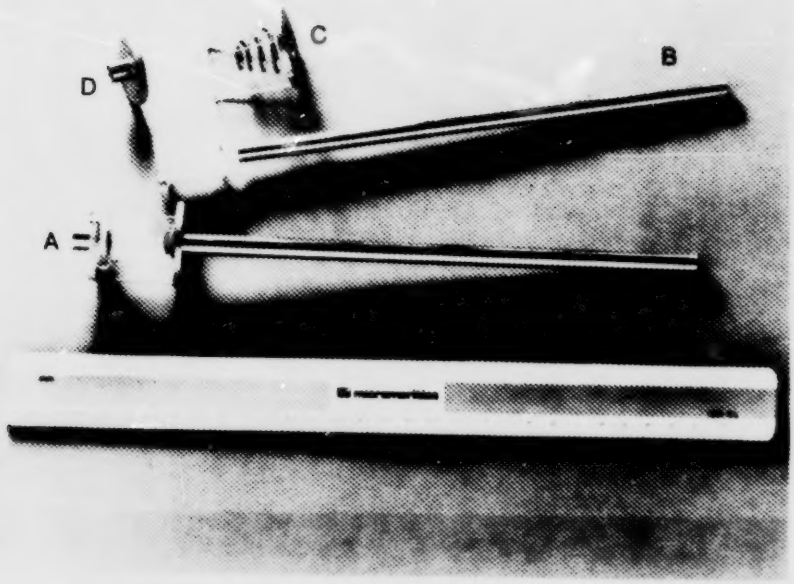

Figure 3.1 Drawing of Standard Aeroacoustics Proctor Soil Penetrometer

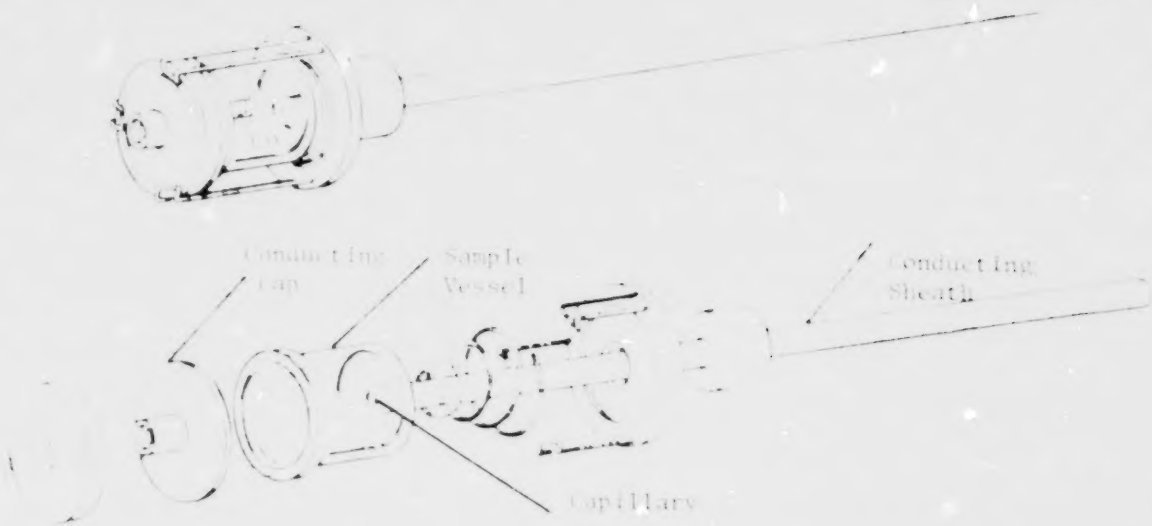

Figure 3.2 Diagram of Microporous Mercury Intrusion Penetrometers

Following evacuation, the penetrometer is filled with mercury such that the small capillary is completely full. The penetrometer is then placed in a hydraulic oil chamber such that an increase in oil pressure will drive the mercury down the capillary and into the sample. The advantage of using mercury is apparent here since the volume of mercury pushed into the sample can be monitored by measuring the change in capacitance between the moving column of mercury and the external conducting sheath. By knowing the exact dimensions of the capillary, it is therefore possible to calibrate the penetrometers such that precise volume measurements can be made.

Commercial penetrometers are available in a variety of sample chamber sizes and capillary volumes ranging from 3 to 15 cc, and 0.38 to 1.8 cc, respectively. Unfortunately, these penetrometers have been designed to measure the porosity of bulk materials (i.e. grains of sample) as well as samples with significant porosity. Problems are therefore encountered when one attempts to measure either non-porous materials or samples with small volumes, such as films, since there is not enough void volume to get a measureable intrusion using standard diameter penetrometers (smallest = 1.5 mm).

For example, if one considers a 25 mm diameter film with a thickness of 100 um and a porosity of 10%, the total available volume for intrusion is 0.049 cm^3 or approximately 13% of the total capillary volume for the most sensitive commercial penetrometer. Further, if the thickness or porosity decreases then the percent change in mercury moving down the standard capillary becomes practically insignificant.

There are two ways to solve this dilemma. Firstly, one could increase the total volume of sample by adding more films. This approach, however, results in a blending of data for the entire set of films which will not provide any information on the variability of individual films. The second method involves designing a high pressure penetrometer with an even narrower bore than commercially available. This latter approach was taken as part of this program.

In conjunction with the manufacturer (Micromeritics), ORF was able to obtain a set of narrow-bore penetrometers with a capillary dimension of approximately 0.5 mm. This corresponds to an almost ten-fold increase in sensitivity which, if used for the example cited above, would result in an overflow situation where all of the mercury in the capillary would be intruded into the sample.

Unfortunately, the development of these penetrometers has lead to new problems in performing the intrusion analyses. Since the penetrometer now has an increased sensitivity, effects which were insignificant with regular penetrometers are now major problems. These effects arise from incomplete filling of the penetrometer resulting in measurable "intrusion" as the pressure increases from 1 to 30 psia (175 um - 6 um) and high pressure compression which result in another measurable intrusion between approximately 2500 - 60,000 psia (0.07 - 0.03 um). Figure 2.19 depicts this behavior as the cumulative intrusion curve for a blank run (no sample) conducted with a high pressure penetrometer. This has the total effect of severely limiting the range of reliable measurements from about 30 psi to 1500 psi (6-0.12 um). Beyond this range, the observed intrusion will be compounded and absolute measurements should be suspect, although the approach could still be employed in a relative manner to examine significant differences in micro-pore structure.

2.3.4.1 Impedance Porosimetry

Previous research conducted at AECL in Chalk River[19] has led to the development of a novel approach for monitoring the filling of pores in micro-thin films. This technique involves the measurement of electrical impedance changes in a film as mercury is forced into the pores of the sample. Since the means of accurately measuring the mercury volume intruded has been the limiting factor for conventional porosimetry, this electrical approach solves this problem in an eloquent and extremely sensitive manner.

Figure 2.19 "Intrus rusion" Curve for Blank Run of
of High Precision Penetrometer

Preliminary investigations of this technique at ORF involved using a HP 4192A LF Impedance Analyzer coupled to platinum paste films screen printed on penetrometer caps. In the first series of tests, the Micromeritics Auto Pore was employed to generate mercury intrusion into the sample, however, problems were encountered in impedance reading stability (both resistive and capacitative components). This was thought to be caused by parallel circuit problems which resulted from using the instrument ground as a conducting media.

Further attempts were made to employ this technique by using an older Aminco 60,000 mercury porosimeter. This instrument offered the advantage of being able to electrically isolate the impedance measurement circuit. Unfortunately, the technique was still found to be quite unstable, possibly due to thermal effects in the hydraulic oil/mercury or the polarization of mercury.

Although the original work in this area examined the pore structure of insulating films (e.g. oxides), it was thought that the technique could be applied to conductive films as well, assuming that the conductivity of mercury was much greater than the conductivity of the film. Unfortunately, due to the stability problems described above, the technique could not be proven conclusively and further study in this area has been suspended.

2.3.5 Gas Adsorption

When a solid is exposed to a gas, the gas molecules will impinge upon its surface, and depending upon the nature of the solid and gas as well as the pressure and temperature, these molecules will have a finite residence time on the surface. This phenomenon is known as adsorption which differs from absorption in which the gas molecules are actually taken into the body of the solid.

By monitoring the volume of gas adsorbed on a surface against the adsorption pressure (relative to the saturation pressure of the gas), it is possible to construct an adsorption isotherm. Measuring the volume of gas adsorbed can be done by a number of conventional methods including ; 1) the mass change of the sample can be monitored (gravimetric determination), 2) the

pressure change of a closed system can be recorded (volumetric determination), or, 3) the amount of gas removed from a flowing stream can be detected (thermoelectric mass flow determination). In each case the measurement can provide one point on the adsorption isotherm which can be employed to reveal information regarding surface area, pore size distribution, and total pore volume.

The determination of surface area from adsorption isotherms has been examined extensively elsewhere [20] and a number of theoretical models currently exist for its evaluation. The most widely employed technique, however, is that known as multilayer adsorption originally proposed by Brunauer, Emmett, and Teller[21] and commonly referred to as the BET theory. Using this approach, it is possible to employ the linear portion of a Type II isotherm (0.05 - 0.35 P/Po, where Po is the saturation pressure) to obtain an estimate of the volume of gas needed to produce a monolayer coverage over the entire surface of the sample (i.e. surface area).

By measuring the total volume of gas adsorbed by the sample at a point slightly less than saturation pressure, the pore volume of a material can also be computed. In addition, by employing a modification of the Kelvin equation which relates relative pressure to the surface tension, contact angle, temperature and pore radius of gases as they condense in a cylindrical capillary, it is possible to compute a pore size distribution. (Incidentally, the Kelvin equation was the basis for Washburn's work on the theoretical model for mercury porosimetry).

The selection of adsorbing gas (adsorbate) will generally depend upon the nature of the solid (adsorbent) and the conditions one wishes to employ. A variety of gases have been employed over the years with mixed results. These include water vapour, n-butane, freon, toluene, benzene, ethyl iodide, n-hexane, xenon, and argon. The gases generally employed, however, are nitrogen and krypton.

Nitrogen adsorption has become the accepted standard for the measurement of surface with an absolute surface area greater than 5 m^2. This is most likely due to the accuracy by which the cross-sectional area of the nitrogen molecule is known (16.2 A) as well as the availability of liquid nitrogen which is used as a means of reducing the sample temperature (-196°C). This permits pore condensation which can be detected and plotted as an adsorption isotherm.

For materials with absolute surface areas less than 5 m^2, krypton is usually employed since it has a saturation pressure of about 2.3 mm Hg at -196°C. (Compared to 729 mm Hg for nitrogen at the same temperature). This minimizes what is known as the "dead space correction" in which the volume of the sample chamber can greatly influence the ability to obtain precise pressure differentials. One difficulty with using krypton, however, is that at liquid nitrogen temperatures, krypton solidifies (triple point = -157°C). This therefore prohibits its application as an adsorbate for pore volume or size distribution measurements.

Ontario Research currently employs a Micromeritics Orr Pore-Volume Surface-Area Analyzer Model 2100 for conducting standard gas adsorption studies. The unit is equipped with both krypton and nitrogen as adsorbates and employs a volumetric technique for measuring the volume of gas adsorbed on solid samples. The measurements are obtained by monitoring the pressure changes in an accurately known dead space, caused by the adsorption of gaseous molecules on a cooled sample surface. Pressure changes down to 10^{-4} Torr can be monitored by a capacitance transducer type barometer. This permits the measurement of samples with an absolute surface area of down to 0.1 m^2.

One difficulty with the commercial equipment employed at ORF is the design of the standard glass adsorption cells which were constructed mainly for the analysis of powders or solids with a greatest dimension of less than 5 mm. This arrangement does not permit the measurement of larger films (i.e. 1" diameter), therefore a series of special sample cells were constructed. These involved using a ground glass conical joint seal with an internal dimension of approximately 30 mm. This custom designed cell is capable of

handling a multitude of thin films (up to approximately 10 cm in stacked height) with a diameter of approximately 25 mm. This allows for the absolute surface area to be increased into a measurable range for krypton analysis.

The one drawback to this system is that the effect of individual films (assuming an absolute area $<0.1\ m^2$) cannot be measured. This could be overcome with the design of a UHV system with small dead volume, more accurate pressure transducers, and possible change of adsorbate gas (i.e. xenon). The construction of this system was beyond the scope of this program, however, it should be seriously considered for future studies since it does provide a rapid and non-destructive technique for evaluating the physical morphology of thin films.

3. EXPERIMENTAL RESULTS ON THIN FILM MATERIALS

To study the feasibility of employing the characterization techniques discussed in Section 2, a number of films with various morphologies and compositions (including films prepared in different manners) were investigated. The first materials studied were platinum paste films since these are currently being used as electrodes in the fuel cell development effort at CANMET. Plasma spraying as a deposition method was examined by evaluating porous nickel films prepared by this process. Some preliminary analyses were also conducted on perovskite coatings (films) produced by the plasma spray technique. Finally, in an effort to standardize and correlate the analyses procedures, a number of controlled morphology silver membrane filters were investigated.

3.1 Platinum Paste Films

To date, fuel cell optimization studies at CANMET have been conducted exclusively with platinum as both the cathode and anode material, the majority of which are platinum pastes or inks developed by Engelhard.[22] As described previously, platinum was chosen since it displays good electro-catalytic properties with regard to the reactant gases for the fuel cell reaction.

Platinum inks and pastes are available in a wide variety of compositions and particle sizes. Special inks such as Englehard #6926 or A-4338 have been specifically developed for oxygen sensing applications when used in conjunction with zirconia electrolytes. These pastes have been designed primarily for brush applications but are certainly amenable to screen-printing. Screen-printing offers the advantages of controlled area application as well as uniformity in applied thickness and texture. Screen-printing also allows for the production of reproducible films with a defined morphological nature.

One current problem facing the development of electrode materials for use in the hydrogen exchanged solid-state fuel cell currently under development at CANMET, is the sensitivity of the electrolyte to temperatures

greater than approximately 150°C. This is believed to limit the performance of the platinum inks since they are designed primarily for high temperature applications and should be fired in excess of 800°C to realize their full conductivity and catalytic reaction activity.

Figures 3.1.1 and 3.1.2 are SEM photomicrographs of platinum paste #6926 which has been brush painted and cured at 500°C and 800°C respectively. In the latter case, the platinum particles have sintered together to form, on a microsopic scale, a highly porous and substantially interconnected metallic film.

On a macroscopic scale, however, the #6926 ink has a tendency to form isolated islands of film which severely affect the overall conductivity. Figures 3.1.3 and 3.1.4 show a 60% 6926 paste (40% toluene) which has been screen-printed on -alumina and then cured in air at 500°C and 800°C, respectively. Depending upon the film thickness, the degree of particle separation may become so great as to restrict all conductivity. This behaviour has also been observed when the 6926 paste was cured in hydrogen at a lower temperature (200°C). Figure 3.1.5 depicts such a film prepared and analyzed at CANMET.

SEM examination of the A-4338 pastes reveals an equally interesting change in film morphology on firing at various temperatures. Figures 3.1.6 and 3.1.7 show the A-4338 paste after screen printing on α-alumina and curing at 100°C and 800°C, respectively. Firing above 600°C appears to produce a highly irregular but porous film with good interconnectivity. This was further confirmed by two-point resistance measurements which showed a decrease in resistance from approximately 40 Ω/cm to 0.8 Ω/cm for the temperature curing range of 100°C to 800°C. Curing in hydrogen at 200°C also gives a film with good conductive properties and a relatively porous structure (Figure 3.1.8 from CANMET). The A-4338 ink is known to contain a finer grind of platinum particles (50% approx. 2-4 um) in comparison to the #6926 paste which is 50% approx. 12 um. This would most likely contribute significantly to the overall performance of the ink as a fuel cell electrode, particularly for low temperature applications.

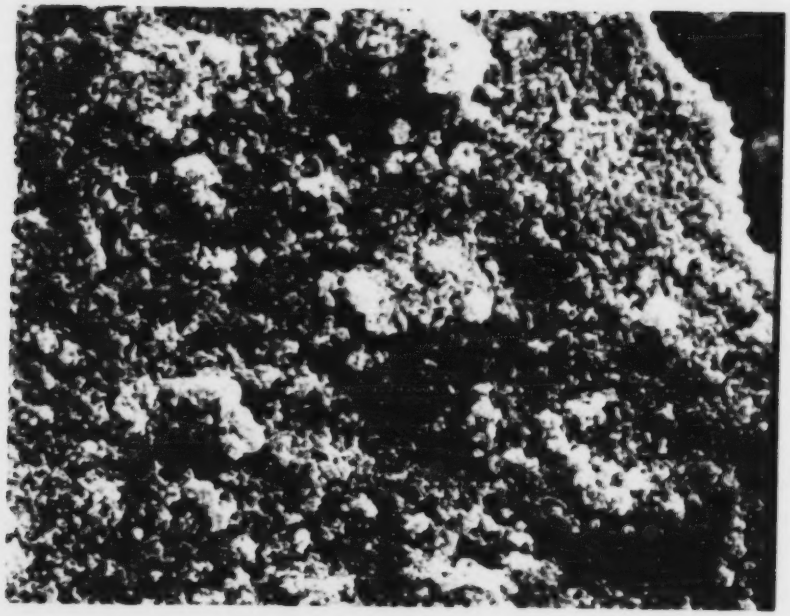

Figure 3.1.1 SEM Photomicrograph of #6926 Platinum Paste cured at 500°C (approx. 3000X)

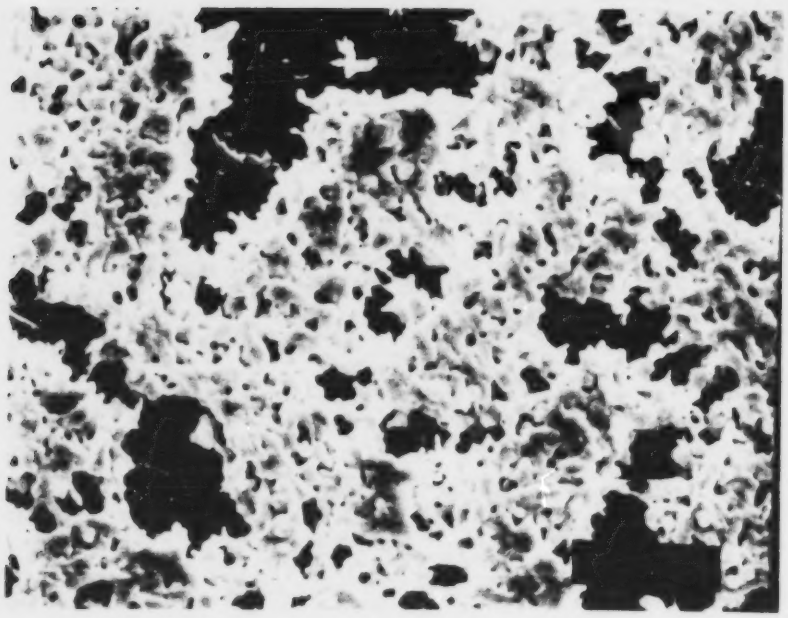

Figure 3.1.2 SEM Photomicrograph of #6926 Platinum Paste cured at 800°C (approx. 3000X)

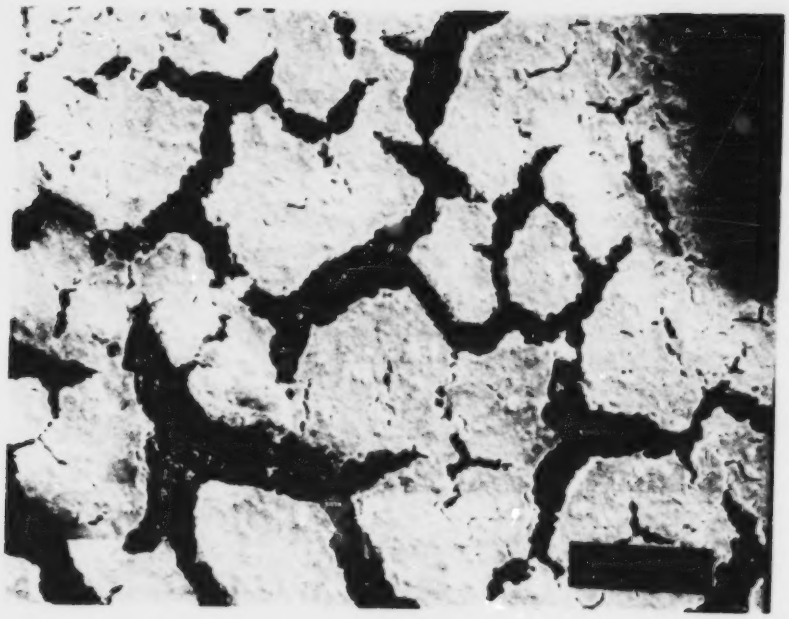

Figure 3.1.3 SEM Photomicrograph of #6926 Platinum Paste cured at 500°C (approximately 150X)

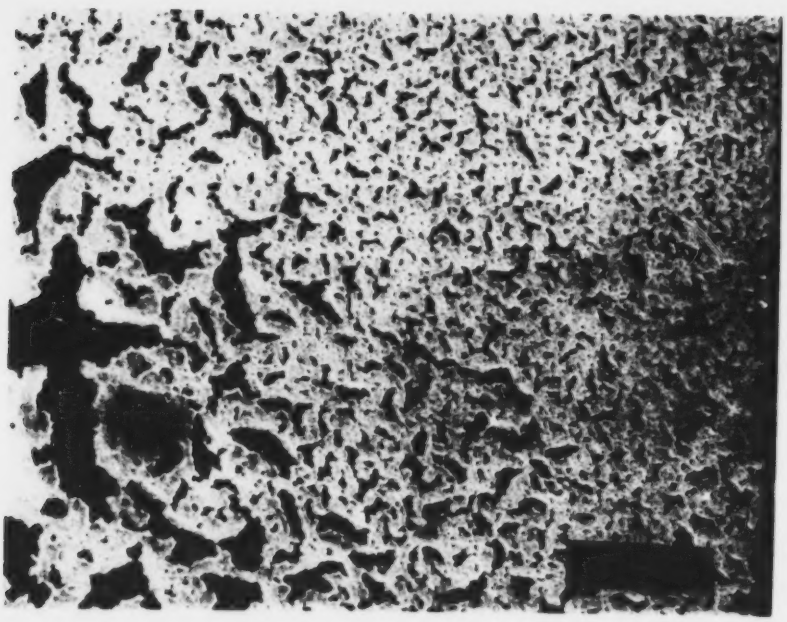

Figure 3.1.4 SEM Photomicrograph of #6926 Platinum Paste cured at 800°C (approximately 150X)

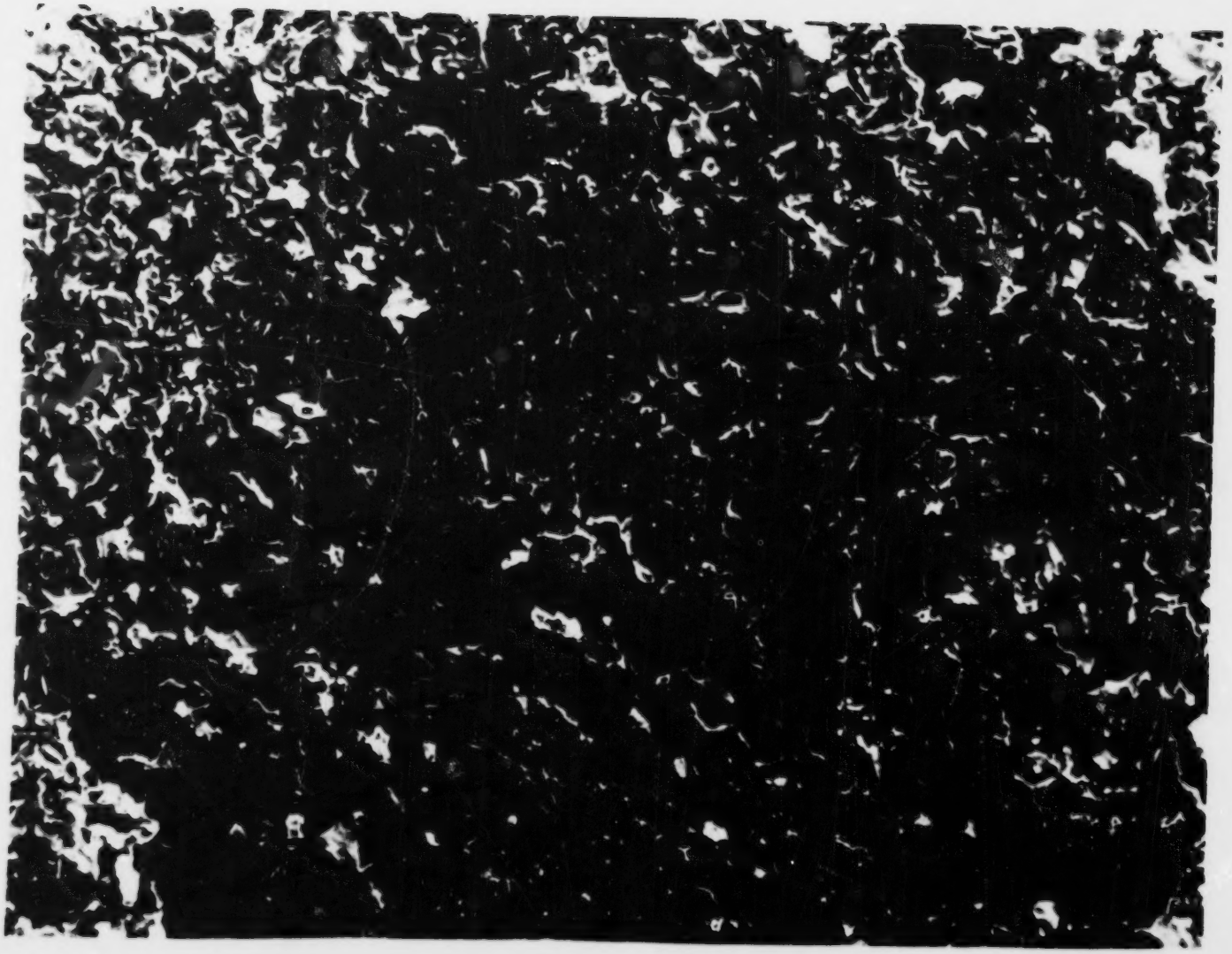

Figure 3.1.5 CANMET SEM Micrograph of #6926 Pt Paste Cured at 200°C in Hydrogen (450X)

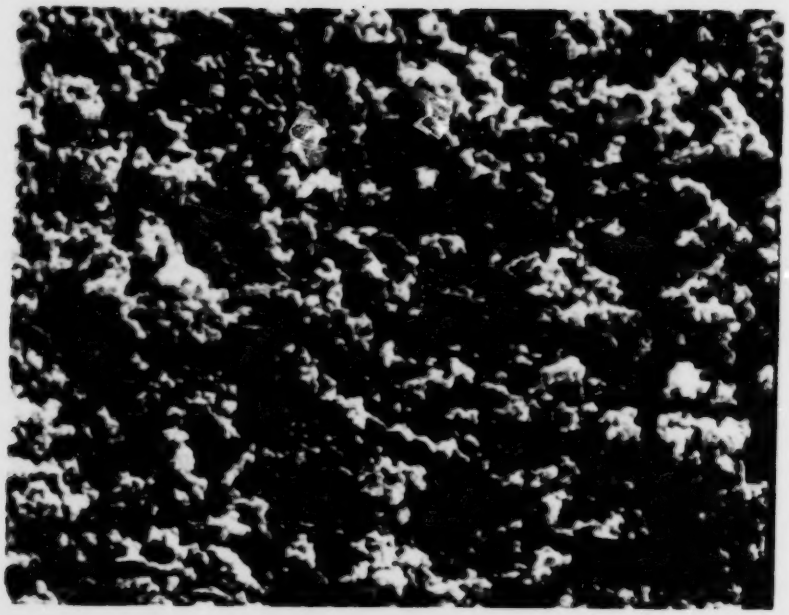

Figure 3.1.6 SEM Photomicrograph of A-4338 Platinum Paste cured at 100°C (approximately 6200X)

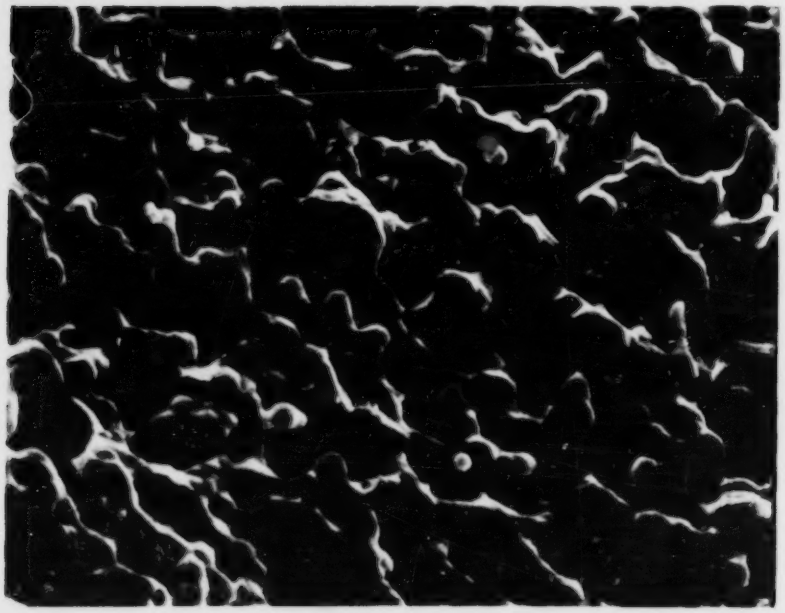

Figure 3.1.7 SEM Photomicrograph of A-4338 Platinum Paste cured at 800°C (approximately 5800X)

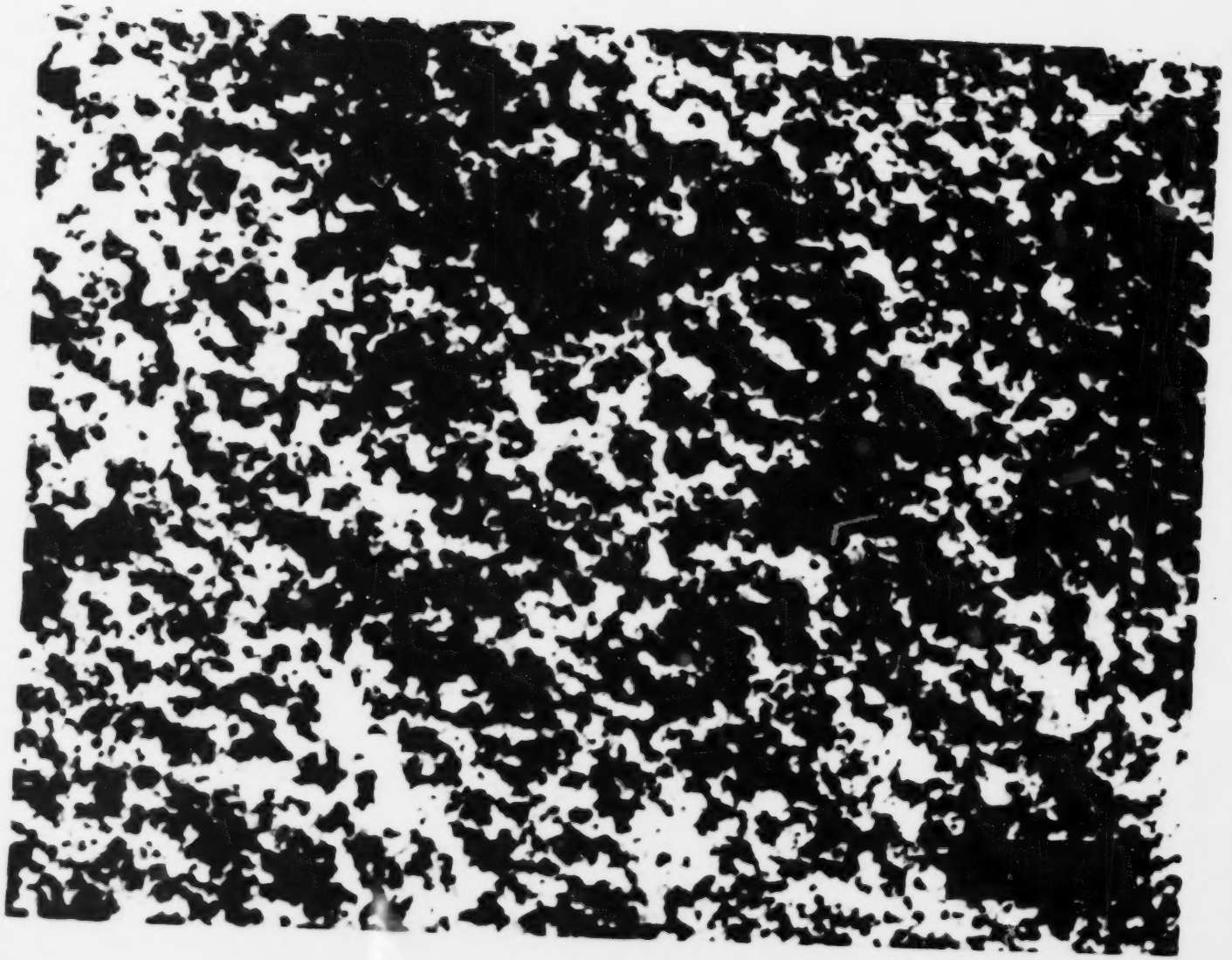

Figure 3.1.5 CANMET SEM Micrograph of A-4338 Pt Paste Cured at 200°C in Hydrogen (4800X)

3.1.1 Image Analysis of Platinum Paste Films

From Figure 3.1.8, it can be seen that any pores which do exist within the platinum paste film are most likely sub-micron in nature (particularly for those films cured at <600°C). Due to the fine nature of these pores, regular epoxy mounting and polishing was unsuccessful in producing a cross-sectioned plane which had sufficient contrast between pores and particles. Viewed under the SEM, the polished samples appeared blurred and smeared such that no pore structure could be measured quantitatively (see Figure 3.1.9).

In an effort to increase the contrast between particles and pores in the platinum film, the vacuum impregnation technique described in Section 2.3.1.4 was employed. Unfortunately, this did not result in any significant improvement for feature identification when viewed under the SEM. This could be due in part to the spatial resolution of the SEM which makes it difficult to develop sufficient contrast between polished platinum particles suspended in a predominantly platinum background.

Examination of the polished paste under an optical microscope, however, revealed that some platinum particles were indeed being polished to such a degree that they reflected light very efficiently. Figure 3.1.10 shows an optical photomicrograph of a polished A-4338 platinum paste at approximately 500 magnification. If it is assumed that the reflecting particles (white phase) are representative of the platinum particles in the paste on one plane, then it is possible to conduct a standard image analysis investigation of the cross-sectional area to evaluate porosity, pore and particle size, as well as three-phase line.

Table 3.1.1 lists the standard morphological parameters for the platinum paste film measured by a variety of image analysis techniques (see Section 2.3.1). From these results, it appears that the platinum paste/film has an average particle size around 2.3 um, which is consistent with the manufacturers claim of an average fineness of between 2-4 um. This analysis also suggests that the average porosity is approximately 70% with a

Figure 3.1.9 Photomicrograph of Reverse Epoxy Polished Platinum Paste

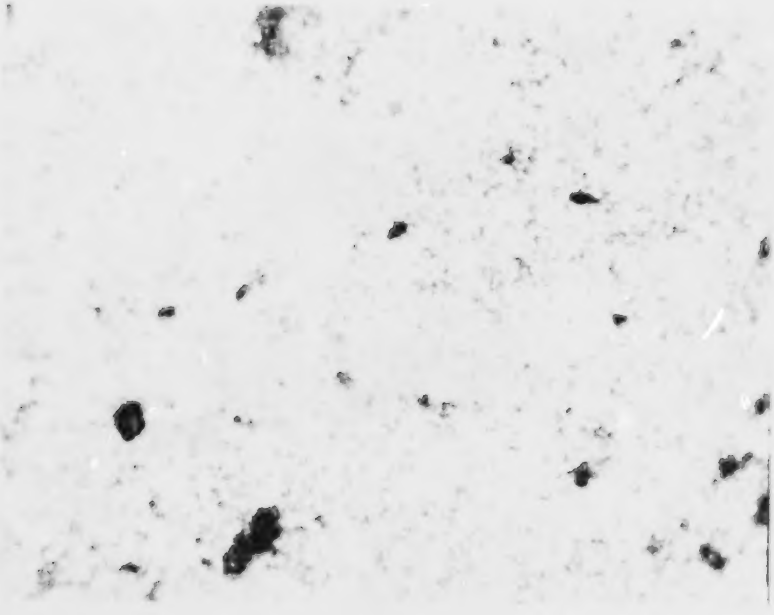

Figure 3.1.10 Optical Photomicrograph of Vacuum Impregnated, Polished A-4338 Platinum Paste (approx. 500X)

Table 3.1.1

Morphological Parameters for Platinum Paste A-4338
Derived from Image Analysis

Image Analysis Technique	Morphological Descriptor			
	Particle Diameter (μm)	Pore Diameter (μm)	% Porosity	Three-Phase Line (cm/cm^2)
Line Scan (Area)	2.5	-	65 (1)	5500 (250)
Lineal	2.2	5.3	72	-
MCD	2.3	3.4	-	-

three-phase line estimate of approximately 5500 cm/cm^2. These values, however, are somewhat limited by the optical resolution of the microscope employed (approximately 0.34 um @ 500X) and should be considered relative to the magnification used.

3.1.2 Profilometry of Platinum Paste Films

Preliminary profilometry work on the platinum films began by examining the surface texture of Engelhard ink #6926. Following examination under SEM (Section 3.1) it was revealed that the bulk morphology of the films appeared to change with increasing firing temperature. To quantify this effect, small strips, approximately 3 mm x 15 mm were screen-printed on a-alumina substrates using the #6926 ink which had been diluted 3:2 with toluene (40%). The test specimens were cured in air at various temperatures ranging from ambient (22°C) to 800°C.

The surface textures of these films were measured together with their average thicknesses, the results of which are presented in Table 3.1.2. From the Ra values, it is apparent that there is a significant increase in roughness with increasing temperature. There also appears to be a striking change in film thickness for those pastes cured at > 400°C.

These effects agree fairly well with the SEM observations which show the formation of a metallic coating for temperatures greater than 600°C. As the individual platinum particles sinter together to form interconnected islands, the porosity increases (thereby "roughening" the film) while the thickness decreases.

Since platinum inks are currently being employed for electrodes in fuel cell research at CANMET, it was decided to investigate the physical differences between films prepared with A-4338 by either hand-painting or screen-printing. Four preparative methods were employed;

Table 3.1.2

Surface Texture vs Curing Temperature for Pt Paste (#6926)

Curing Temp (^{o}C)	Unfiltered, Skidless, 10 mm Scan Length		
	Ra (μm)	Ra (μm)	Thickness (μm)
Room	5.2	6.4	42
100	5.4	7.2	41
200	5.8	7.2	44
400	7.1	8.7	41
600	9.2	11.5	30
800	9.3	10.8	30

1) Screen-printing and curing at room temperature (22°C)
2) Screen-printing and curing at 100°C in air
3) Hand-painting and curing at room temperature (22°C)
4) Hand-painting and curing at 100°C in air.

Table 3.1.3 lists the average (and standard error) for a few of the surface texture parameters measured. It appears that screen-printing has a tendency to coarsen the surface roughness (Ra) of the platinum ink coatings and increase the mean spacing (Sm). This may be due, in part, to partial replication of the screen mesh pattern (400M or approximately 38 um opening) to the deposited film. Table 3.1.3 also shows that, the inks cured at 100°C seem to have a slightly rougher texture.

One of the anticipated benefits of employing a screen printing technique for preparing electrode materials is that of sample reproducibility and overall uniformity. Table 3.1.4 shows the variations in film thickness with preparation method. Figures 3.1.11 and 3.1.12 show a typical scan length profile for each of the two methods employed (screen-printing vs hand-painting). From these results, it is obvious that hand-painting produces very irregular films with large deviations in film thickness, while screen-printing provides relatively consistent films of nearly uniform thickness.

During these analyses, it was noted that screen-printed films did not lose as much weight in drying as did the hand-painted films (see Table 3.1.4). As expected, curing at 100°C tends to reduce the weight of the films (both screen-printed and hand-painted), however, there appears to be an approximate 7% difference in the percentage weight loss between the screen-printed and hand-painted films. This effect may be due, in part, to the formation of a surface liquid as a result of the high shear action generated when "smoothing" hand-painted films. During drying (curing), this surface liquid would be evaporated thereby producing a lighter film. This

Table 3.1.3

Surface Texture Parameters for Platinum Paste Films
Phase Corrected, 0.8 mm, Skidless

Sample/Method	Ra (μm)	Sm (μm)	Δq (deg)
1) Screen-Printed Rm Temp Curing	0.66 (11)	54(9)	6.1(0.5)
2) Screen-Printed 100° Curing	0.79 (12)	56(11)	7.2(0.4)
3) Hand-Painted Rm Temp Curing	0.45 (4)	39(3)	5.8(0.4)
4) Hand-Painted 100°C Curing	0.59 (6)	38(4)	7.8(0.4)

Table 3.1.4

Comparison of Screen Printed and Hand Painted Pt Paste Films

Preparation	Sample	Wt Loss (%) on drying	Min-Max Thickness (μm)	Avg Thickness (μm)
Screen-Printed Room Temp (22°C)	1	13.4	10 - 16	12.6
	2	12.8	10 - 16	13.6
	3	15.9	11 - 17	12.1
	4	12.9	11 - 14	13.0
		12.8	6 - 12	9.7
	Avg	13.6 (1.3)	-	12.2 (1.5)
Screen-Printed 100°C	6	16.4	8 - 12	9.8
	7	14.8	11 - 18	13.9
	8	14.8	11 - 15	12.7
	9	14.4	12 - 16	13.5
	10	14.8	10 - 14	12.4
	Avg	15.0 (0.8)	-	12.5 (1.6)
Hand-Painted Room Temp (22°C)	13	20.8	10 - 28	15.0
	14	19.6	6 - 15	10.0
	15	21.6	6 - 22	12.4
	Avg	20.7 (1.0)	-	12.5
Hand-Painted 100°C	16	21.9	6 - 29	14.4
	17	24.5	3 - 12	6.7
	18	20.8	2 - 10	5.5
	Avg	22.4 (1.9)	-	8.9 (4.8)

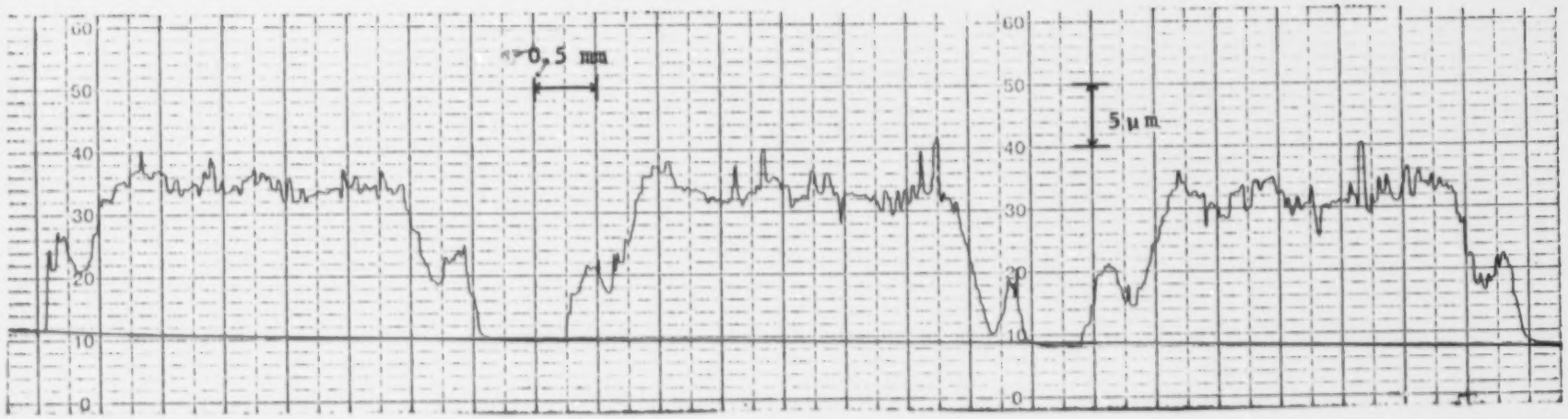

Figure 3.1.11 Profilometry Scan for Three Strips of Screen-Printed Platinum Paste (A-4338)

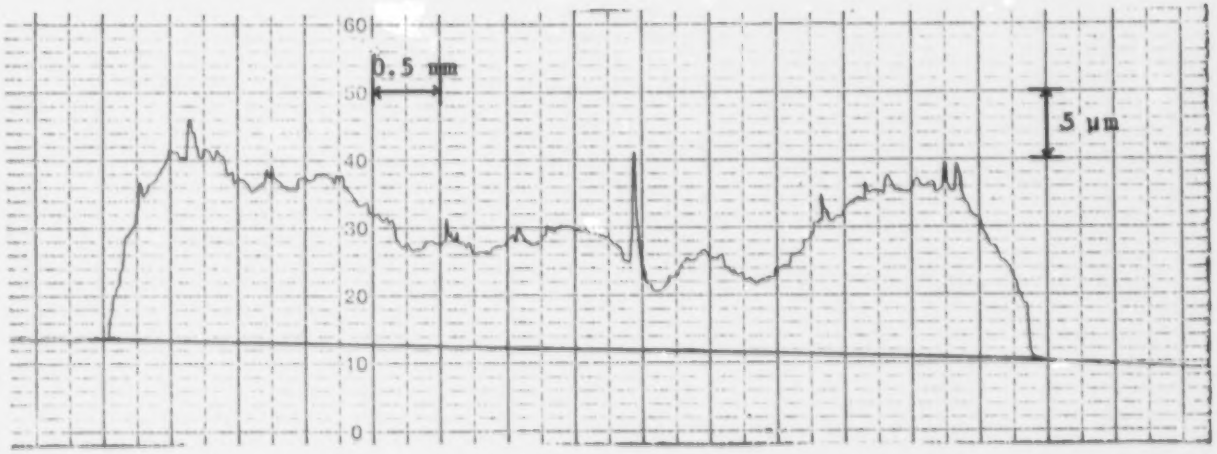

Figure 3.1.12 Profilometry Scan of Hand-Painted Platinum Paste (A-4338)

effect could have direct implications on bulk morphological properties of the film (e.g. bulk density, pore size, etc.) especially as the solvent "trapped" within the screen-printed films is forced to escape when curing at higher temperatures.

3.1.3 Permeametry of Platinum Paste Films

Permeametry or gas flow experiments were not conducted on platinum films due to the friability of the uncured pastes and problems associated with preparing the film on a well characterized porous substrate. The difficulty in this approach is that since the support must be porous, the liquid ink is expected to penetrate the surface pores to some degree thereby giving an inaccurate estimate of permeability.

3.1.4 Porosimetry of Platinum Paste Films

Due to the thin nature (approx. 10-20 um) of the platinum paste films, it was not possible to perform mercury porosimetry on these materials. Attempts could be made to increase the sample volume by repeated painting of the film, however the cost associated with such an analysis would be prohibitive.

3.1.5 Gas Adsorption of Platinum Paste Films

Attempts were made to measure the surface area of A-4338 platinum paste using the Micromeritics Orr Pore-Volume Surface Area Analyzer by increasing the absolute area present in the adsorption cell. Approximately 200 mm^2 of hand-painted A-4338 paste (on glass slides) was introduced into the customized large adsorption cell for krypton analysis. This corresponded to a total film mass of approximately 0.1 g.

Using this approach it was not possible to get an accurate reading of surface area. This therefore implies that the surface area of the film must be less than approx. 3 m^2/g in the uncured state (assuming a sensitivity of

0.01 m^2/g and a total weight (slide and film) of 30g). This would indicate that the unfired platinum film does not appear to have good catalytic properties, most likely due to the presence of organic binders, etc.

3.2 Plasma Sprayed Nickel Films

Preliminary studies began by examining the nature of films produced by a plasma spraying technique. As discussed in Section 2.2.2, plasma coatings are known to have a sandwich-like structure and, depending upon spray conditions, can have a variety of pore morphologies. Figures 3.2.1 and 3.2.2 show a cross-section of a plasma sprayed nickel coating (Ni powder 56C supplied by Metco[23]) prepared under two different conditions. In Figure 3.2.1 the coating was sprayed using an Ar/H_2 plasma (Ar; 100 psi @ 89 ft^3/hr, H2; 50 psi @ 10ft^3/hr) with a power setting of 60V and 500A. The powder flow was 6 kg/hr and the working distance was 6". The coating in figure 3.2.2 was sprayed under identical conditions except that the plasma current was reduced to 300 A (thereby decreasing the plasma temperature) and the working distance was increased to 10".

From these figures, it is obvious that there is an apparent increase in total "porosity" caused by decreasing plasma current and increasing working distance. It is interesting to note the nature of the features which are interpreted as "pores" in both of these coatings. Although both films contain a significant number of "large" cavities which actually are pores, the majority of features are long and thin and appear perpendicular to the spray direction.

These structures are most likely due to the formation of metal oxides which are produced on the surface of a molten droplet as it passes through the air. Upon impact, the droplet splatters to form long, thin oxides, commonly referred to as "stringers". Unfortunately, true pores of this shape can also be formed during the film deposition and distinguishing between these features by conventional examination (SEM or optical) can be extremely difficult if not

Figure 3.2.1 SEM Photomicrograph of Cross-Sectioned Ni Plasma Sprayed Coating (T = 500 A, WD = 6") Mag approx. 325X

Figure 3.2.2 SEM Photomicrograph of Cross Sectioned Ni Plasma Sprayed Coating (T = [illegible], WD = 10") Mag approx. 325X

impossible. Figures 3.2.3 and 3.2.4 show the nature of these laminate structures in more detail. This confirms the sandwich-like structure of these plasma sprayed films.

The ability to produce porous coatings using the plasma spray technique has led to its application for the fabrication of electrodes for electrochemical devices. Previous research conducted at Queen's University under DSS contract number 21ST.23440-4-9204 has indicated that plasma spraying of molybdenum on Na -alumina is a suitable technique for producing electrodes. Other studies at the Technical University of Nova Scotia (TUNS) have also shown that perovskite powders can be successfully plasma sprayed on nickel mesh to produce electrodes for electrolyzer applications. Based upon these results, it was decided to pursue the characterization of plasma sprayed materials in an attempt to better understand their physical morphology which may, in turn, be related to electrochemical behavior.

To study the effect of spray conditions (e.g. plasma power and/or working distance) and film thickness on reproducibility, a number of plasma coatings were prepared both in a supported and unsupported fashion.

The supported films were prpeared at TUNS by spraying Metco powder 56C (nickel) on galvanized steel disks approximately 1" in diameter. The plasma conditions at powder flow were identical to those described earlier (Ar; 100 psi @ 89 ft^3/hr, H^2; 50 psi @ 10 ft 3/hr, 60V, powder flow = 6 kg/hr). The plasma current and working distance were then varied to produce 7 coatings for each setting. The settings chosen were; Set 1) 500A, 6", Set 2) 300A, 6", and Set 3) 300A, 10". The thickness of these films as measured by optical microscopy ranges from 0.27 mm to 0.30 mm.

The unsupported films were prepared primarily for permeability measurements in which a free standing film was necessary to remove any substrate effects on gas flow. These films were prepared at the Ontario Research plasma spray facility by attempting to duplicate the plasma conditions and powder flow employed for the supported films produced at TUNS. The substrates employed, however, were - alumnina disks approximately 1" in

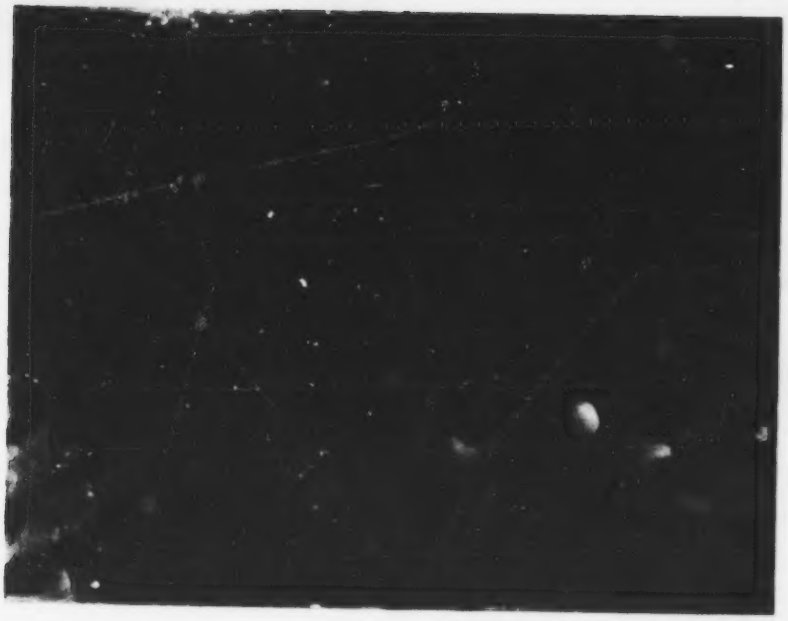

Figure 3.2.3 Detailed SEM Photomicrograph of Laminate Structures in Ni Plasma Sprayed Coating (I = 300 A, WD = 6") Mag approx. 3100X

Figure 3.2.4 Detailed SEM Laminate Structures in Ni Plasma Sprayed Coating (I = 300 A, WD = 10") Mag approx. 6900X

diameter. Previous experimentation at TUNS indicated that if the α-alumina disks were roughened by grit blasting and preheated to remove excess and adsorbed moisture, then nickel could be bonded in a reasonable fashion to the ceramic substrate. If, however, the substrate was not pre-treated (both roughening and heating) then the plasma coatings did not display good bonding characteristics and could be easily removed. Figure 3.2.5 shows a SEM micrograph of a cross sectioned portion of a nickel coated alumina substrate which depicts the poor bonding usually associated with ceramic/metal interfaces. (In most industrial applications, a bond coat is used to cushion the thermal coefficient difference between coatings and substrates which generally causes this poor bonding effect).

Using this technique (e.g. non-treated -alumina substrates), a number of unsupported films of various thicknesses were prepared by increasing the number of passes of spray using a plasma current of 500A and a 6" working distance. Three sets were prepared as follows; Set 1) (1 x double pass), Set 2) (2 x double pass), and Set 3) (3 x double pass). Since each set varies only by the number of double passes, then thicknesses (and hence weights) are expected to increase proportionately. Due to problems in keeping thicker films bonded to the substrate for the period of time to complete all the required passes, the number of suitable samples decreases with the number of passes employed. For this study, 6 specimens of Set 1), 5 specimens of Set 2), and 2 specimens of Set 3), were found acceptable for in-depth analyses. The averaged thicknesses of these unsupported films, as measured by optical microscopy, are: set 1) 0.11 mm, set 2) 0.21 mm, set 3) 0.30 mm.

The analyses conducted on both the supported and unsupported films are described in the following sections.

3.2.1. Image Analysis of Ni Plasma Films

In the cross-sectional examination of thin films, there are two planes commonly employed, thickness and rea sections. Figures 3.2.1 to 3.2.4 are examples of thickness sections which are generally employed to assess both porosity and interfacial bonding. Although some information on pore structure

Figure 3.2.5 SEM Micrograph of Ceramic (Alumina)/ Metal (Nickel) Interface with no Bond Coat (Mag approx. 6000X)

can also be generated from the examination of these sections, it is felt that for porous electrode applications, where the gas flow is parallel to the thickness axis, areal cross-sections may be more indicative of the pores by which the gas molecules must travel. In each case, however, it must be noted that the true pore morphology and degree of tortuosity can only be given by a three dimensional assessment of the complete pore network.

3.2.1.1 Supported Films

A sample from each set of spray conditions evaluated was selected and vacuum impregnated, pressure cured, area cross-sectioned and polished, and examined with the optical microscope. Figures 3.2.6 to 3.2.8 show typical optical photomicrographs for each sample analyzed. As discussed earlier, the dark phase is a combination of true pores and metal oxide laminates. Close examination reveals that the pores, oxides, and metal are very irregular in shape, indicative of the random nature of the plasma spray process.

It can also be observed that as the plasma power is decreased and the spraying distance increased, there appears to be an increase in the ability to discriminate more individual particles (white phase). In the latter case (i.e. Set 3, Figure 3.2.8), distinct "grain boundaries" and oxides are readily observable as heavy "swirls" which give rise to a very erratic structure.

As stated earlier, discrimination between the actual pores and oxides is extremely difficult, especially for optical photomicrographs where the depth of field is relatively limited. When attempting an automated measurement technique, such as image analysis, this discrimination is complicated in that only grey level separation can be achieved. One possible alternative would be to employ a shape selection criteria which would preclude the "stringers" from being analyzed. Unfortunately, this can only be accomplished using the line scan logic for pore diameters which would severely limit the range of parameters measured. It was therefore decided to analyze the entire dark phase to make relative assessments regarding the changes in

Figure 3.2.6 Optical Photomicrograph of Impregnated Polished Plasma Spraved Supported Nickel Film for Set 1 (500A, 6") Mag. approx. 100X

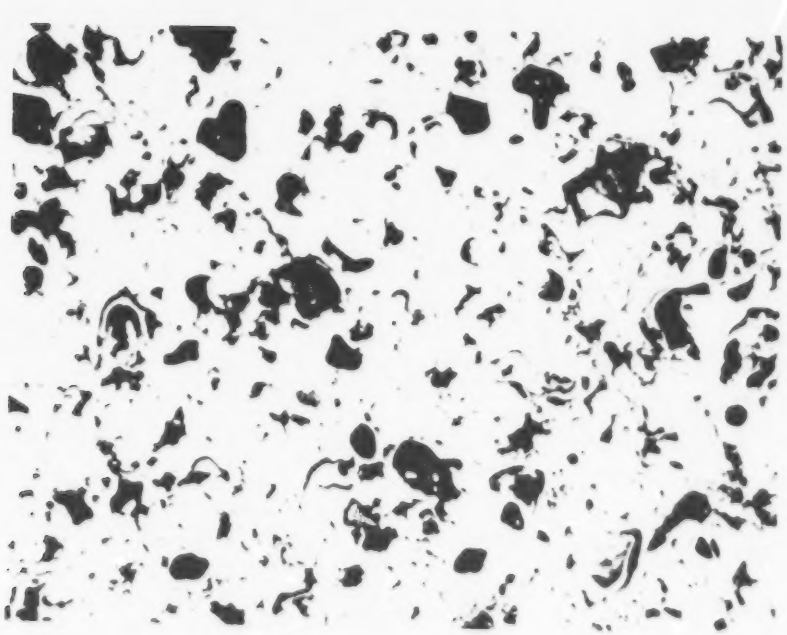

Figure 3.2.7 Optical Photomicrograph of Impregnated Polished Plasma Spraved Supported Nickel Film for Set 2 (300A, 6") Mag. approx. 100X

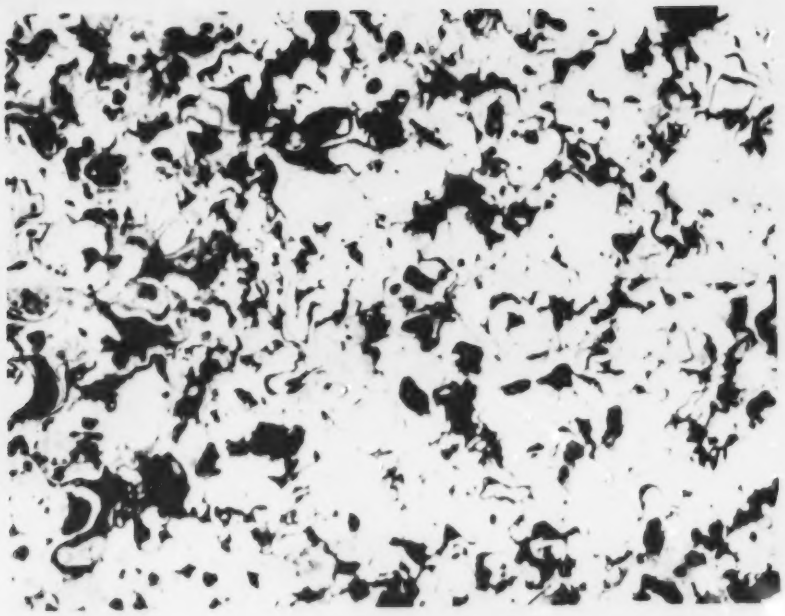

Figure 3.2.8 Optical Photomicrograph of Impregnated/Polished Plasma Sprayed Supported Nickel Film for Set 3 (300A, 10") Mag approx. 100X

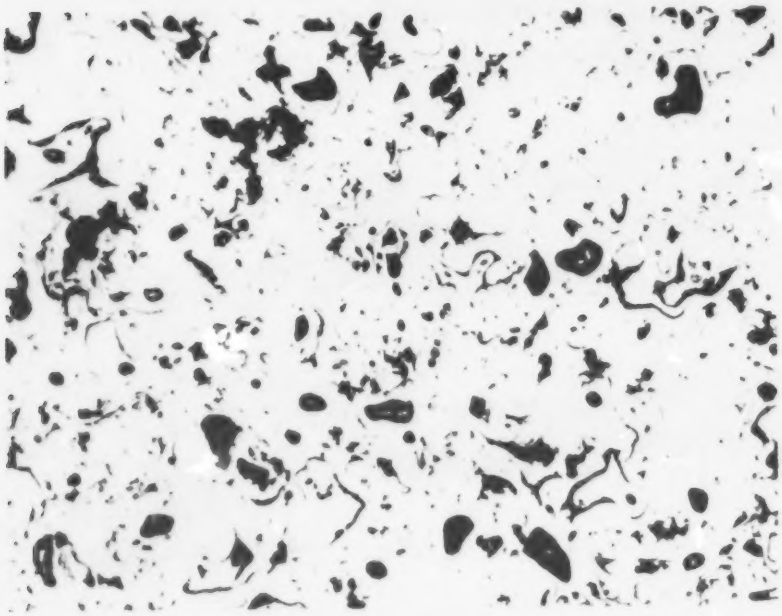

Figure 3.2.9 Optical Photomicrograph of Impregnated/Polished Plasma Sprayed Unsupported Nickel Film(1 x double pass @ 500A, 6") Mag = 100X

"pore" structure. For this reason, the values generated by image analysis are only internally consistent with the optical photomicrographs and should not be taken as absolute.

Quantitative assessment of the dark phase by image analysis reveals some interesting behavior. By examining several fields of view, it is possible to calculate the mean values of "pore" and/or particle size, as well as "porosity" and "three phase line estimates" based upon hundreds of component features. Table 3.2.1 gives these average values for the three sets of plasma films analyzed. From these results, it appears that as the "pore" diameter remains approximately the same, the particle diameter (or pore spacings) decreases which has the effect of increasing both "porosity" and "3-phase line estimates". This would indicate that when the molten or semi-molten particles which have a lower thermal mass (resulting from lower plasma power or enhanced cooling from increased spraying distances) impact on the substrate/film, the porosity of the resultant film increases. This would therefore provide some degree of flexibility in preparing porous plasma sprayed electrodes for gas flow electrochemical cell applications (i.e. fuel cells).

3.2.1.2 Unsupported Films

Figure 3.2.9 to 3.2.11 show the optical photomicrographs for a representative field of view on each sample analyzed from the three sets of unsupported films prepared at ORF. Qualitative assessment of these cross sections would indicate that they do indeed appear to be similar to the supported film of Set 1 which was produced using identical spray conditions (500A, 6" working distance). Numerical evaluation by image analysis, however, reveals that there is no obvious trend for relating the "porous" structure to film thickness. In fact, the reproducibility of the films, in general, becomes highly suspect. Table 3.2.2 lists the morphological descriptors calculated from an extensive image analysis investigation on these unsupported films. These results indictate that although the thinnest and thickest films (Set 1 and Set 3, respectively) show excellent agreement in all categories, Set 2 appears signiciantly different both in particle size and porosity.

Table 3.2.1

Morphological Properties via Image Analysis for Supported Plasma Sprayed Nickel Films

Sample	IA Technique	Morphological Descriptor			
		"Pore" Diameter(μm)	Particle Diameter(μm)	"% Porosity"	"3-Phase Line"(cm/cm^2)
Set 1 (500A, 6")	Line Scan (Area)	13.6	-	16.6(2.2)	360
#4	Lineal	16.4	73.8	17.3	-
	MCD	18.6	73.5	-	-
Set 2 (300A, 6")	Line Scan (Area)	13.6	-	19.7(2.2)	400
#3	Lineal	17.8	69.9	19.6	-
	MCD	21.4	65.5	-	-
Set 3 (300A, 10")	Line Scan (Area)	13.8	-	21.0(1.4)	450
#3	Lineal	15.6	58.1	20.5	-
	MCD	18.8	57.0	-	-

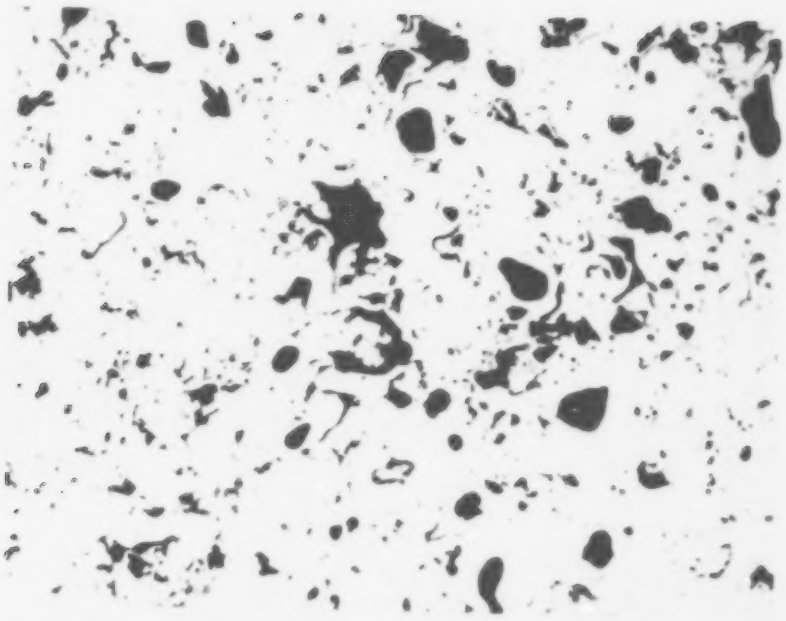

Figure 3.2.10 Optical Photomicrograph of Impregnated/Polished Plasma Sprayed Unsupported Nickel Film (2 x double pass @ 500A, 6") Mag - 100X

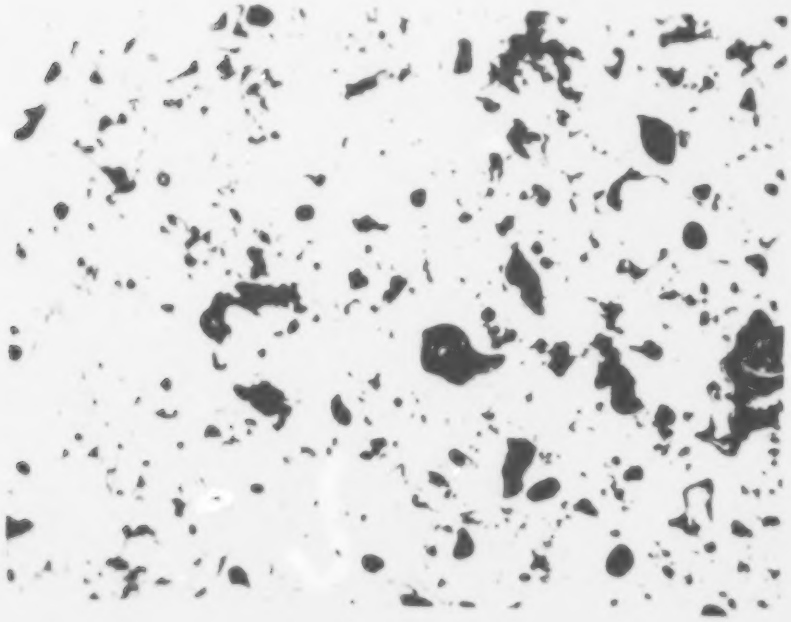

Figure 3.2.11 Optical Photomicrograph of Impregnated/Polished Plasma Sprayed Unsupported Nickel Film (3 x double pass @ 500A, 6") Mag - 100X

Comparison of the morphological values generated in Table 3.2.2 with those measured for Set 1 of the supported plasma sprayed films (see Table 3.2.1), also indicates a reasonable discrepancy, considering these films were sprayed under identical conditions. One possible explanation, however, is that these films were prepared at two different facilites (Supported-TUNS, Unsupported-ORF), both of which use different powder feed arrangements (fluidized bed vs gravity flow) and gun supports (hand held vs computer controlled). For these reasons, it is felt that accurate comparisons should only be assessed on samples which are internally consistent (i.e. prepared at the same site under the same conditions).

Overall, the image analysis results tend to indicate that there is a great degree of variability in producing films by plasma spraying that have a consistent morphology. Although there does appear to be some trends with regard to the effect of spray conditions on pore structure, the irregular nature of the films (both within the same film and between films) makes the current characterization of individual films by image analysis very problematic.

3.2.2 Profilometry of Nickel Plasma Films

3.2.2.1 Supported Films

Each of the seven supported films produced using the three sets of conditions described earlier were analyzed for surface texture by conducting five 1.25 mm traces using the Talysurf 6 profilometer while employing a skid arrangement and an ISO filter mode of 0.25 mm (see Section 2.3.2). Table 3.2.3 lists the measured roughness parameters and standard deviations for each sprayed disk (along with the film weight). Table 3.2.3 also includes a "best five" average after dropping high and low values for each value listed.

From the results generated in Table 3.2.3, it appears that as plasma current is decreased (from 500A to 300A), the surface roughness increases as expected. Unexpected, however, is the increase in film weight. One possible

Table 3.2.2

Morphological Properties via Image Analysis for Unsupported Plasma Sprayed Nickel Films

Sample	IA Technique	Morphological Descriptor			
		"Pore" Diameter(μm)	Particle Diameter(μm)	"% Porosity"	"3-Phase Line"(cm/cm^2)
Set 1 (1 x double pass)	Line Scan (Area)	11.7	-	20.6(4.4)	450(70)
	Lineal	14.9	54.0	21.0	-
	MCD	19.4	60.1	-	-
Set 2 (2 x double pass)	Line Scan (Area)	10.2	-	15.2(3.1)	420(70)
	Lineal	12.6	71.7	14.3	-
	MCD	16.1	66.5	-	-
Set 3 (3 x double pass)	Line Scan (Area)	12.1	-	20.6(5.1)	450(90)
	Lineal	14.9	53.9	20.9	-
	MCD	20.1	60.3	-	-

explanation is the variability in producing uniform films from a hand-held gun (Technical University of Nova Scotia). (This irreproducibility was also observed for nickel sprayed coatings prepared at ORF when weight deviations of approximately 0.1 g were noted). Another possible explanation, however, may be the partial melting of nickel particles suspended in a lower power plasma (i.e. lower temperature). As these particles strike the film/substrate surface they are bonded to each other at their outer molten surface yet retain a solidified component which gives rise to an increase in mass. At higher powers the entire powder may be molten and hence much better dispersed within the plasma spray such that finer droplets (i.e. smaller mass) impact on the substrate.

As spray distance is increased, these semi-molten particles have a better opportunity to cool and thereby avoid bonding to the substrate/film. This may result in less film deposition and therefore a lower film weight and a less rough surface as only smaller molten particles will be building up the film coating. Possible evidence for this effect may be observed as a decrease in film weight and surface roughness from Set 2 to Set 3. (Table 3.2.3).

3.2.2.2 Unsupported Films

The unsupported specimens described in Section 3.2 were measured for surface texture using the Talysurf 6 in a skidded, unfiltered mode with a scan length of 10 mm. The average values and standard deviations for five runs on each sample are given in Table 3.2.4. Due to the change in sampling mode and length, the surface texture values for the supported and unsupported films are not expected to agree. The values for the larger scan lengths (unsupported) are higher due to the effect of surface form as well as texture over the 10 mm trace.

From Table 3.2.4, it is shown that there is little difference between the surface texture of all three film types (within the standard deviations of the average values) which indicates that from a surface texture point of view, increasing the film thickness in a plasma spray operation has no effect on surface roughness.

Table 3.2.3

Surface Texture Measurements of Supported Nickel Plasma Films

Sample	Weight (g)	Surface Texture Parameters Skid, ISO 0.25 mm Ra (μm)	Sm (μm)	λq (μm)
Set 1 (500A, 6")				
1	0.76	6.9(1.4)	121(26)	103(21)
2	1.15^{+}	8.8(2.4)$^{+}$	147(31)$^{+}$	122(37)
3	1.00	6.1(1.1)	101(25)$^{-}$	94(14)
4	0.76	7.2(1.1)	119(22)	94(14)
5	0.54^{-}	6.6(0.6)	101(17)	92(14)
6	0.75	6.0(0.5)$^{-}$	110(9)	91(9)$^{-}$
7	0.64	7.6(0.9)	131(20)	111(10)
Avg (Minus Hi & Lo)	0.78(13)	6.9(0.6)	116(11)	99(8)
Set 2 (300A, 6")				
1	1.27	9.2(1.2)	149(23)	132(17)
2	1.32	8.9(1.2)	124(32)	127(18)
3	1.13	7.8(1.5)$^{-}$	139(37)	115(23)
4	1.12	8.4(1.3)	122(36)$^{-}$	109(15)$^{-}$
5	1.45^{+}	10.3(3.7)$^{+}$	201(61)$^{+}$	131(38)
6	1.39	10.1(1.4)	174(38)	159(11)$^{+}$
7	1.03^{-}	9.4(1.7)	156(37)	130(18)
Avg (Minus Hi & Lo)	1.25(12)	9.2(0.6)	148(19)	127(7)
Set 3 (300A, 10")				
1	0.59	9.5(1.0)$^{+}$	175(47)$^{+}$	131(11)$^{+}$
2	0.53	7.4(1.3)	133(18)	120(16)
3	0.69	7.2(0.5)	114(18)$^{-}$	108(9)
4	0.60	6.3(1.7)	118(43)	97(14)$^{-}$
5	0.84^{+}	7.7(1.3)	172(52)	109(17)
6	0.37^{-}	6.9(0.6)	133(41)	112(9)
7	0.75	7.0(2.0)	121(42)	111(20)
Avg (Minus Hi & Lo)	0.63(9)	7.2(0.3)	135(22)	112(5)

Table 3.2.4

Surface Texture Parameters for Unsupported Nickel Plasma Sprayed Coatings

	Unfiltered, Skidded, 10 mm Scan Length, Avg 5 Runs				
Sample	Ra (μm)	Rq (μm)	Sm (μm)	λq (μm)	Δq (deg)
1-1	16.9(4.9)	21.0(6.3)	295(73)	283(77)	25.1(0.9)
1-2	16.1(1.6)	20.0(2.0)	300(53)	259(24)	26.0(0.4)
1-3	15.5(2.0)	19.1(2.3)	284(57)	254(30)	25.5(0.8)
1-4	18.8(5.7)	23.5(6.7)	310(104)	305(82)	25.9(0.6)
1-5	13.2(0.9)	16.2(1.0)	232(28)	206(15)	26.4(0.4)
1-6	17.0(2.5)	20.8(2.9)	298(49)	263(31)	26.5(0.7)
Avg	16.3(1.9)	20.1(2.4)	287(28)	262(33)	25.9(0.5)
2-2	13.4(0.6)	16.8(0.7)	269(34)	229(7)	24.8(0.5)
2-3	14.6(1.8)	18.3(2.4)	255(50)	236(27)	26.1(0.6)
2-4	14.8(2.1)	18.6(2.6)	238(40)	242(39)	26.0(0.5)
2-5	16.3(3.0)	20.2(3.6)	282(60)	266(46)	25.7(0.6)
2-6	14.1(0.8)	17.7(0.9)	270(53	242(14)	25.5(0.9)
Avg	14.6(1.1)	18.3(1.3)	263(17)	242(14)	25.6(0.5)
3-1	15.0(1.1)	18.7(1.4)	284(36)	247(20)	25.6(0.4)
3-2	13.4(1.1)	16.8(1.4)	246(34)	226(22)	25.3(1.0)
Avg	14.2(1.1)	17.8(1.3)	263(30)	237(15)	25.4(0.2)

Spray Condition: 500A, 6"
Set 1 1 x double pass
Set 2 2 x double pass
Set 3 3 x double pass

Unsupported Films

3.2.2.2.1 Fractal Descriptors

The application of fractal descriptors for characterizing the physical nature of edges and surfaces is a relatively new approach first theorized in 1977 by Mandelbrot.[24] Since its inception, fractals have been employed to study gas adsorption [25], detection breakdown in insulators,[26] crack propogation[27] and interfaces in immiscible fluids[27, 28] to name a few. The majority of applications, however, have dealt with the characterization of physical profiles (either particle shape/ruggedness or surface texture).[29]

A fractal can be conceptualized as the fractional component of a feature which displays some properties of both 1 and 2, or 2 and 3 dimensions. As an example, consider a straight line which is known to have a fractal dimension of 1.000. As this line becomes more rugged and convoluted, its space filling ability (2 dimensional) increases such that its fractal dimension approaches 2 which is a flat plane (totally filled area). Profiles can therefore be treated as continuous lines, each of which will have its own unique fractal dimension.

There currently exists a number of methods for evaluating the fractal dimension of a profile. In most cases, the fractal is calculated from the slope of a Richardson plot, which is a logarithmic relationship between the length of the perimeter and the length of the "yardstick" by which it has been measured. This plot can be computed from values deduced by a random walk strategy, structured walk, or even a digital image analysis technique involving dilation logic developed by Flook.[30]

In the course of this program, a number of fractal analysis techniques were attempted to apply to the unsupported nickel plasma sprayed films. These involved a manual random walk strategy across the profiles output from the Talysurf 6 printer, a numerical random walk calculated with the individual profile points, and attempts at employing dilation logic with the LeMont OASYS image analyzer.

Figure 3.2.12 shows a portion of a typical profile for an unfiltered trace across an unsupported nickel plasma sprayed films. Using the random walk technique described by Kaye[29], it is possible to construct a Richardson plot of log P (perimeter estimate) versus log (normalized step length). Table 3.2.5 lists the fractal values (δ) measured by using step lengths of between 0.1 to 0.005 for one 10 mm trace from each unsupported film analyzed. Table 3.2.5 also lists the calculated surface texture parameters for each unique trace. These results indicate, that for these samples, there does not appear to be any correlation between fractal dimension and any of the three surface texture parameters, nor does there appear to be any significant difference between any of the three sets of film thicknesses based upon fractal descriptors.

In an effort to automate the extremely tedious and laborious task of computing the fractal descriptor based upon a manual random walk technique, a computer software program was written to solve for the fractal value numerically. Basically, any profile analyzed by the Talysurf 6 profilometer is broken into 1000 data points each of which represents an equally spaced horizontal point on the profile, corresponding to the vertical amplitude of the point.

A program was written in Pascal to operate on the Apple IIe computer (see Appendix B). The program follows the analogy of the manual random walk technique, however, it can operate down to a minimum spacing of 0.1% of total scan length thereby increasing the sensitivity of the approach. Unfortunately, it has not been possible, as yet, to interface the Talysurf 6 to the Apple IIe, therefore all data must be entered manually. For this reason, only one profile has been attempted (Set 2-No.4) for which the computer generated fractal value is 1.61 for step lengths from 0.1 to 0.002.

In another attempt to automate the fractal analysis procedure, the dilation logic developed by Flook and employed by Kaye[31] was assessed for its ability to generate fractal values. However, due to current limitations in the dilation/erosion logic of the ORF operated LeMont OASYS image analysis system, this approach could not be successfully implemented. As the LeMont

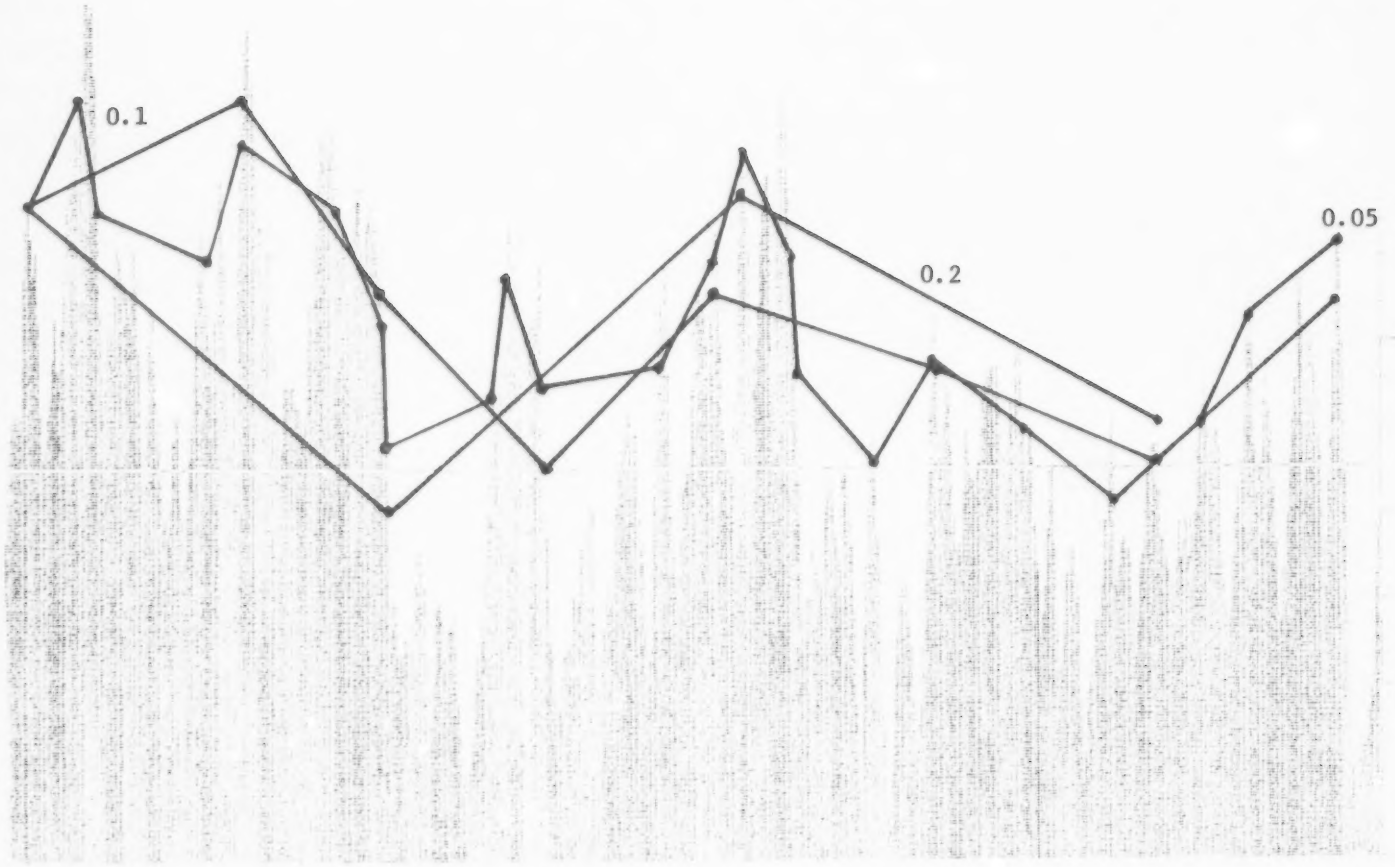

Figure 3.2.12 Manual Random Walk Strategy for Computing Fractal Dimension (Profile of Ni Plasma Sprayed Film)

Table 3.2.5

Comparison of Fractal Descriptors with

Surface Texture Parameters for Unsupported Nickel Plasma Sprayed Coatings

	Unfiltered Scan, 10.0 mm, Skidded, Individual Run			
Sample	δ	Ra (μm)	λq (μm)	Δq (deg)
Set 1-1	1.53	11.8	195	25.4
1-2	~ 1.51	15.3	253	25.3
1-3	1.64	15.4	244	26.3
1-4	1.45	14.6	257	25.4
1-5	1.66	12.0	198	25.7
1-6	1.56	17.3	227	25.8
Avg	1.56(8)	14.9(1.8)	196(87)	25.6(4)
Set 2-2	1.50	14.2	231	25.5
2-3	1.61	13.2	223	25.2
2-4	1.50	17.4	286	24.7
2-5	1.52	14.5	255	24.0
2-6	1.58	15.3	248	25.5
Avg	1.54(5)	14.9(1.6)	249(25)	25.0(6)
Set 3-1	1.59	14.1	234	25.2
3-2	1.54	13.9	231	25.6
Avg	1.57(4)	14.0(1)	233(3)	25.4(3)

Spray Conditions: 500A, 6"

Set 1 — 1 x double pass

Set 2 — 2 x double pass

Set 3 — 3 x double pass

software stands now, the degree of dilation/errosion is orientation dependent. This has the effect of adding too many pixels for features on the diagonals thereby giving over-exaggerated area determinations and poor Richardson fits. Discussions with LeMont personnel have indicated that they are aware of the problem and are working to implement a new erosion/dilation logic in the near future.

Based upon the results of Table 3.2.5, it is felt that although the fractal characterization of surfaces from profiles generated by profilometry is certainly novel and provides a new parameter for describing surfaces, this application of fractals does not give any more relevant information than a number or combinations of standard surface texture parameters computed by the Talysurf 6 system (see Appendix A). Fractals are therefore believed to be best applied to interfaces which cannot be measured by traditional techniques.

3.2.3 Permeametry of Ni Plasma Films

In a previous section (3.2), the preparation of unsupported plasma sprayed nickel films was discussed. It was pointed out that to conduct permeability measurements on porous films, it is necessary to either support the film on a well-characterized porous substrate whose pore morphology is significantly larger than the test film (to avoid the support becoming the restrictive flow component) or to analyze totally unsupported films.

In this program, permeability measurements were used to evaluate the reproducibility of preparing porous electrodes using a plasma spray technique as well as to define the effects of changing spray conditions (e.g. plasma power, working distance) on the overall pore morphology. These two conditions are extremely important when one is attempting to produce gas electrodes with identical and controlled morphologies.

3.2.3.1. Plasma Film Reproducibility

To study the similarity of films produced under identical conditions a number of porous nickel coatings were prepared by plasma spraying a

non-roughened, non-preheated alumina disk 25 mm in diameter at standard conditions of 500A and 6" spraying distance (See Section 3.2).

Figure 3.2.13 shows the observed flow/pressure curve for 6 films prepared by a single double pass of the automated spray gun. The film weights vary from 0.25g - 0.35g which may be related to the variability of the gravity feed flow system employed to introduce the nickel powder into the plasma. It is interesting to note, however, that the resistance to flow does not vary, in all cases with weight change (and therefore thickness). This would indicate that a unique pore structure may be generated for each film. This behaviour may be expected since plasma spraying is a truly random process and the build-up of a film is determined by a variety of complex variables (e.g. powder size, flow, plasma temperature, position, etc.).

Figure 3.2.14 shows the curves generated by the 6 films prepared by two-double passes using the same conditions as for the single pass samples. This corresponds to an approximate doubling of film weight (0.58 to 0.72g). This increase in film weight and thus the thickness significantly affects the flow characteristics by decreasing the flow rate by almost an order of magnitude. Once again, the flow behavior is very erratic which indicates random and unique pore morphologies.

Figure 3.2.15 depicts the flow curves for the 2 samples prepared by a 3 double pass spray. The variation in flow behavior is also evident even at these lower flow rates. Table 3.2.6 gives the slope of the lines determined in Figures 3.2.13-15 along with the sample identification and film weight.

These three sets of data indicate that, as expected, when the thickness of the film is increased there is a significant decrease in gas flow through the material. It does appear, however, that plasma spraying, although capable of producing porous electrode materials, is not a technique by which one can satisfactorily predict the true pore morphology of the resultant film. It is suspected that a more in-depth statistical analysis using many

Table 3.2.6

Gas Flow/Pressure Slopes for Unsupported Nickel Plasma Sprayed Films

Sample I.D.		Weight (g)	Slope (Q/P) (ℓ/min.psi)
Set 1	1	0.25	0.182
	2	0.34	0.123
	3	0.32	0.174
	4	0.32	0.165
	5	0.34	0.143
	6	0.35	0.149
Set 2	1	0.66	0.020
	2	0.67	0.016
	3	0.67	0.025
	4	0.69	0.016
	5	0.58	0.022
	6	0.72	0.011
Set 3	1	1.02	0.011
	2	1.08	0.010

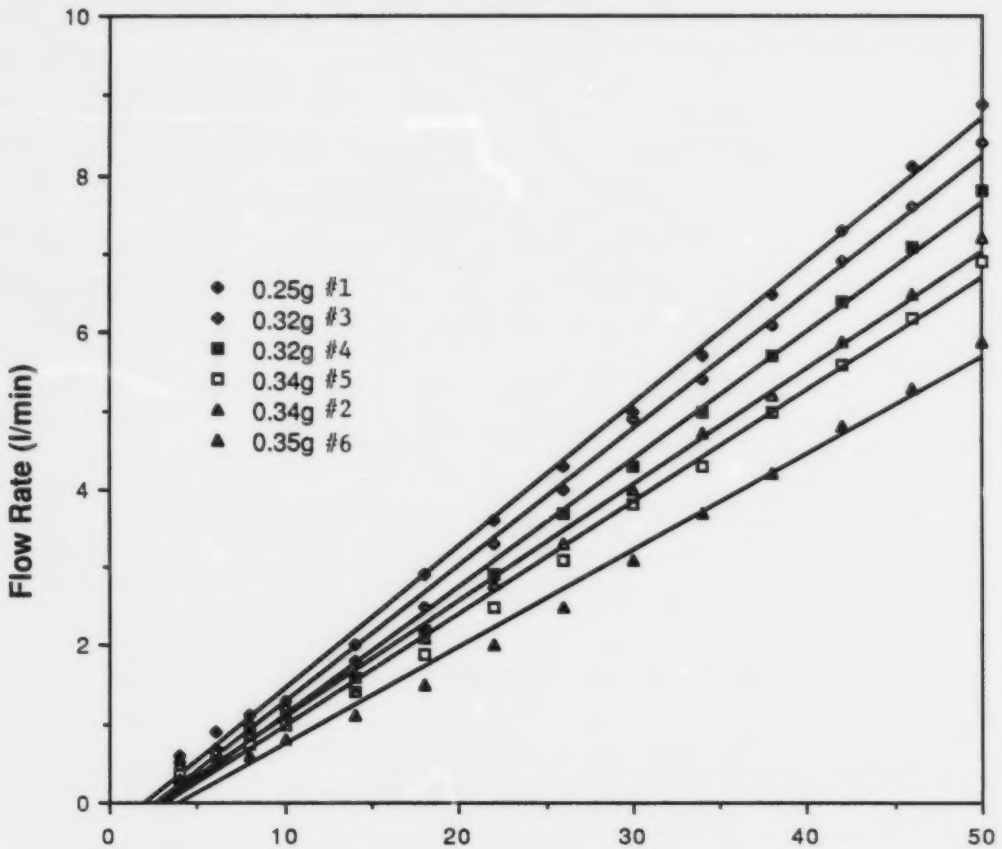

Figure

Figure 3.2.13 Permeability Measurements of Set 1 (Single Pass) Nickel Plasma Sprayed Films

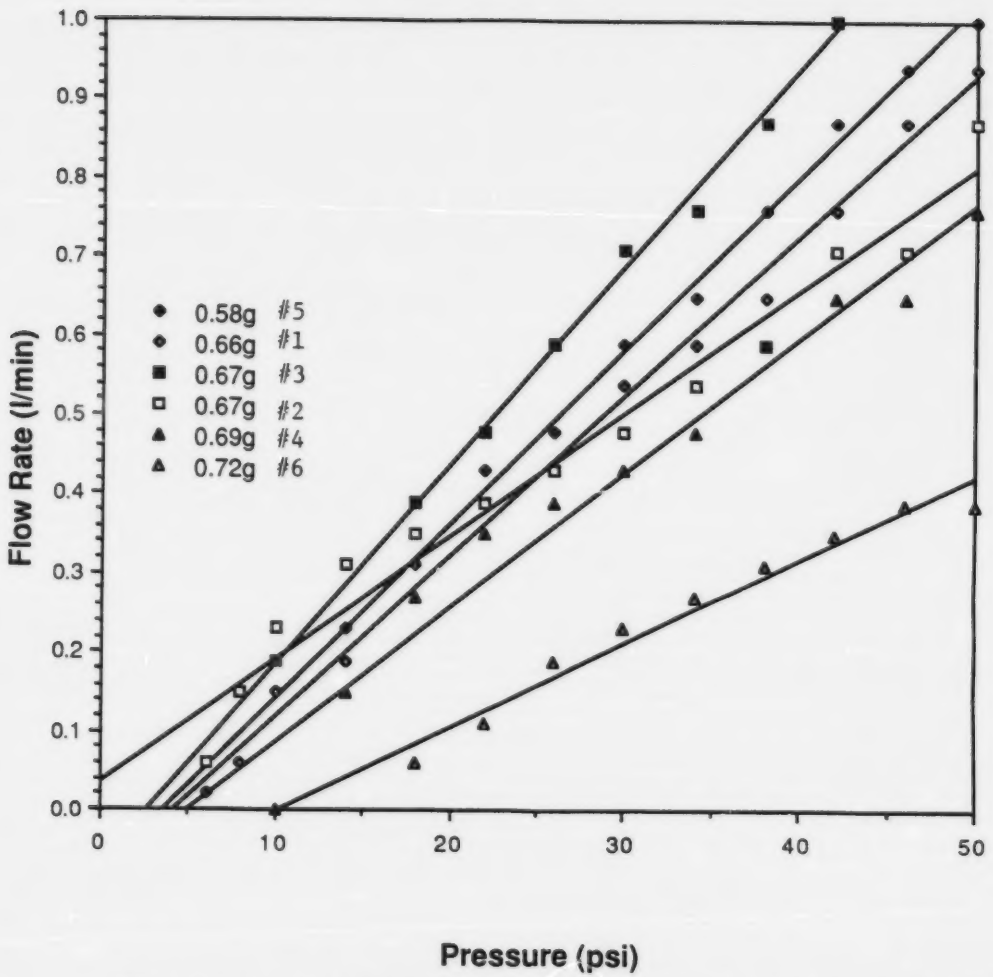

Figure 3.2.14 Permeability Measurements of Set 2 (Double Pass) Nickel Plasma Sprayed Films

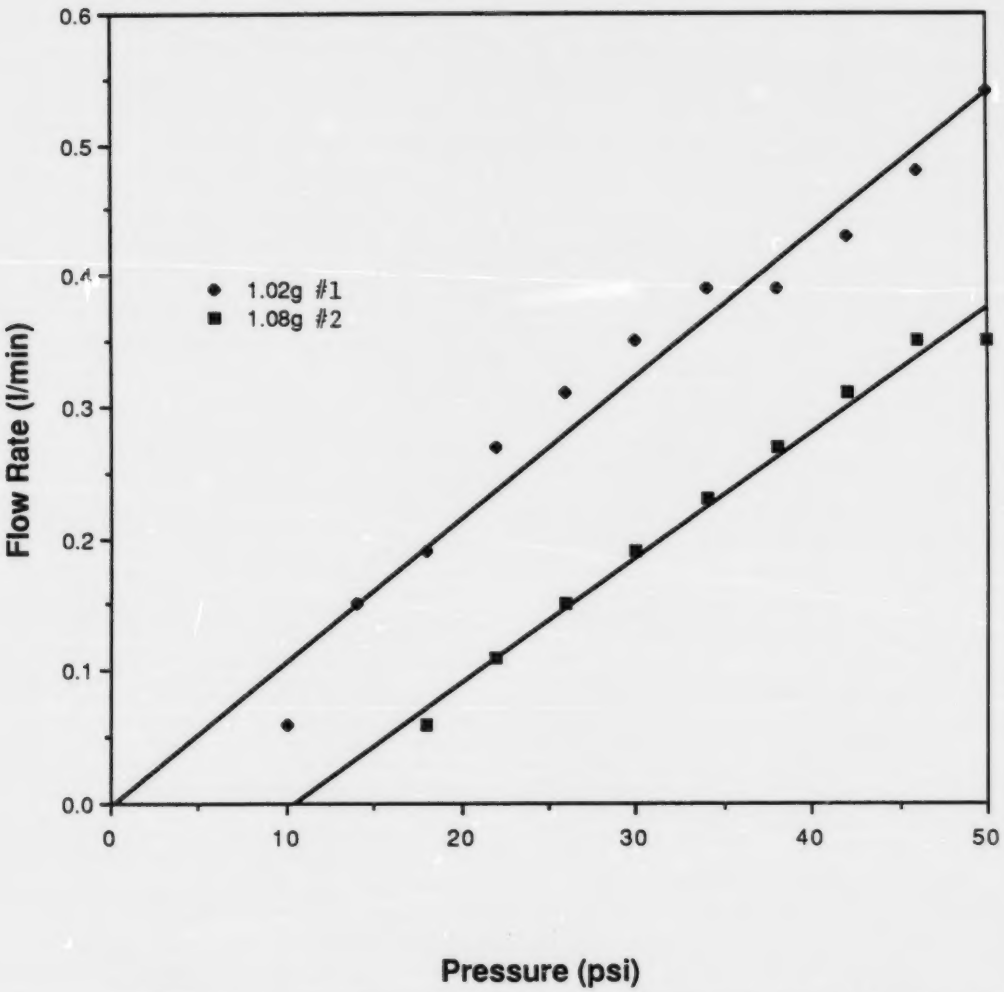

Figure 3.2.15 Permeability Measurements of Set 3 (Triple Pass) Nickel Plasma Sprayed Films

more films could reveal the limits of variability with this process. If this range is found to be satisfactory, then the plasma spray technique could be a viable method of electrode preparation.

3.2.3.2. Effect of Plasma Spray Conditions

To investigate the effects of spray conditions (i.e. plasma power and spray distance), a number of films were prepared in a manner similar to that described in the previous section except a nickel-aluminum composite powder was employed (Metco Powder 404). This material was originally chosen since the aluminum could be leached out with boiling KOH thereby affecting the degree of porosity.

Figure 3.2.16 shows the measured flow curves for the six samples prepared. The effect of spray conditions is somewhat masked by the changes in sample weight (thickness), however by examining Table 3.2.7, a number of general conclusions can be drawn. For example, in comparing samples 2 and 3 which have nearly the same weight, it is noted that increasing the spray distance by 4 inches, greatly increases permeability and therefore porosity/pore structure. On the contrary, increasing plasma power (300A to 500A) appears to decrease porosity although no firm conclusion can be drawn from this data owing to the problems of sample reproducibility as discussed in Section 3.2.3.1. These results appear to be relatively consistent with the SEM examination of nickel films discussed in Section 3.2.

3.2.4 Porosimetry of Ni Plasma Films

As discussed in an earlier section (2.3.4), the application of mercury intrusion porosimetry is generally employed for the determination of porosity and pore size distribution in samples with a relatively large void volume. The development of high precision penetrometers during this program at ORF, has enabled mercury porosimetry analysis to be extended by approximately one order of magnitude into the smaller sample volume end which allows for the partial measurement of pore structure on individual plasma sprayed films. Since it has been shown (Section 3.2.3) that the plasma

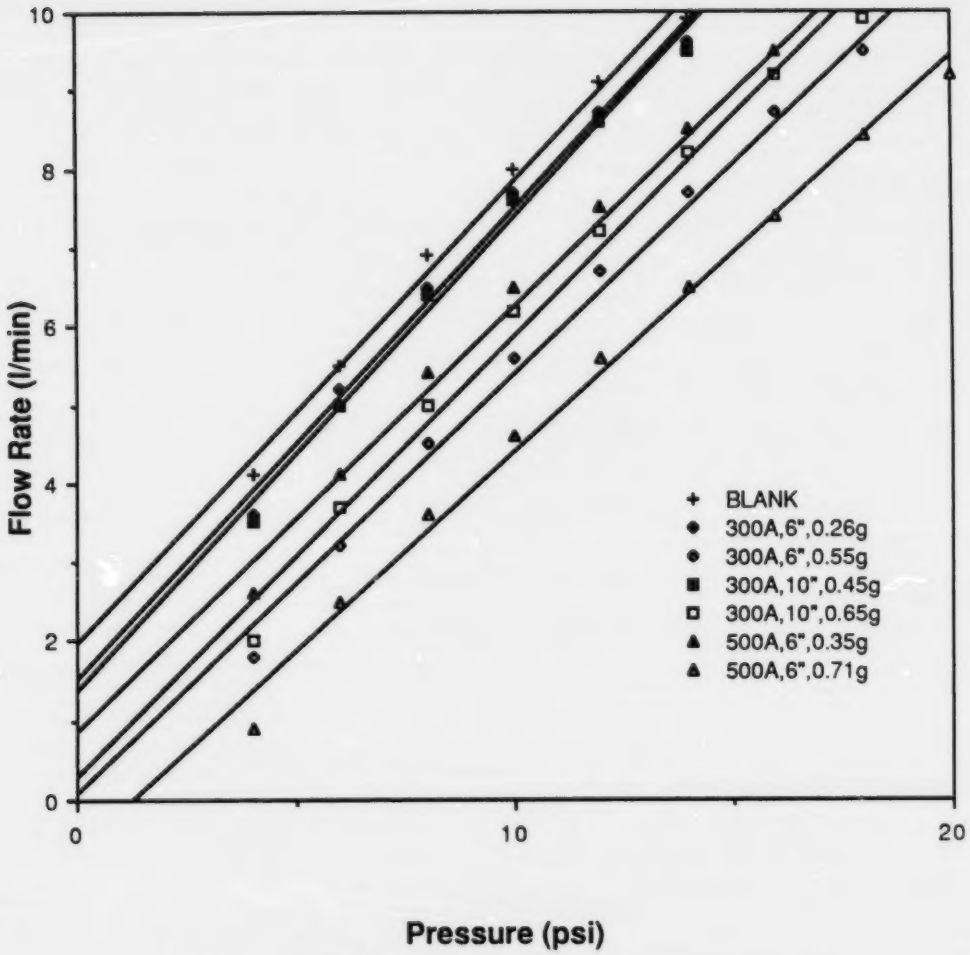

Figure 3.2.16 Comparison of the Permeability of Plasma Films (Powder 404) Sprayed Under Various Conditions

Table 3.2.7

Comparison of Plasma Spray Conditions via Film Permeability

Sample	Sample					
	1	2	3	4	5	6
1) 300A, 6", Low						
2) 300A, 6", High	T					
3) 300A, 10", Low	D,T	D				
4) 300A, 10", High	T,D	T,D	T			
5) 500A, 6", Low	P,T	T,P	P,D	T,D,P		
6) 500A, 6", High	P,T	T,P	T,D,P	P,D	T	

T = thickness effect

P = plasma power effect

D = spray distance effect

sprayed nickel coatings appear to be fairly irreproducible with regard to pore morphology, the ability to measure and compare singular films provides another opportunity to investigate the feasibility of the plasma spraying process.

3.2.4.1 Unsupported Films

The three types of unsupported plasma sprayed nickel coatings prepared using a different number of spray passes (see Section 3.2) at 500A and 6" W.D. were evaluated. Mercury intrusion porosimetry was conducted from 10 psia to 60,000 psia using the Micromeritics AutoPore 9200. This realizes a pore size range of between 18 um to 0.003 um. Figures 3.2.17, 3.2.18 and 3.2.19 show the observed cumulative intrusion curves for a sample of each set.

These surveys show the behavior noted in Section 2.3.4, that at high pressures, mercury compression and other effects show up as sample intrusion. To avoid complicating the analysis, the pressure range 30 psi - 1500 psi was chosen, which corresponds to a pore size range of 6 um - 0.12 um. This selection thereby omits the extremely fine pores which are overlapped with compression effects and avoids the larger "pores" (i.e. intrusion between 20-10 um) which are most likely due to the filling of surface irregularities (e.g. surface texture).

From the intrusion curves, it appears that there is an increase in the volume of pores approximately 1 um - 0.6 um in diameter as the number of passes is increased. This effect, however, is complicated by the scaling factors employed in Figures 3.2.17 to 3.2.19. To isolate this effect more clearly, the intrusion volumes (cc/g) for the range 6 um - 0.12 um are plotted as Figure 3.2.20. From these curves, there appears to be a trend that as the thickness of the film is increased there is a shift in pore size (to larger pores) and pore volume.

Each set was repeated (duplicate analysis) and the revised results (30-1500 psia) are presented in Table 3.2.8. By averaging each of the two porosimetry runs, it appear that there is, indeed, a trend towards higher

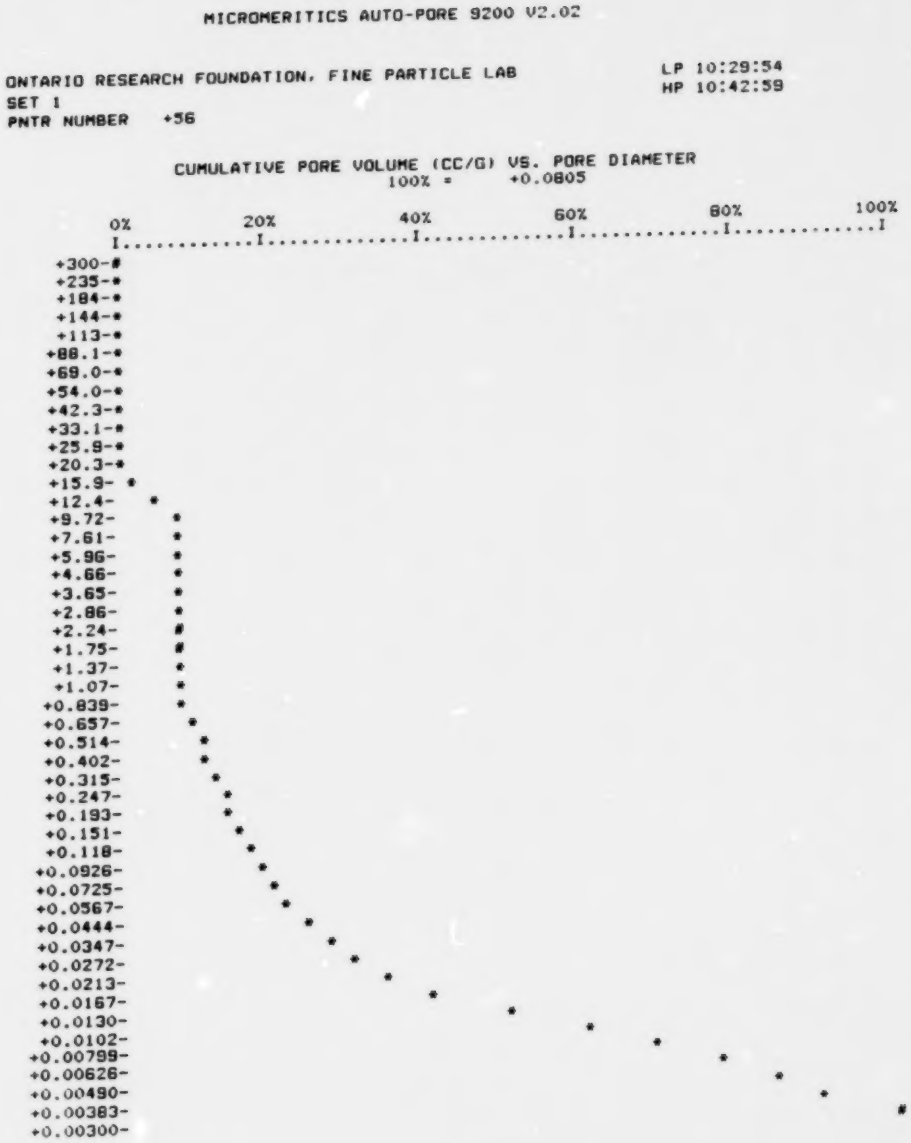

Figure 3.2.17 Cumulative Intrusion Curve for Unsupported Plasma Sprayed Nickel Film (1 x double pass)

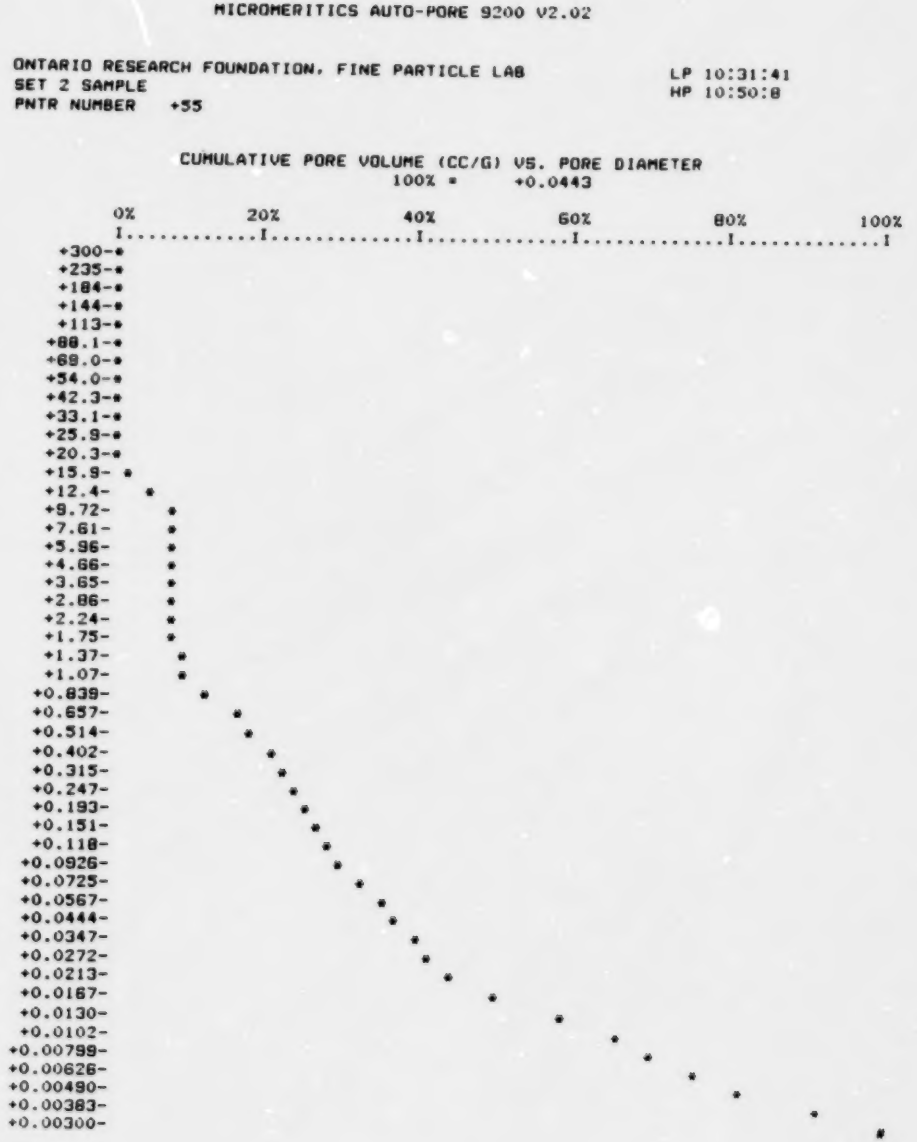

Figure 3.2.18 Cumulative Intrusion Curve for Unsupported Plasma Sprayed Nickel Film (2 x double pass)

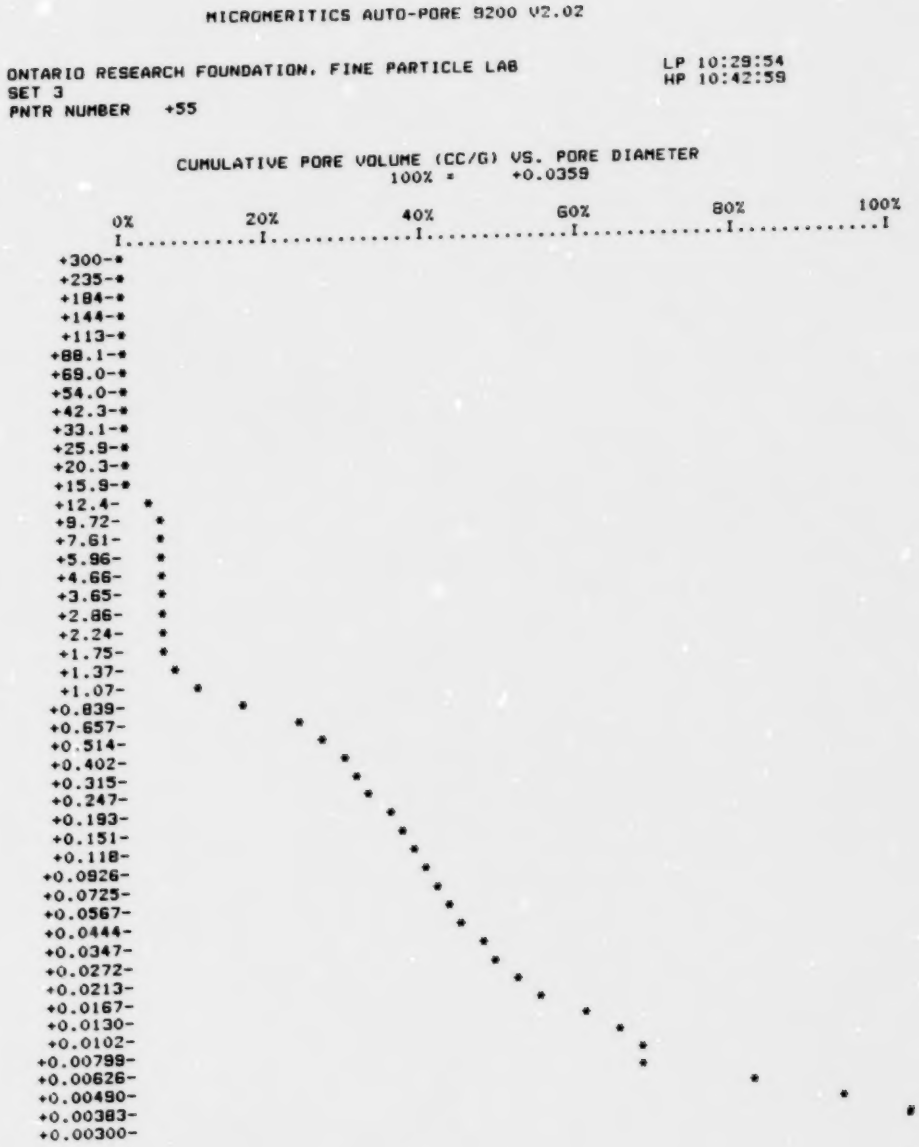

Figure 3.2.1[illegible] Cumulative Instrusion Curve for Unsupported Plasma Sprayed Nickel Film (3 x double pass)

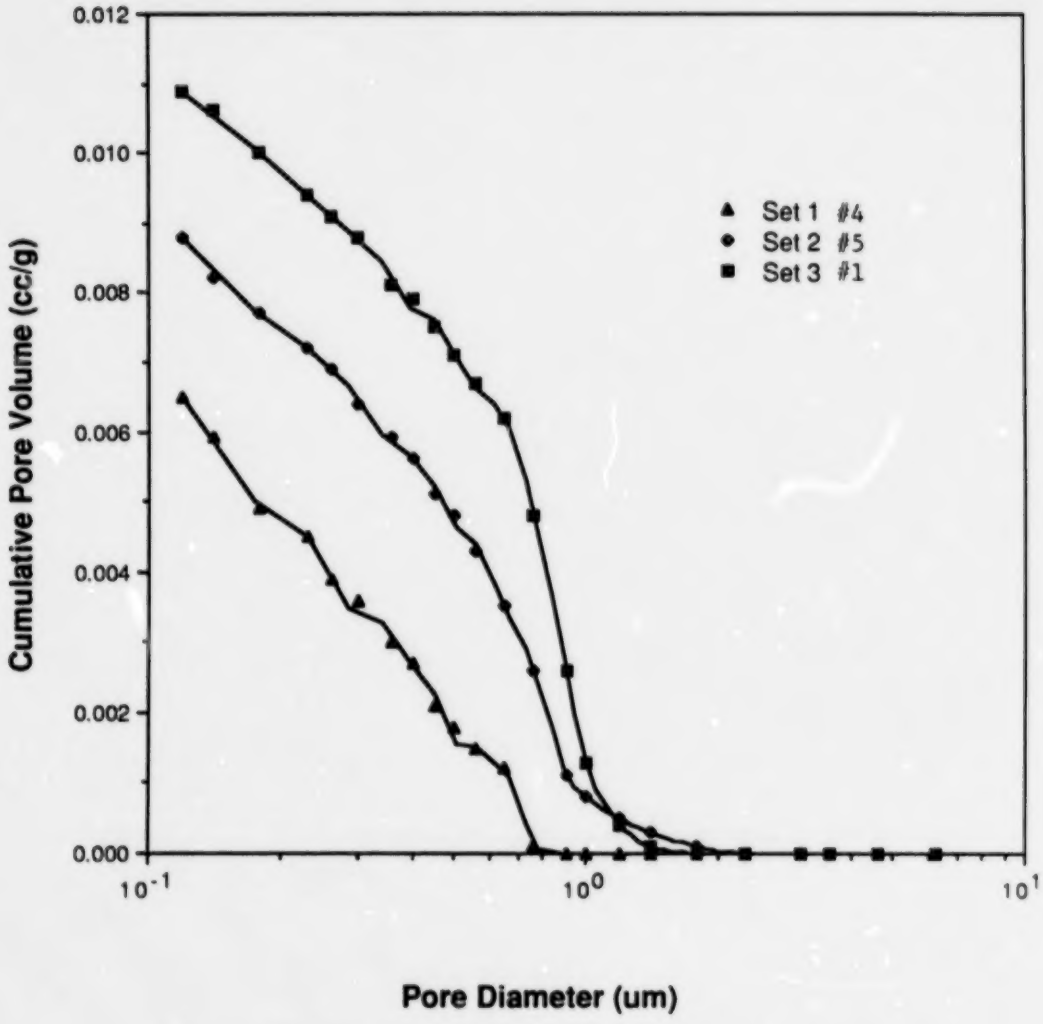

Figure 3.2.20 Mercury Intrusion Curves for Unsupported Nickel Plasma Films

porosity with increased film thickness. As the thickness is increased, the average pore diameter also appears to increase. The pore area, however, remains relatively constant as the surface area for the volume (or number) of larger pores approximates the surface area of the smaller pores.

In an effort to obtain another measurement of porosity for these samples, the degree of mercury entrapment was monitored by recording the increase in weight for the samples following high pressure intrusion. By assuming that of the weight change was attributable to mercury being trapped in the pores of the sample, a volume could be calculated (based upon the density of mercury) and related to the original sample volume by knowing the theoretical density of nickel (8.90 g/cc) and the sample weight. These measurements are given in Table 3.2.8. with the regular porosimetry results. These results also indicate a trend towards higher porosities with increased film thickness.

At present, this effect is not totally understood, however, one possible explanation may be related to powder segregation in the gravity feed device. As a powder "settles" due to the vibrations in the feeder, smaller particulates will migrate to the bottom leaving larger particle on top. If this takes place in the powder feeder, then with time, the size of particulates entering the plasma will increase in size (assuming a bottom feed stream), thereby results in films of increased porosity and pore dimension as the spray droplets actually increase in size. This would result in a slight porosity gradient with films that are built up by the multi-pass approach.

3.2.4.2 Supported Films

Duplicate porosimetry analysis was performed on samples for the three sets of plasma spray conditions employed while spraying nickel on galvanized steel disks; 1) 500A, 6A", 2) 300A, 6", 3) 300A, 10". Table 3.2.9 gives the intrusion results which are adjusted for the pressure region of interest between 30-1500 psia (6 um-0.12 um). For these samples, the observed intrusion was assumed to be due to the films porosity and the support's pore volume was considered negligible.

Table 3.2.8

Mercury Porosimetry Analysis of Unsupported Plasma Sprayed Nickel Films (500A, 6" W.D.)

	Set 1 (1 x double pass)		Set 2 (2 x double pass)		Set 3 (3 x double pass)	
Parameter	#4	#6	#6	#5	#1	#2
Intrusion Volume (cc/g) 30 - 1500 psia	0.0065	0.0018	0.0077	0.0088	0.0109	0.0074
Pore Area (m^2/g) 30 - 1500 psia	0.094	0.031	0.089	0.092	0.097	0.081
Average Pore Diameter (μm) 30 - 1500 psia	0.28	0.23	0.35	0.38	0.45	0.37
% Porosity (30 - 1500 psia)	5.5	1.6	6.4	7.3	8.8	6.2
Average % Porosity	3.6(2.8)		6.8(0.6)		7.5(1.8)	
Mercury Entrapped (cc)	0.0026	0.0029	0.0069	0.0056	0.0105	0.0114
Weight Sample (g)	0.32	0.35	0.71	0.58	1.01	1.07
% Porosity	6.7	6.9	8.0	7.9	8.5	8.7
Average % Porosity	6.8(0.1)		7.9(0.1)		8.6(0.1)	

Table 3.2.9

Mercury Porosimetry Analysis of Supported Plasma Sprayed Nickel Films

Parameter (30 - 1500 psia)	Set 1 (500A, 6")				Set 2 (300A, 6")		Set 3 (300A, 10")	
	#1	#3	#5	#6	#1	#2	#1	#2
Intrusion Volume (cc/g)	0.0216	0.0100	0.0131	0.0181	0.0096	0.0114	0.0174	0.0200
(avg)		0.0157(52)			0.0105(13)		0.0187(18)	
Pore Area (m^2/g)	0.106	0.079	0.093	0.086	0.058	0.070	0.093	0.108
(avg)		0.091(12)			0.074(9)		0.101(11)	
Avg Pore Diameter (μm)	0.81	0.51	0.56	0.84	0.66	0.65	0.75	0.74
(avg)		0.68(17)			0.66(1)		0.75(1)	
% Porosity	16.1	8.2	10.4	13.9	7.9	9.2	13.4	15.1
(avg)		12.2(3.5)			8.6(0.9)		14.3(1.2)	
Film Weight (g)	0.76	1.00	0.54	0.75	1.27	1.32	0.60	0.53

Due to the variability encountered for the duplicate analysis of the Set 1 samples, four samples in total were analyzed, each of which gave quite unique results. Figure 3.2.21 shows the observed intrusion curves for each sample in this set which highlights the difference between films of supposedly identical structure. This indicates that for these plasma sprayed films the reproducibility in preparing coatings/films of consistent morphology is rather poor, and therefore limits the conclusions which can be drawn from changing spray conditions. It does appear, however that there is an increase in porosity and pore diameter when the spray distance is increased. This is consistent with other studies including permeability and image analysis which suggests that molten particles exiting from the plasma have a chance to cool before impacting with the piece to form the film. This results in a more open pore structure and increased porosity.

3.2.5 Gas Adsorption of Plasma Sprayed Nickel Films

As with the platinum paste films (Section 3.1.5), it was necessary to increase the absolute surface area of the plasma sprayed films under study by conducting a multiple sample analysis using the custom built large adsorption cells. Six sample sets were analyzed corresponding to both the supported (various plasma conditions) and unsupported (thickness variation) films. Krypton adsorption was employed for the analyses and the results are reported in Table 3.2.10.

For the supported films, adsorption on the galvanized steel surfaces was assumed to be negligible due to its non-porous nature, and specific surface area estimates relate to the film weight only. From these results, it appears that there is little significant difference between the films analyzed, with the possible exception of the unsupported three by double pass samples (Set 3). One possible explanation is that with increased working distance the molten droplets have a better opportunity to cool, thereby destroying some microstructural features (e.g. nanopores) which would give rise to an increased surface area. The pore area of approximately 0.07 m^2/a as

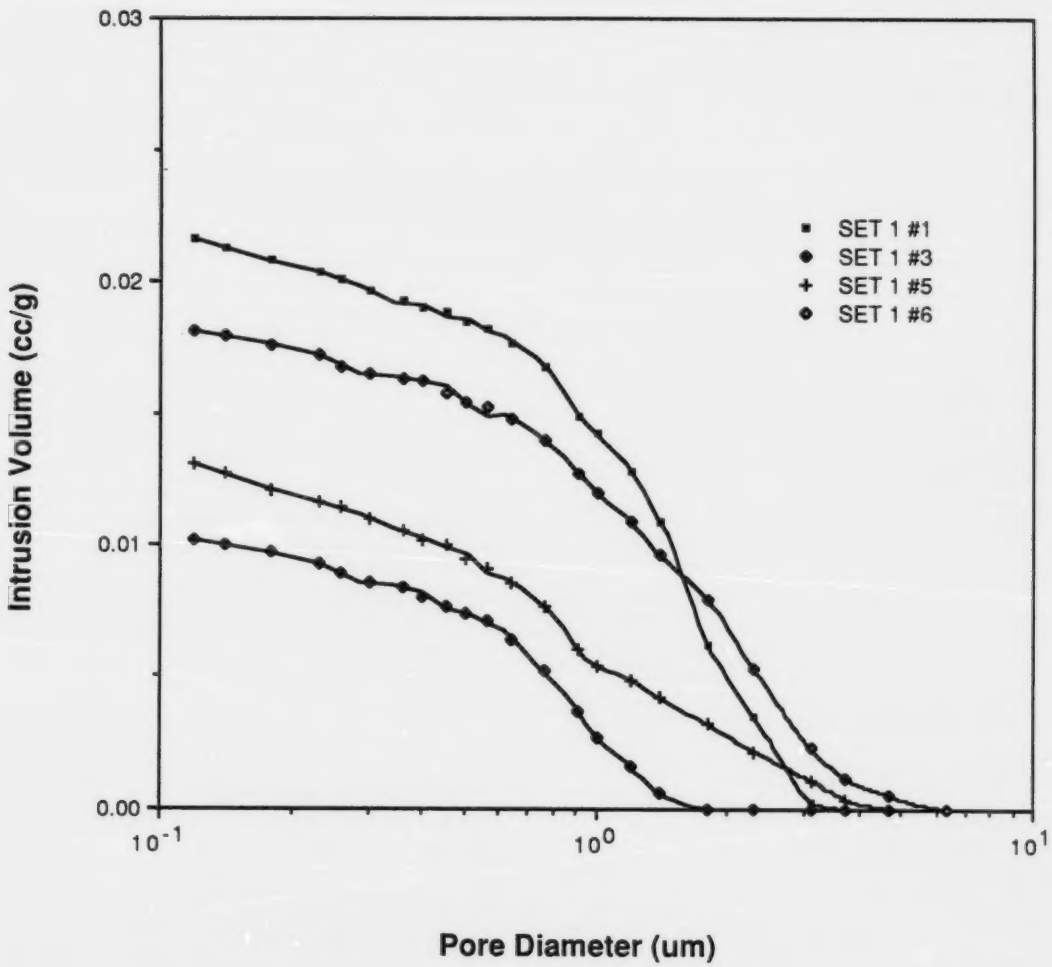

Figure 3.2.21 Mercury Instrusion Curves for Set 1 Samples (500A, 6") of the Supported Nickel Plasma Sprayed Films

Table 3.2.10

Specific Surface Areas of Plasma Sprayed Nickel Films

Substrate	Spray Conditions	Specific Surface Area (m^2/g)
Galvanized Steel	500A, 6"	0.075(7)
Galvanized Steel	300A, 6"	0.064(5)
Galvanized Steel	300A, 10"	0.067(6)
Unsupported	500A, 6" 1 x double pass	0.070(3)
Unsupported	500A, 6" 2 x double pass	0.065(1)
Unsupported	500A, 6" 3 x double pass	0.048(4)

determined by mercury porosimetry is in good agreement with the surface area of 0.05 - 0.08 m^2/g resulted from gas absorption analysis.

In general, however, it is assumed that the present instrument is still not sensitive enough to distinguish between subtle differences in film surface areas.

3.3 Perovskite Films

The application and benefits of employing perovskite type materials for electrodes in electrochemical devices have been discussed earlier (Section 2). It was originally hoped that $La_{0.8}Sr_{0.2}Co_{0.8}Ni_{0.2}O_{3-x}$ perovskite films would be prepared by a separate CANMET contract awarded to the Atlantic Industrial Research Institute (AIRI) in Halifax. Unfortunately, this work could not be completed due to the difficulties in producing flowable powders with good integral strength. Attempts at AIRI did result in powders with sufficient sphericity. However, these powders had very poor crush strengths which resulted in their deterioration in the powder feeder. This severely limited the spray operation and resulted in an approximate 10% coating efficiency (i.e. 90% loss). Arrangements were subsequently made with Metco to use their proprietary procedures (involving special binders) for producing a suitable power. To date, this work has not been completed by Metco and the contract with AIRI has been cancelled.

As a preliminary investigation, a number of mixed composition coatings plasma sprayed by AIRI for Electrolyser (Noranda Research Centre) were supplied to ORF by Dr. R. LeRoy of Electrolyser. The powders were developed by Sherritt-Gordon Mines of Fort Saskatchewan, Alberta and were prepared by a proprietary process which results in a chemical composition of $Co_{0.6}Ni_{0.3}(316\ \text{Stainless Steel})_{0.1}O_{3-x}$. Figure 3.3.1 and 3.3.2[32] show the surface morphology and cross sectional nature of these sprayed coatings using plasma conditions of 500A, 55V, 12" working distance, and a 6.6 lbs/hr feed rate.

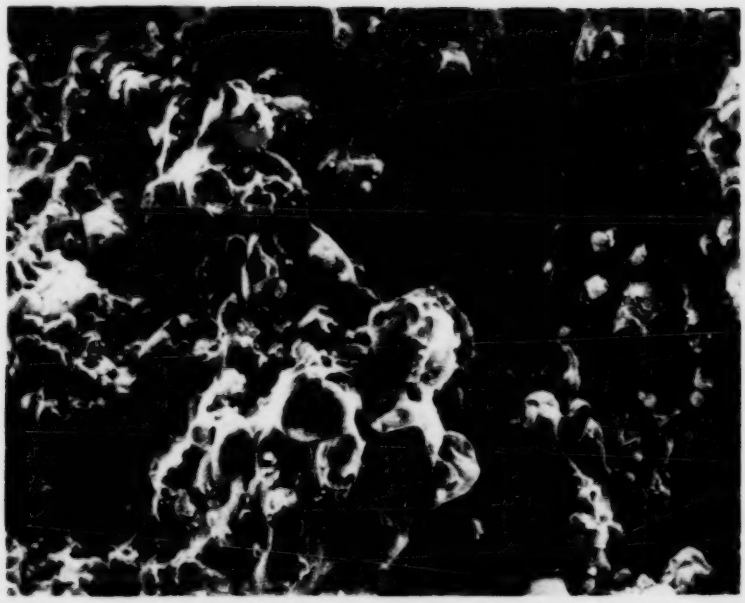

Figure 3.3.1 SEM Micrograph of $Co_{0.6}Ni_{0.3}$ $(316SS)_{0.1}$ O_{3-x} Plasma Coating Surface (500X)

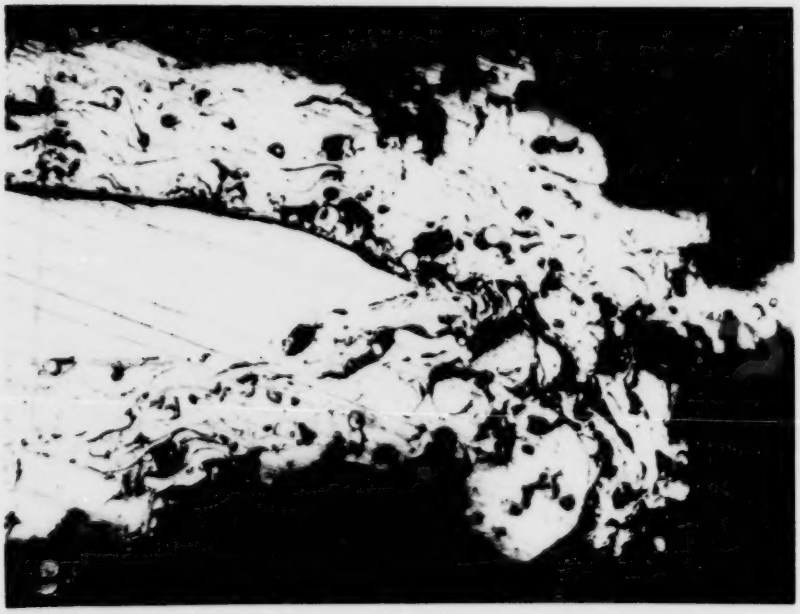

Figure 3.3.2 SEM Micrograph of $Co_{0.6}Ni_{0.3}$ $(316SS)_{0.1}$ O_{3-x} Plasma Coating Cross Section (200X)

A portion of this material was sent to the Micromeritics laboratory in Atlanta where surface area analysis was conducted using the automated Digisorb 2600. This unit operates on the standard multi-point adsorption isotherm (BET) theory for calculating specific surface area, however as it is entirely micro-computer controlled, the sensitivity of the instrument is increased to measure samples with an absolute area as low as 0.01 m^2. The measured surface area of the $Co_{0.6}Ni_{0.3}(316SS)_{0.1}O_{3-x}$ film was found to be 0.065 m^2/g based upon film weight and assuming that the surface area of the support (Ni mesh) was negligible.

One other composition prepared at AIRI and analyzed by Micromeritics was a plasma coating of $Ni_{0.39}Al_{0.59}Mo_{0.02}O_{3-x}$. Figure 3.3.3 and 3.3.4[32] show the SEM micrographs of this material which has a surface area of 0.375 m2/g. This increase in surface area is most likely attributable to the change in the microstructure of the material which was sprayed using plasma conditions of 700A, 70V, 12" working distance and a 2.2 lbs/hr feed rate.

Preliminary plasma tests on the $La_{0.8}Sr_{0.2}CO_{0.8}Ni_{0.2}O_{3-x}$ perovskite powders prepared at AIRI have been able to produce small quantities of the coating supported on nickel mesh. Figures 3.3.5 and 3.3.6 show the surface morphologies for the films which have an approximate surface area of 0.3 m^2/g, as measured at ORF using the Micromeritics Orr Pore-Volume Surface Area Analyzer Model 2100. Unfortunately, insufficient quantities were available for the other types of characterization studies conducted in this program.

3.4 Silver Membranes

Problems associated with the reproducibility of plasma sprayed films (Section 3.2) have shown that in order to attempt any correlation between physical characterization techniques, it was essential to have a supply of standardized films which had a consistent pore morphology. Silver membrane filters produced by Osmonics [33] were subsequently employed to evaluate the various characterization techniques discussed in Section 2.3. These metal membranes offered the advantages of being relatively uniform, having a

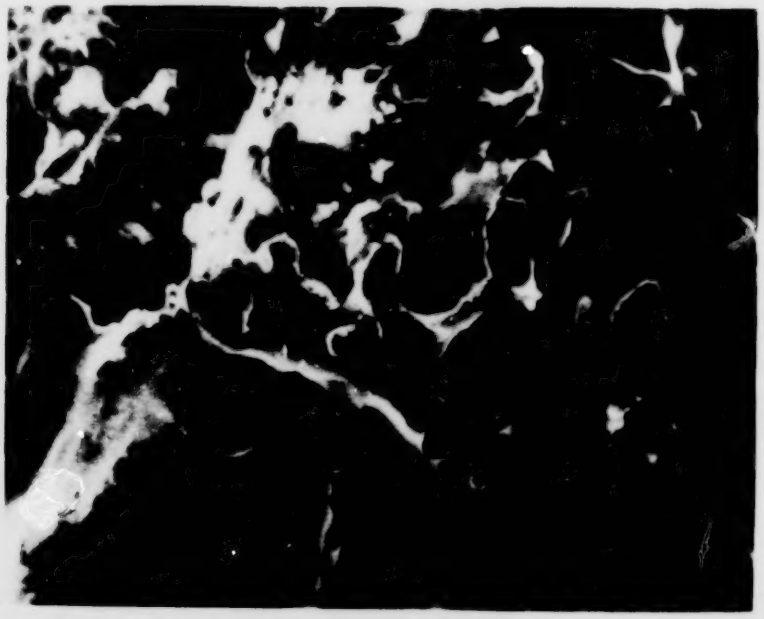

Figure 3.3.3 SEM Micrograph of $Ni_{0.30}Al_{0.50}Mo_{0.02}O_{3-x}$ Plasma Coating Surface (500X)

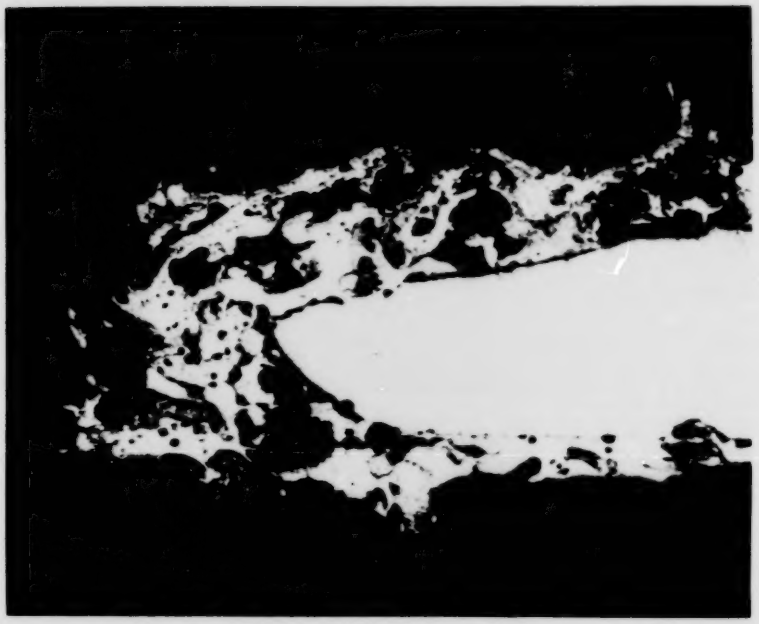

Figure 3.3.4 SEM Micrograph of $Ni_{0.30}Al_{0.50}Mo_{0.02}O_{3-x}$ Plasma Coating Cross Section (200X)

Figure 3.3.5 SEM Micrograph of Plasma Sprayed Perovskite Coating on Nickel Mesh (approx. 65X)

Figure 3.3.6 SEM Micrograph of Suface Structure for Plasma Sprayed Perovskite Coating (approx. 6500X)

controlled porosity and pore retention rating (ranging from 5 um to 0.2 um), and approximating the physical dimensions of other electrode materials which have been studied in this program (e.g. thicknesses of between 40-70 um).

Figures 3.4.1 and 3.4.2 show the virgin surface of a 5 um filter and demonstrate the morphological nature of these silver membrane filters. The manufacturing process, which is strictly proprietary, appears to be a result of a powder sintering action, possibly in conjunction with a volatile organic pore former. The result is a very porous and tortuous structure with well defined particle retentive abilities.

3.4.1 Image Analysis of Ag Membranes

Five silver membrane pore ratings (5 um, 1.2 um, 0.8 um, 0.45 um, and 0.2 um) were selected for in-depth quantitative image analysis using the LeMont OASYS image analysis system. In each case, a 25 mm diameter membrane was prepared by mounting in standard metallurgical epoxy followed by grinding and polishing it down to the minimum of a 1 um diamond paste finish. Polished samples were either gold coated for subsequent SEM examination or in some cases (for pore ratings greater than 0.5 um) analyzed directly by optical microscopy techniques. In both situations, it was found imperative to treat or analyze the samples immediately to avoid oxidation (tarnishing) of the exposed silver metal which distorted the pore structure image.

Figures 3.4.3 to 3.4.7 show the SEM photomicrographs for the five cross-sectioned and polished membranes selected. Of striking contrast in this set is the difference in the continuous (interconnected) phase between the 5 um, 1.2 um, and 0.8 um membranes as well as between the 0.45 um and 0.2 um membranes. In the former case, the voids (pores) appear interconnected while the solid phase (silver) appears as isolated particles. The opposite is observed for the finer pore rated membranes in which the pores now appear as isolated voids and the silver phase is continuous. This has a significant effect on the pore/particles size determination as computed by an area determination (see Section 2.3.1.2). In the case where joined features are of interest a lineal or chord length analysis is more appropriate for evaluating feature size.

Figure 3.4.1 SEM Photomicrograph of 5 μm Rated Ag Membrane Surface (approx. 300X)

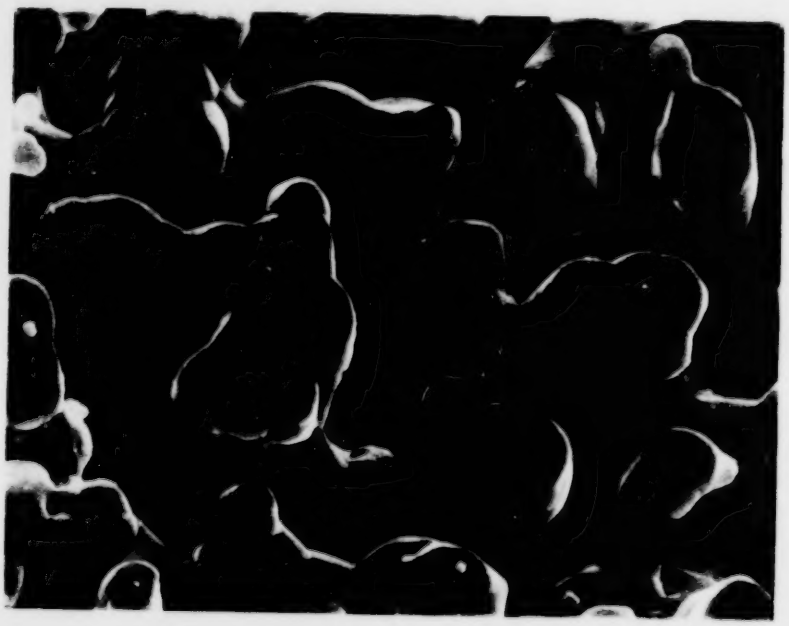

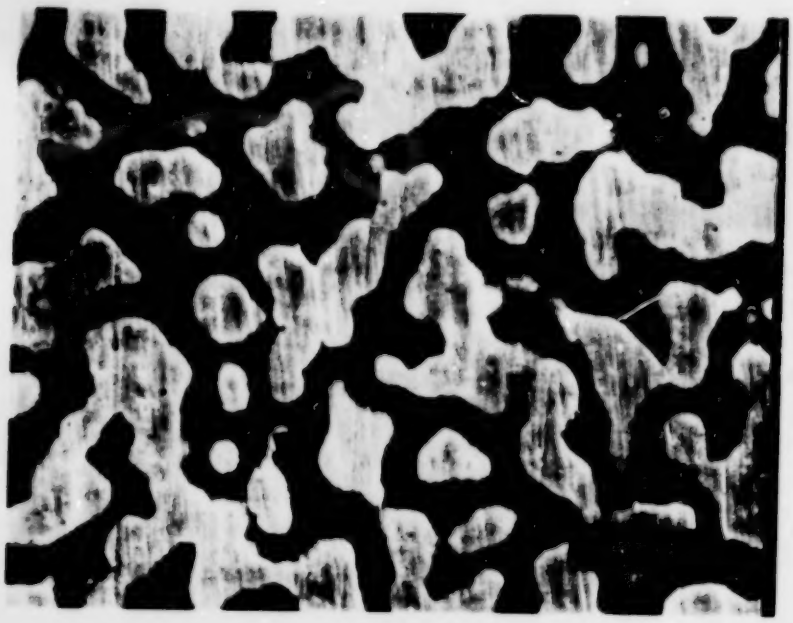

Figure 3.4.3 SEM Photomicrograph of Polished 5 μm Ag Membrane (approx. 1600X)

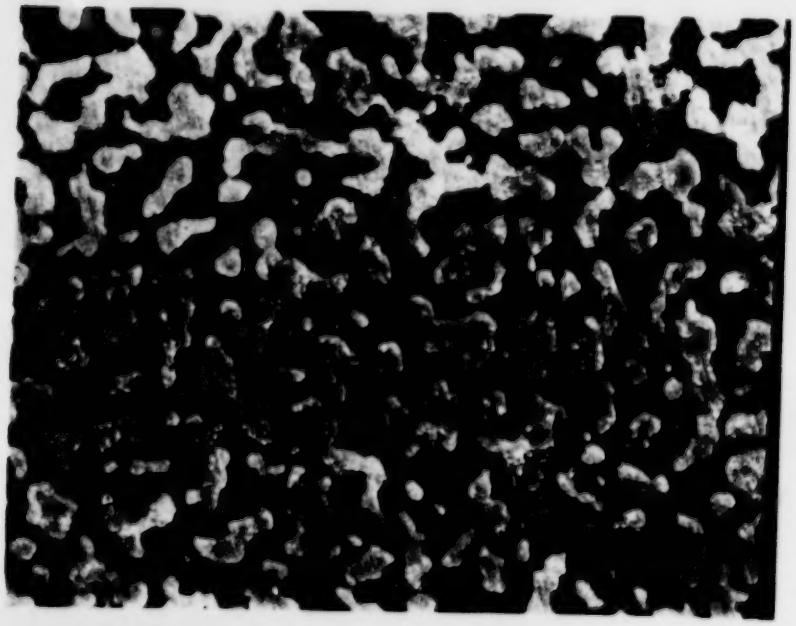

Figure 3.4.4 SEM Photomicrograph of Polished 1.2 μm Ra[illegible] Membrane (approx. 1600X)

Figure 3.4.7 SEM Photomicrograph of Polished 0.2 m Ag Membrane (approx. 1800X)

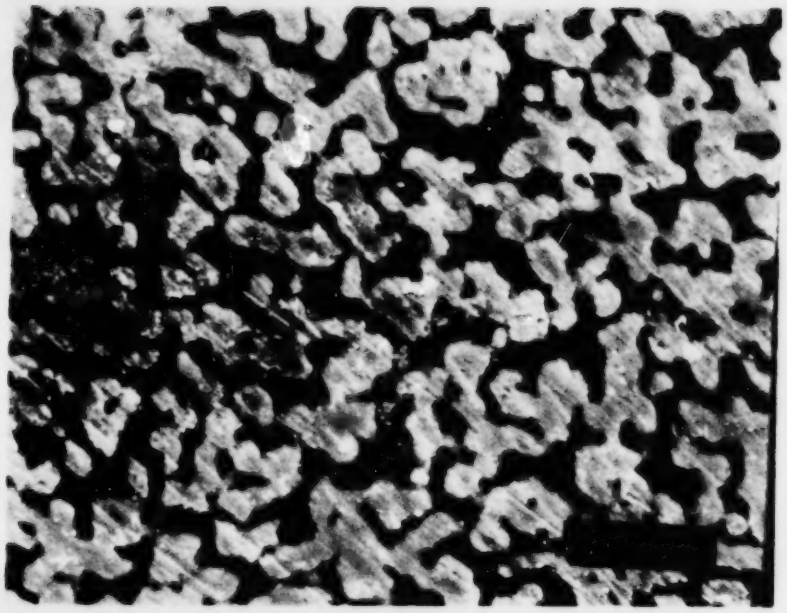

Figure 3.6.3 SEM Photomicrograph of Polished [illegible] Membrane (approx. 1900X)

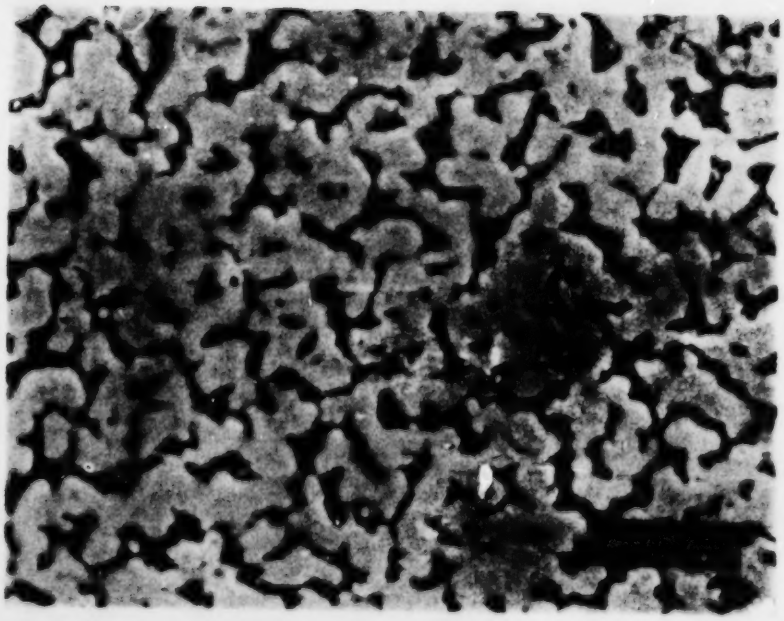

Figure 3.6.4 SEM Photomicrograph of Polished [illegible] Membrane (approx. 1900X)

Table 3.4.1 gives the mean particle/pore diameter measured by a chord length distribution analysis. In each case, between 7 to 10 frames (photomicrographs) were analyzed with 5 lines/frame. This corresponds to between 250 and 500 individual feature measurements.

As can be seen from this table and from the photomicrographs, the particle diameters remain relatively constant while the pore diameters decrease in size. There exists a very good correlation between the pore diameters measured by the lineal approach and the minimum crossing distance (MCD) technique developed specifically for evaluating porous structures (see Section 2.3.1.3).

Table 3.4.1 also shows the measured average particle diameter using the line scan or area equivalent diameter logic. As with the chord length or line scan analysis, the particle diameters remain relatively constant until the silver particulates become the continuous phase (i.e. pore rating <0.5 um) whereupon the measured particle diameters become greatly exaggerated and somewhat meaningless.

The decrease in pore diameter while maintaining a consistent particle diameter results in a decrease in overall porosity. As with the feature dimension analysis, the porosities of the silver membranes can be measured in a number of ways. Table 3.4.2 lists the percent porosity for each polished membrane filter using both a line scan (area) technique and a chord length to total length analysis (both voids and particles). From this table, it is apparent that for porous silver membranes with less than approximately 30% porosity, the solid phase becomes continuous.

One other important parameter that can be derived from image analysis is the perimeter to area ratio for selected features (either pores or particles). Assuming one were able to examine particles of the electrode situated at the electrolyte (i.e. interface), this perimeter would correspond to what is know as the 3-phase line estimate. It can therefore be assumed

Table 3.4.1

Pore and Particle Diameters for Ag Membranes via Image Analysis

	Pore Diameter		Particle Diameter	
Pore Rating (μm)	Minimum Crossing Distance (μm)	Avg Chord Length (μm)	Line Scan Area (μm)	Avg.Chord Length (μm)
5.0	3.2	4.3	5.9	4.8
1.2	2.2	2.5	5.8	2.7
0.8	1.5	1.9	4.9	3.4
0.45	1.2	1.2	7.6	3.6
0.2	1.0	1.0	8.5	4.0

Table 3.4.2

% Porosity (Voids) for Ag Membranes via Image Analysis

Pore Rating (μm)	% Porosity		
	Area Determinations[1]	Chord Length (Particles)	Chord Length (Voids)
5.0	44(9)	47	47
1.2	47(4)	48	48
0.8	34(2)	35	35
0.45	24(6)	26	24
0.2	20(2)	20	20

1. Standard error derived from averaging 5-10 fields of view

that if a porous body has a random yet uniform structure, such as the silver membranes, then any cross-sectioned plane should approximate any other and hence the 3-phase line calculated on any section would be an estimate of the value at the interface.

Table 3.4.3 gives the measured values for the five membranes analyzed. Except for the 5 um membrane, all the filters appear to have a similar 3-phase line or perimeter/area ratio. This is somewhat expected since, as was shown earlier, the particles remain relatively constant in size while the porosity decreases to account for a smaller pore dimension. Overall, however, the particle perimeter per unit area does not change significantly.

In summary, it has been shown that for the ideal case (silver membranes), image analysis can provide a number of important physical parameters which may prove useful in evaluating electrode behavior/morphology relationships in future.

3.4.2 Profilometry of Ag Membranes

Initial investigations began by measuring the surface roughness of virgin surfaces for the five silver membranes under study. Samples were mounted on a vacuum holding device developed at ORF as part of this program to secure thin materials. Ten traces were acquired on each membrane using the skidless, standard stylus (approximately 2 um tip radius) and using the phase corrected mode at a sampling length of 0.08 mm. The small sampling length was chosen to avoid problems in sample leveling which often become dominant when operating in a skidless mode.

Table 3.4.4 lists the mean values and standard errors for a number of surface texture parameters. From these results, it is apparent that there exists a strong correlation between virgin surface texture and particle retention rating for the silver membranes. This effect is most likely attributable to the physical dimensions of the pore diameters. However, it is

Table 3.4.3

Three Phase Line Length Estimate for Ag Membranes

Pore Rating (μm)	Three Phase Line Estimate ($\mu m/\mu m^2$)[1]	(cm/cm^2)
5.0	0.34 (4)	3400
1.2	0.64 (5)	6400
0.8	0.64 (3)	6400
0.45	0.62 (12)	6200
0.2	0.61 (4)	6100

1. Standard error derived from averaging 5-10 fields of view

Table 3.4.4

Standard Surface Texture Parameters for Silver Membrane Surfaces

Particle Retention Rating (µm)	PC/0.08 mm/skidless		
	Ra (µm)	Rq (µm)	Sm (µm)
5	0.55(3)	0.69(3)	12.4(7)
1.2	0.36(1)	0.46(2)	11.6(7)
0.8	0.31(2)	0.38(2)	10.4(7)
0.45	0.16(1)	0.20(1)	7.6(3)
0.2	0.13(0)	0.16(1)	8.4(6)

also complicated by the fact that by using the standard stylus tip, smaller irregularities (e.g. pores) can be under-detected which leads to the interpretation of a smoother surface.

Profilometry can also be used to study the thickness and uniformity of features. In an effort to cross-correlate the porosity measurements observed through image analysis, four silver membrane types were selected for volumetric/gravimetric determination of porosity. Three fresh individual samples of each membrane material were mounted on the vacuum holder such that the filter edge could be easily measured. A minimum of five edges per membrane were measured to provide a reasonably accurate estimate (and standard deviation) for membrane thickness. From this thickness measurement, and by knowing the membrane area (25 mm diameter), a total volume could be computed. This volume was then related to the actual mean weight of a membrane and by using the specific gravity of pure silver (10.5 g/cc), a porosity value could be obtained.

Table 3.4.5 lists the measured dimensions and weights as well as the calculated porosity. Only the 0.2 um membrane weight has a standard error associated with it since three individual membranes were weighed. The other values are an average from the total weight of twenty identical membranes determined during the surface area analysis in Section 3.4.5). The porosity values agree reasonably well with those calculated in Section 3.4.1 (see Table 3.4.2). Observed deviations are most likely due to the variance in measuring the membrane thickness and weight.

3.4.2.1 Direct Pore Measurements

In an attempt to correlate surface texture measurements with pore dimensions, the profilometer was employed to scan ten 0.4 mm sections of each different pore rated silver membrane filter (5 um - 0.2 um). The traces were stored and printed using the maximum horizontal magnification of 1,000X and vertical magnifications of between 10,000 to 50,000X.

Table 3.4.5

Gravimetric/Volumetric Determination of Porosity for Silver Membranes

Absolute Particle Retention (μm)	Weight (g/membrane)	Thickness (μm)	Porosity (%)
1.2	0.126(9)	52(4)	53
0.8	0.170	70(4)	53
0.45	0.180	51(5)	32
0.2	0.126	37(2)	34

These direct traces were subsequently measured using the digipad input of the LeMont OASYS image analyzing computer. The width of valleys (possibly pores) at the center line average (CLA) were assessed and averaged to provide the results in Table 3.4.6. Resolution for this technique was ± 0.6 um. Figures 3.4.8 a-e show portions of the scans employed for each membrane analyzed along with estimates of the pore dimensions (noted as dotted lines along the CLA).

From Table 3.4.6, it is apparent that although this measurement technique does show a relative decrease in pore diameter with decreasing pore rating, the direct stylus scan does not appear to be sensitive enough to detect changes below approximately 0.5 um. This is most likely due to the physical limitations incurred by the size of the stylus tip (approximately 2 um).

3.4.2.2 Impregnation/Dissolution of Silver Membranes

To increase the sensitivity of measuring pore dimensions by profilometry, a novel approach was studied which involved vacuum impregnating a 1.2 um silver membrane with Spurr Low-Viscosity Embedding Media epoxy, followed by sectioning and polishing. An acidic wash was used to dissolve the silver component leaving the impregnated pores in relief to be measured. To improve the resolution of this technique, a high-resolution stylus was employed (approximately 1.5 um diameter). Table 3.4.7 relates the changes in surface texture for both the polished silver and epoxy following successive immersions in a nitric acid solution suspended in a low-power ultrasonic bath. Figures 3.4.9 a) to 3.4.9 d) show a sample trace for each of the treatments conducted.

From these results, it does indeed appear that for the silver membrane the surface texture is becoming more rough with increased time of etching. It was originally hoped that this increase would be due to a selective dissolution of the silver phase leaving the impregnated pores to stand as "islands" which could be easily measured by profilometry. SEM

Table 3.4.6

Pore and Particle Diameters for Ag Membranes via Profilometry

Absolute Pore Rating(μm)	Mean Spacing Sm(μm)[1]	Pore Diameter(μm)[2]	Particle Diameter(μm)[3]
5	12.4	5.5	6.9
1.2	11.6	5.1	6.5
0.8	10.4	4.8	5.6
0.45	7.6	3.6	4.0
0.2	8.4	3.6	4.8

1. From surface texture measurements (see Table 3.4.4)
2. From CLA estimate of pore size (see Figures 3.4.8 a-e)
3. Calculated from Sm - Pore Diameter

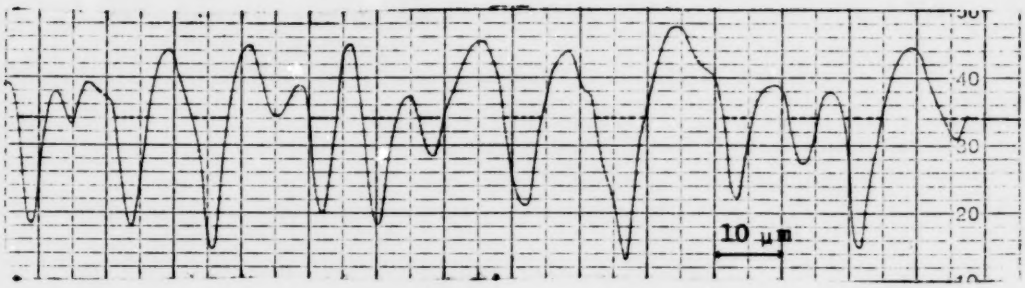

Figure 3.4.8(a)
5 µm Membrane
Vx=10,000
Hx= 1,000
1 µm

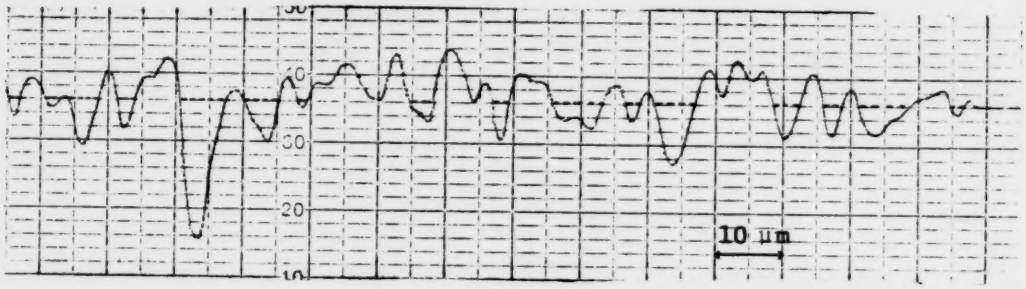

Figure 3.4.8(b)
1.2 µm Membrane
Vx=10,000
Hx=1000
1 µm

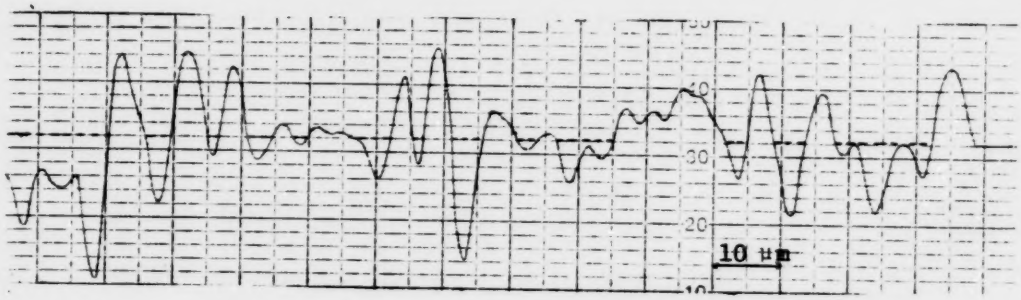

Figure 3.4.8(c)
0.6 µm Membrane
Vx=20,000
Hx= 1,000
0.5 µm

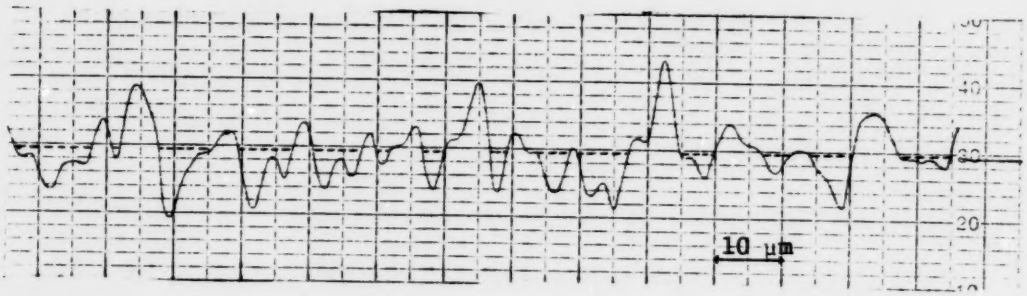

Figure 3.4.8(d)
0.45 µm Membrane
Vx=20,000
Hx=1,000
0.5 µm

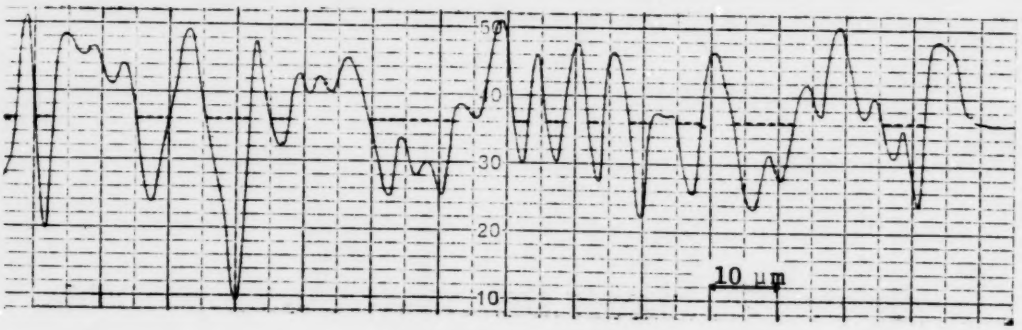

Figure 3.4.8(e)
0.2 µm Membrane
Vx=50,000
Hx=1,000
0.2 µm

Table 3.4.7

Surface Texture of Impregnated/Polished/Etched 1.2 μm Silver Membrane

	Surface Texture for HR Stylus, 0.25 mm PC, Skidless					
	Impregnated Silver Membrane			Epoxy Surface		
Treatment	Ra (μm)	Rq (μm)	Sm (μm)	Ra (μm)	Rq (μm)	Sm (μm)
1) Virgin	0.047(1)	0.061(5)	10.2(3)	0.028(2)	0.037(4)	15.5(1.3)
2) 1 hr, 1MHNO_3	0.056(2)	0.076(3)	10.9(6)	0.031(6)	0.041(8)	15.3(1.8)
3) 2)+ ½hr, 2MHNO_3	0.086(6)	0.114(7)	10.7(3)	0.032(3)	0.042(5)	15.9(1.2)
4) 3)+ ½hr, 2MHNO_3	0.340(18)	0.421(24)	10.2(5)	0.032(3)	0.044(6)	15.7(1.1)

Figure 3.4.9 Profilometry Trace of Etched Silver Membrane (1.2 μm)

a) Virgin Surface
V=100,000
H=500

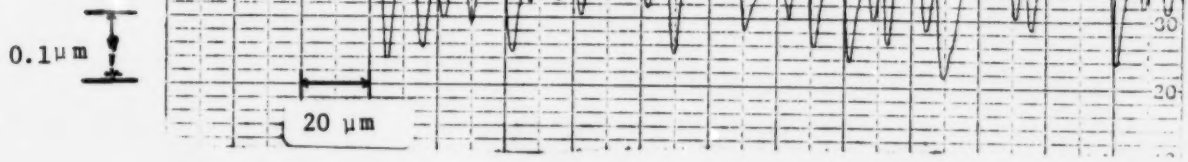

b) 1 hr 1MHNO$_3$
V=50,000
H=500

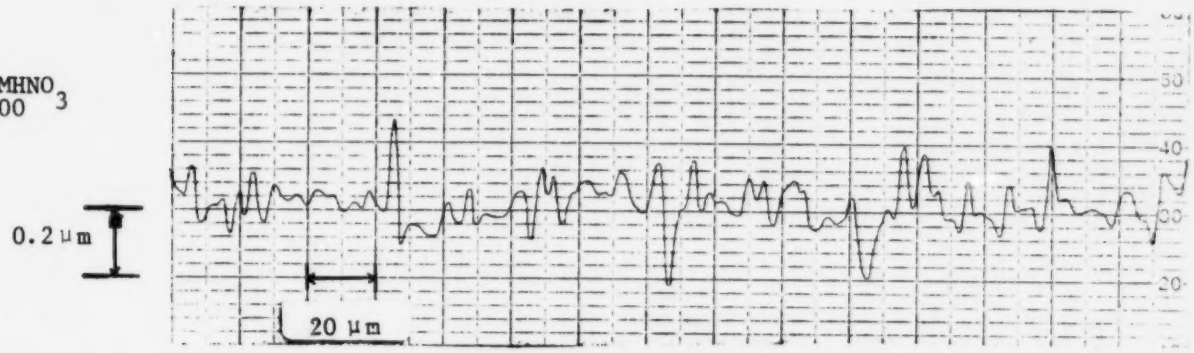

c) 1 hr 1M HNO$_3$ +
½ hr 2MHNO$_3$
V=50,000
H=500

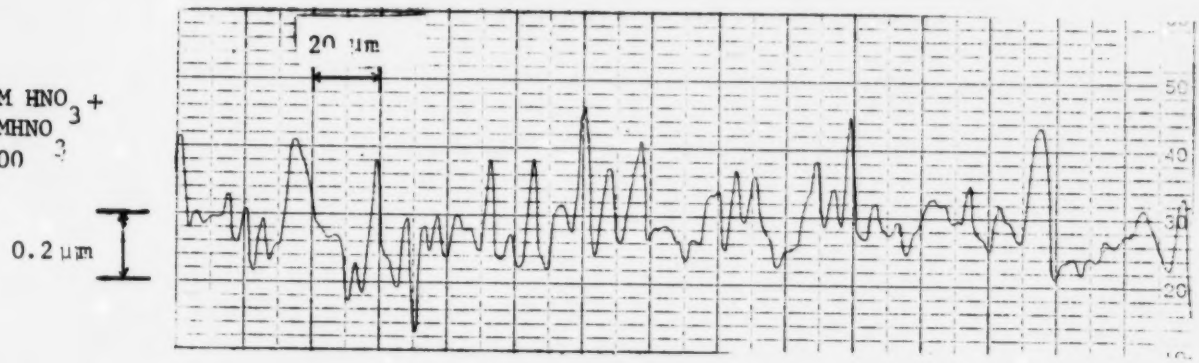

d) 1 hr 1MHNO$_3$ +
1 hr 2MHNO$_3$
V=20,000
H=500

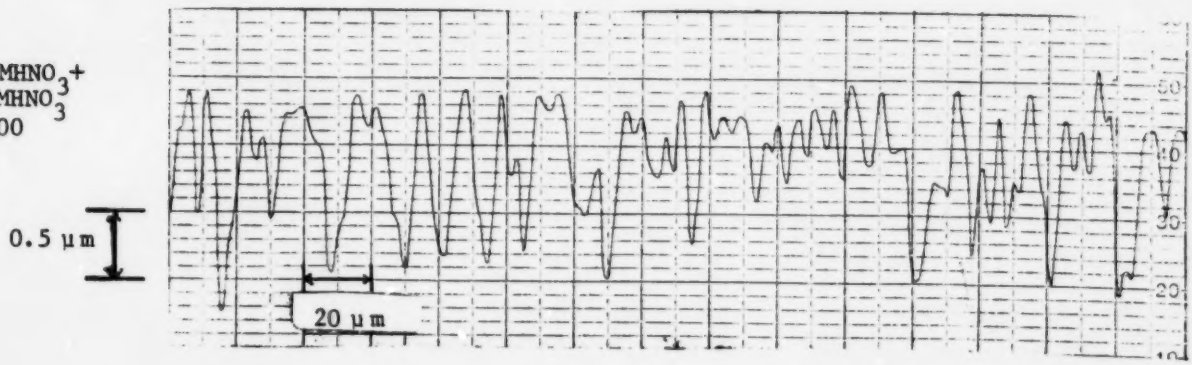

examination of the etched sample, however, reveals that although the silver has been dissolved, the interstitial epoxy does not appear to remain as separated islands.

Figures 3.4.10 and 3.4.11 show the silver membrane surface after treatment 4) (1 hr 1 M HNO_3 + 1 hr 2 M HNO_3). The silver appears to have well rounded edges as compared to the untreated sample (see Figure 3.4.4, which shows the epoxy does indeed impregnate the sample). This suggests that the epoxy in the pores is also being removed either by chemical (acid attack) or physical (ultrasonic bath) means. It is therefore difficult to draw any significant conclusions regarding the pore dimensions using these results. For other materials, however, this approach may provide an alternative means of evaluating void structure in porous films.

3.4.3 Permeametry of Silver Membranes

Following the procedure described in Section 2.3.3, the five particle retention rated silver membranes were measured for gas flow versus pressure head using helium. Figure 3.4.12 shows the excellent fits for the five materials, all of which correspond to the behaviour displayed by other filter membranes, (e.g. Nuclepore, Millipore). Basically, only the 0.2 um membrane is either sufficiently non-porous or with fine enough pore diameter to produce any significant change in the flow/pressure curve from the blank run.

The 0.2 um membrane was subsequently selected for investigation of its flow/pressure characteristics using the reactant gases for the "ideal" fuel cell, hydrogen and oxygen. Figure 3.4.13 shows the measured flow curves for the same flowmeter setting. As shown in Section 2.3.3.1, the needle valve into the rotameter tube acts as a flow resistor which limits the gas passage for the various gases. This has the effect of lowering gas flow through the rotameter, depending upon gas composition.

The overall effect of the 0.2 um silver membrane is therefore strictly relative to the blank run for the gas of interest only (i.e. percent change in air flow). From these results, it would appear that oxygen passes

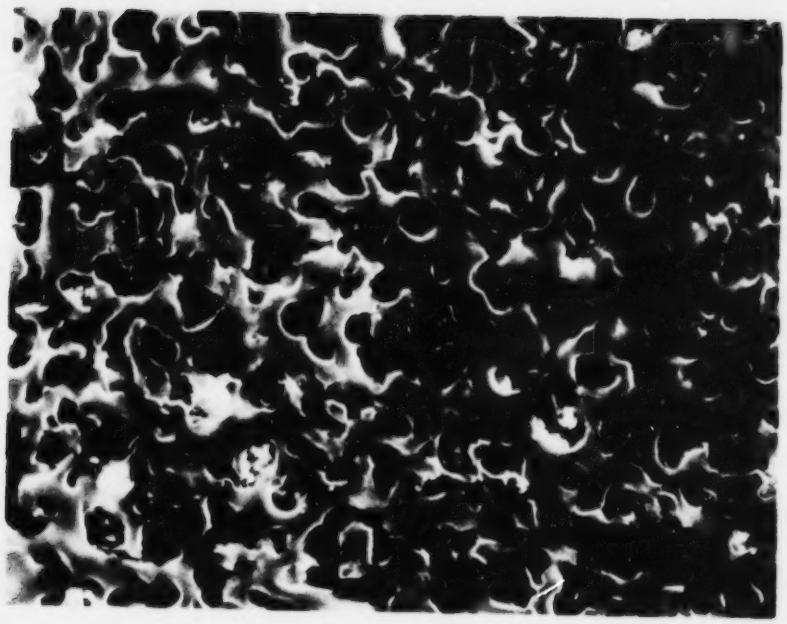

Figure 3.3.4D SEM Micrograph of BN05 Treated 1.2 m Silver Membrane (approx. 1,000x)

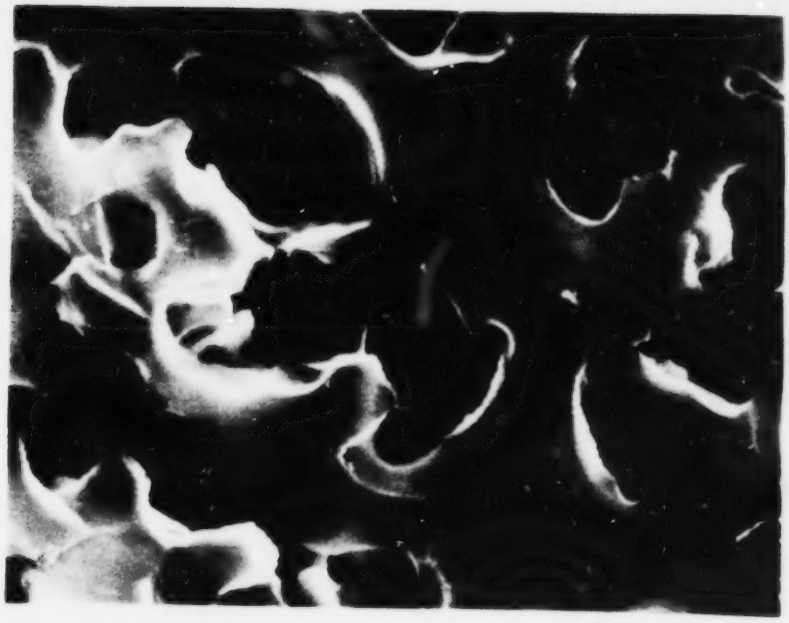

Figure 3.3.4E SEM Micrograph of BN05 Treated 1.2 m Silver Membrane (approx. 4,000x)

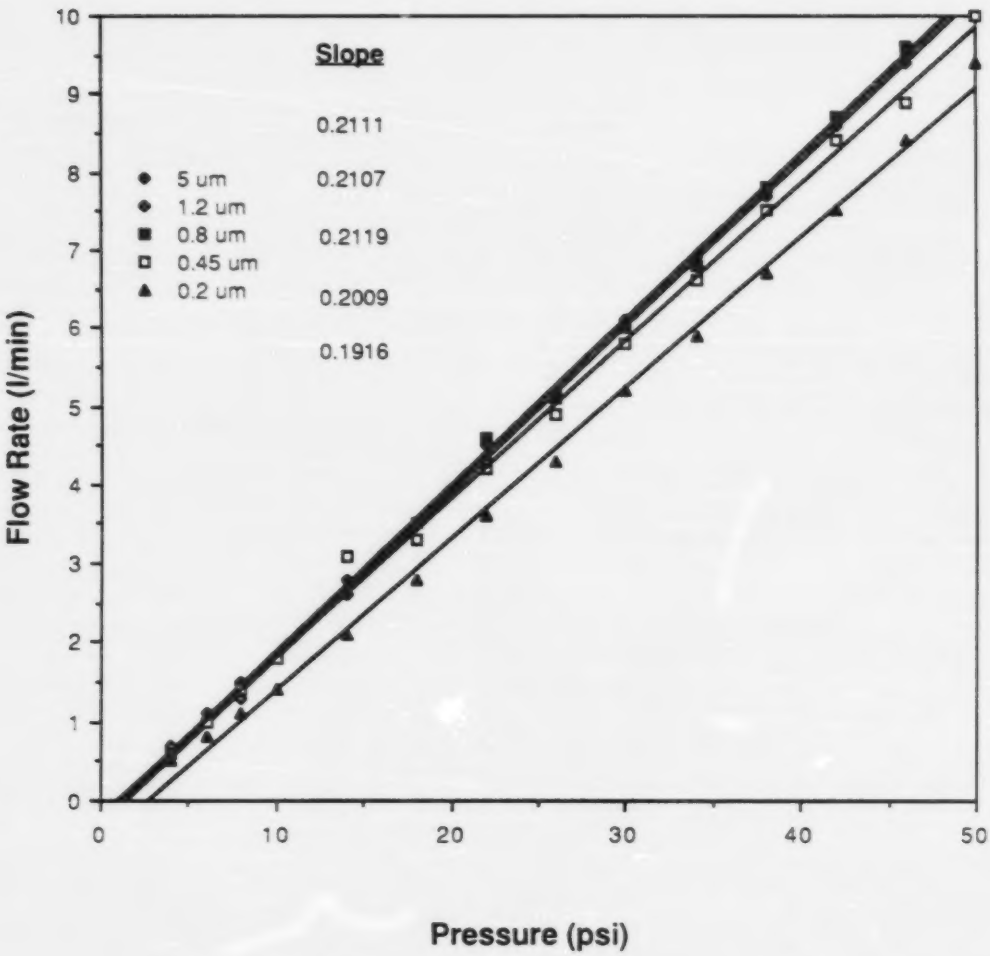

Figure 3.4.12 Permeability Measurements for Silver Membrane Filters (Helium)

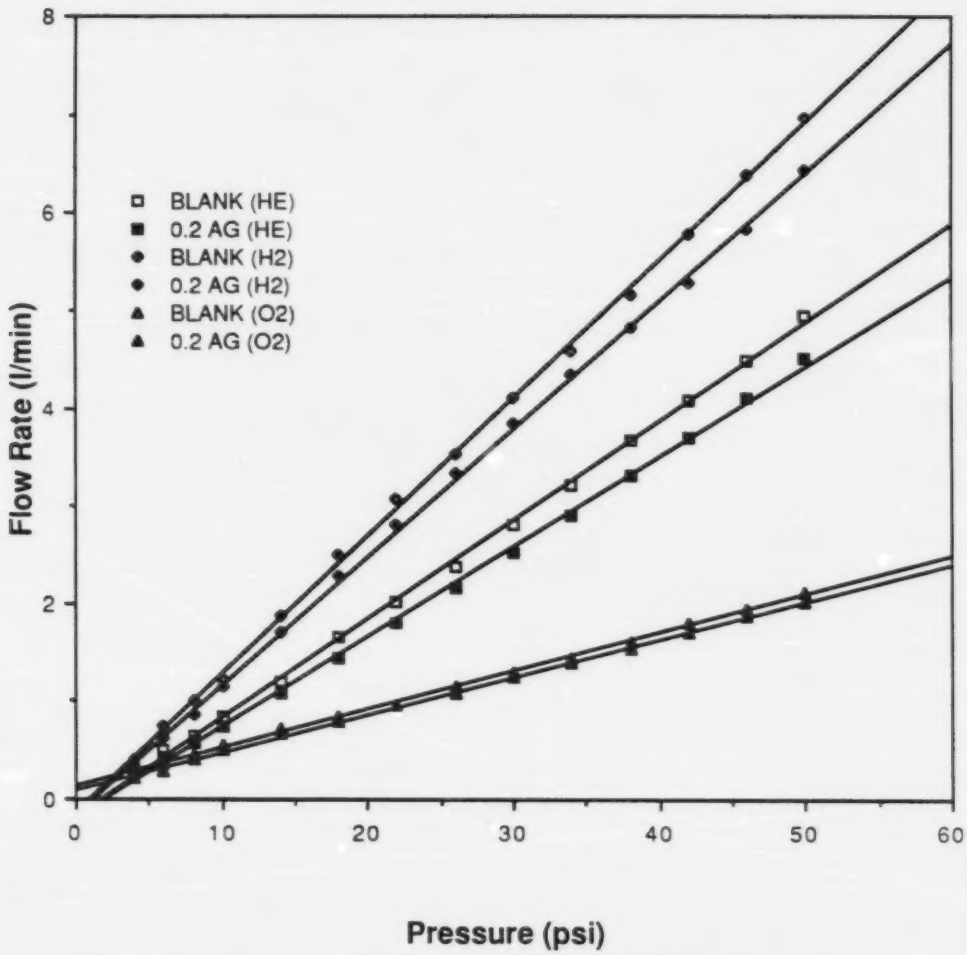

Figure 3.4.13 Comparison of Permeability for 0.2 μm Silver Membrane with Different Gases

through the 0.2 um membrane with greater ease than hydrogen or helium although the absolute gas flow is much lower. This may be related to the mean free path (MFP) of oxygen which is approximately half of the MFP for hydrogen. Table 3.4.8 lists the mean percent change in gas flow velocity (/min) over the pressure range of 8-50 psi versus the various gases employed. From these results, it can be shown that the passage of reactant gases through porous membranes is directly related to the MFP of the gas. This may have obvious consequences when considering the design of porous fuel cell electrodes for various reaction mechanisms or reaction rates.

3.4.4 Porosimetry of Ag Membranes

Due to the formation of silver-mercury amalgam, it was not possible to conduct mercury porosimetry analysis on the silver membranes. Future developments at Ontario Research into the area of Wood's metal porosimetry (Bismuth-Lead-Tin-Cadmium compounds) may prove to be useful not only in conducting standard high-pressure intrusion analysis but in the physical characterization of porous bodies by "freezing" the Wood's metal in the pores and then examining the pore shape etc. by SEM/optical image analysis techniques.

3.4.5 Gas Adsorption of Ag Membranes

Due to the small absolute surface area of each individual membrane and the limit of sensitivity with the commercial equipment operated at Ontario Research (Micromeritics Orr Pore-Volume Surface-Area Analyzer Model 2100), it was necessary to increase the sample volume by measuring twenty membranes in unison. Table 3.4.9 lists the specific surface areas measured as well as the surface area per unit volume (cm^2/cm^3) of membrane material. The 5 um membrane was not measured due to the unavailibility of twenty virgin samples.

Table 3.4.9 also lists the estimate of surface area based upon the stereological measurement of the three-phase line (or perimeter) by image analysis. Although the agreement between the B.E.T. technique and image analysis is not as good as one would expect, the values are in the same order

Table 3.4.8

Gas Flow Resistance From 0.2 μm Silver Membrane

Gas	Mean Free Path[1] (μm)	Percent Decrease in Gas Flow
He	0.275	10.1(1.4)
H_2	0.174	7.9(2.3)
O_2	0.099	5.6(2.6)

1. Boltzmann MFP at 20°C and 75 cm Hg

Table 3.4.9

Surface Area of Silver Membrane Filters

Particle Retention Rating (μm)	Specific Surface Area (cm^2/g)	Volumetric Surface Area (cm^2/cm^3)	Stereological[2] Surface Area Estimate (cm^2/cm^3)
1.2	1600	7900	6400
0.8	1320	6500	6400
0.45	1320	9500	6200
0.2	1130	7750	6100

1. Based upon thickness values measured by profilometry (see Table 3.4.5)

2. From image analysis measurement of three-phase line

of magnitude and agree to within 35% (worst case). Possible deviations would be expected due to the inability of the image analysis technique to measure minute crevices or pores which would certainly be accessible to be monitored by the krypton gas adsorption, resulting in an increase in surface area.

4. CONCLUSIONS

The conclusions drawn here are related to the suitability of each technique examined to evaluate thin film morphology, the interdependence of all the techniques, and the methods employed to prepare thin film materials. These conclusions form the basis of recommendations for further areas of research both with regard to more refined techniques and the direct application of the knowledge gained in this study for the characterization of thin film electrodes for electrochemical device applications.

4.1 Individual Techniques

The purpose of this program has been to identify, test, and refine characterization techniques for the physical examination of thin film morphology. The five techniques selected in this study for in-depth evaluation have all been shown capable of producing morphological data, providing certain restrictions regarding material types, preparative method, and the absolute sensitivity of the instruments employed are considered. The interpretation and cross-correlation of this data is somewhat complicated, however, due to film irreproducibility and the destructive nature of some techniques (eg. mercury porosimetry, impregnation). This has resulted in an assessment of each technique with regard to its practicality (i.e. advantages/disadvantages) in producing reliable information which can be employed to monitor the physical properties of novel electrode materials developed in the future.

A summary of the typical results of measurements using the various techniques is given in Appendix C.

4.1.1 Image Analysis

Image analysis is seen as perhaps the most versatile method currently available for studying film morphology. The technique has been shown to provide data on all the physical properties which are considered relevant to electrochemical behavior (i.e. pore size, particle size, pore/particle

interface length, and total porosity). The sensitivity of image analysis is only limited by the ability to produce input images of sufficient contrast and resolution. (The size of features is generally not considered a problem since atomic level discrimination can be achieved with state-of-the art transmission electron microscopy imaging).

The main drawback to image analysis, as seen in this study, is the difficulty in producing an image which adequately differentiates pores and solids. In materials of simple composition and semi-regular pore structure, such as the silver membranes investigated in this program, standard preparative methods such as epoxy impregnation were found suitable for developing this discrimination. In films with multi-phase components (e.g. oxides in metal plasma films, organics in platinum pastes) or micro-porosity (either low porosity or extremely fine pores), other preparative methods or even alternative image forming techniques (e.g. acoustic microscopy) may be necessary.

Advanced imaging techniques have not been examined in this program and the imaging methods employed were limited to simple SEM and optical micrographs. This was due, in part, to equipment/materials availability and the overall objective of the program which was to investigate a number of techniques which would provide relevant physical data on porous films. To this end, the application of image analysis as a technique has been shown to be a viable approach for quantifying important physical features in thin films and should be further examined when relating these properties to electrochemical behavior.

4.1.2 Profilometry

Although profilometry offers the advantages of being able to generate physical data on thin film materials in a non-destructive and rapid manner and without the need for involved sample preparation, its application to the direct investigation of bulk film morphology must be viewed in consideration of a number of effects. Profilometry examines surface effects only and is generally applied to the interaction of surfaces with other materials (e.g.

bearing ratios, corrosion, erosion). On a macro scale, gross deviations in the surface are indeed related to the bulk morphology (e.g. "swiss-cheese"), however on a micro-scale, physical forces involved in the formation of a surface may distort the interface such that it does not represent or "mirror" the porous structure contained below. This disparity is particularly evident for films which are formed by methods involving a high degree of surface interaction (e.g. pressing, painting).

Profilometry can be employed, however, to generate meaningful bulk morphological data through the use of more involved sample preparation/techniques. Basically, if one can obtain an unadulterated section of a thin film which is representative of the porous structure, then "surface" scans can produce profiles which are related to the morphology. Unfortunately, sectioning generally imparts some degree of sample destruction particularly on a micro scale. Efforts such as those described in Section 3.4.2.2, are therefore seen as viable approaches for implementing profilometry as a standard analysis technique.

One further consideration to employing profilometry for evaluating micro-porous materials has been the physical size of the diamond tip stylus used in acquiring a profile. In the measurement of controlled pore structure materials (silver membranes, Section 3.4.2.1), it was concluded that by using a standard tip stylus (approximately 2 um) pore diameters down to 0.5 um could be assessed in a routine manner. Below this level the sensivity drops off due to the inability of the stylus tip to enter the pore. This limitation can be improved slightly by using the high resolution stylus which has a tip diameter of approximately 1.5 um.

For the purposes of this study and with regard to further work on electrochemical device electrode development, profilometry is seen as a good means of monitoring film thickness and variability. This often can be employed to assess the reproducibility of a particular preparative method, and as such, if one can guarantee similar bulk morphologies through other techniques, profilometry can be employed as a secondary or indirect means of non-destructive quality control.

4.1.3 Permeametry

Permeametry offers the simplest means of evaluating a films total porous nature. Relative differences in the films physical properties (i.e. thickness, pore size distribution, % porosity) are easily differentiated with regard to which material and unique morphology can pass a particular volume of a specific gas per unit time. This has obvious consequences when relating the permeability of porous electrodes to the behaviour of electrochemical devices and provides a direct measurement of a film's suitability in this area.

As discussed earlier, to conduct permeability measurements, it is necessary to study unsupported films or at least films supported on a well characterized and highly reproducible substrate. This restricts the application of this technique for the measurement of the flow properties of an electrode directly since most electrolytes (substrates) commonly employed are very non-porous and non-permeable. As a result, the films evaluated by peremeametry in this study were of a free-standing nature and no porous substrates were employed. The results have indicated that permeability measurements are particularly useful for studying the variables in producing porous coatings (e.g. plasma films) and for evaluating film reproducibility.

Difficulties encountered in relating theoretical models to the flow behavior of films indicate that the exact quantification of pore dimension is extremely difficult and controlled by such effects as porosity, tortuosity, pore shape, and thickness. Permeametry has therefore been shown to be best applied in a secondary manner for studying mainly the deposition conditions and reproducibility involved in film production as opposed to measuring actual electrode morphological features.

4.1.4 Mercury Porosimetry

Traditional mercury intrusion porosimetry using conventional equipment has been shown to have rather limited applications when applied to thin films. The main difficulty is in the total sample volume which, as seen in this study, must be of sufficient quantity to permit detection of the

intruded mercury. For the customized penetrometers developed as part of this program, the technique has been shown to be suitable when applied to single films approximately 50 um or greater in thickness with porosities in excess of approximately 5%. (Although the volume of sample can be increased by adding more samples, this has the effect of "averaging" results over large populations, something which may not be desirable particularly if one is interested in film variability). The technique employed in this study has been shown to be restricted in pore range due the problems resulting from the more sensitive penetrometers (see Section 2.3.4). The lower size range is presently limited to about 0.1 um.

Mercury porosimetry was found to be a destructive technique, dependent upon pore shape and tortuosity (as well as surface texture as was shown in the nickel plasma films), and materials specific (e.g. silver and gold amalgams). The technique is also not sample selective which means it does not discriminate between portions of the sample. This implies that films are best analyzed in an unsupported fashion or at the very least, supports must be smooth and non-porous (i.e. glass, metals) to avoid complicating the intrusion curves.

Overall, mercury porosimetry, as it stands currently, cannot be viewed as a practical means of assessing thin film morphology until alternative methods can be implemented for increasing the sensitivity of monitoring the intrusion of mercury into the pores. Although preliminary attempts at impedence porosimetry measurements did not result in a usable technique, further study in this area could result in an improved technique for characterizing physical structures.

4.1.5 Gas Adsorption

Like conventional mercury porosimetry, gas adsorption has been found to be somewhat limited by the size of samples which can be analyzed. Through specially designed cells, it has been possible to extend the sensitivity of this technique down to 0.1 m^2 with equipment operated at ORF. New commercial instrumentation is capable of measuring down to 0.01 m^2, however to meet the

demands of most thin film applications, where only small amounts of material (e.g. milligrams) are present, a high vacuum system employing ultra-sensitive detection equipment is necessary.

To improve sensitivity and generate physical data, it has been possible to increase the sample volume by increasing the number of samples. This, however, blends any variability between individual films. The limitation in sample size has also negated one of the prime advantages of employing gas adsorption, namely, the ability to obtain pore size distributions and pore volume (porosity) estimates through nitrogen adsorption isotherm analysis.

Although its application to materials in this program has been limited due to the equipment employed, gas adsorption is still seen as a useful technique since the approach offers a non-destructive means of directly evaluating surface activity. Assuming that the amount of sample cooling (-196°C) does not influence materials properties and hence does not render an electrochemical device inert, then gas adsorption can be used as a quality control tool to check the initial behavior of electrodes and monitor their performance with time and usage.

4.2 Correlation of Characterization Techniques

The confidence one places in parameters obtained by a particular technique is governed not only by its theoretical basis but also by its interdependence and relation to the values generated by other measurement methods. This is particularly true when one does not have any "yardstick" to use as a comparison and must draw conclusions solely on data generated on either novel materials and/or by new approaches.

In this program, the five techniques discussed in section 4.1 have been employed in various degrees to examine the physical properties of a variety of thin film materials. For the most part, correlation of these techniques has been less than satisfactory for a number of reasons.

These include absolute sensitivity of the method, materials complexity (i.e. oxides), support interferences, variability between individual films and preparative methods, the destructive nature of some techniques, and also the way in which a parameter is measured.

Tables 4.1, 4.2 and 4.3 provide a summary of the relationship between individual techniques for two materials studied (i.e. silver membranes and plasma sprayed nickel). Both the platinum paste and perovskite films are omitted due to the lack of physical data generated. For each of these tables, the correlation to gas adsorption measurements has been omitted due to the sensitivity of the instrument employed, as well as the fact that the surface area values are a result of blended samples (i.e. more than one sample per film type). For those techniques where sufficient testing on a suitable number of samples was conducted, some conclusions as to the interdependence of these methods could be established.

For the silver membranes which have a well defined porosity and uniform pore structure, a correlation was found to exist between the pore size measured by image analysis and the surface texture of the membranes (see Table 4.1). Figure 4.1 shows the nature of this relationship. It is also apparent that there is an empirical relationship between pore size and permeability, such that gas flow is hindered at smaller pore diameters. This implies that there must be a connection between surface roughness and permeability. Obviously if this connection could be established for other materials, then one would have a simple non-destructive test for evaluating pore structure via profilometry.

For the plasma sprayed nickel films few correlations could be established. With the supported films (Table 4.2), permeametry measurements were obviously not performed while the destructive nature of the image analysis sample preparation technique and mercury porosimetry made any comparative testing on exact samples impossible. The presence of contaminant

Table 4.1

Relationships Between Characterization Techniques for Silver Membranes

	Image Analysis	Profilometry	Permeability
Profilometry	C		
Permeability	C	C	
Porosimetry	X	X	X

C = Correlation Exists

X = Tests not Performed

N = No Correlation Found to Exist

Table 4.2

Relationships between Characterization Techniques for Supported Plasma Films

	Image Analysis	Profilometry	Permeability
Profilometry	N		
Permeability	X	X	
Porosimetry	X	N	X

Table 4.3

Relationships Between Characterization Techniques for Unsupported Plasma Films

	Image Analysis	Profilometry	Permeability
Profilometry	N		
Permeability	N	N	
Porosimetry	X	C	C

C = Correlation Exists

X = Tests not Performed

N = No Correlation Found to Exist

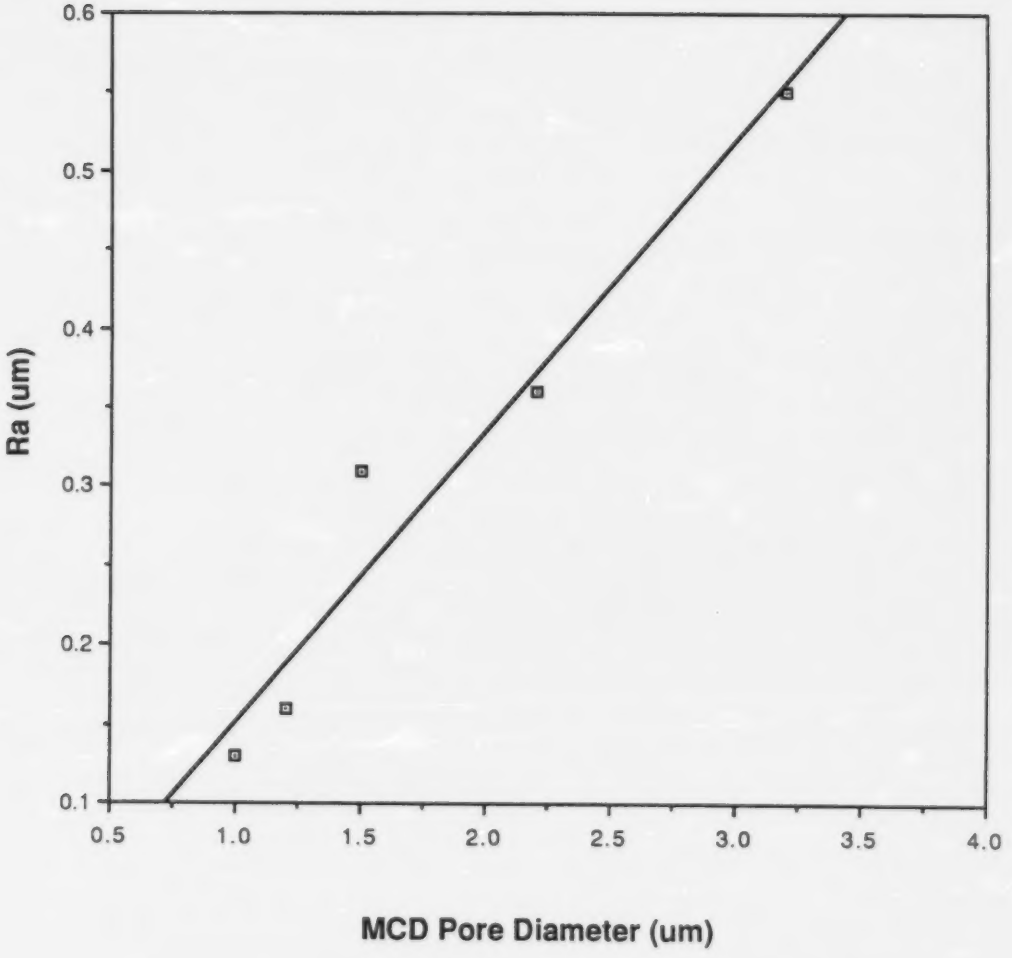

Figure 4.1 Correlation of MCD Pore Diameter versus Surface Roughness for silver membranes

oxides which appear "as pores," make the image analysis approach a relative technique for the comparison of porous plasma films. No firm correlation could be established between profilometry and porosimetry for these supported samples.

In Appendix C, it is noted that the values of the pore diameter of the plasma sprayed nickel films obtained by image analysis and mercury porosimetry differ substantially. Other than the variability of film samples, the major reason for the difference conceivably is owing to the difficulty experienced during the image analysis work in differentiating pores and metal oxides as discussed in Sections 3.2.1.1 and 4.1.1. The uncertainty in such differentiation tends to produce overestimated values of the pore diameter. On the other hand, no problems of similar magnitude were found in the mercury porosimetry measurements. In fact, due to the nature of the plasma spray process for film preparation, the nickel particles were in a molten state when sprayed and splattered onto the surface of the substrate, forming a layered structure and filling the inter-particle voids while consolidating. This leads to the belief that the particle diameter of a plasma sprayed film is likely to be considerably larger than the pore diameter.

Based on these considerations, it is expected that the results of mercury porosimetry measurements are more accurate than those of image amalysis.

The unsupported nickel plasma sprayed films show a few loose correlations with regard to the porosimetry analysis (Table 4.3). For samples within the same set, thereby having similar thicknesses and being prepared under identical conditions, it was noted that an increase in average pore diameter and porosity (as measured by porosimetry) corresponds to an increase in gas permeability. A similar relation exists with the surface texture of these samples (2 from each set) which indicates that as the porosity/pore size increases, the mean surface roughness increases. To be more specific on these correlations, it would be necessary to analyze many more samples.

Overall, the interdependence of these five techniques appears to be somewhat limited for the materials analyzed. This is believed to be a result of both sample and method variability (sensitivity) as well as the difficulties in isolating one parameter from a set of measurements (i.e permeability, profilometry). To better understand the importance of the values generated, the ultimate correlation of morphological properties with electrochemical behavior should be examined, whereupon relevant techniques can then be selected and further refined while non-essential methods can be eliminated from further study.

4.3 Film Preparation Methods

Two basic methods of producing thin film materials were examined in this study; metallized pastes suitable for hand painting or screen-printing and films (coatings) produced through plasma spraying. Each approach offers the advantages of being relatively inexpensive (depending upon materials), being able to cover large areas with a variety of compositions, and having the ability to be automated for larger scale production. Some distinct differences, however, were observed which should be considered when examining their application as a potential electrode production technique.

With the metallized pastes (i.e. platinum), pores are formed indirectly through the removal of organic components during curing/firing. This can place limitations on the substrates (electrolytes) employed with regard to the thermal stability of the system. If this problem can be overcome, then paste application of electrode materials through either a painting/printing operation or even tape casting will be a viable approach for forming very thin (down to 10 um), reproducible films. These films have the potential of having a high degree of the original particle's microstructure which can thereby lead to increased surface activity.

Plasma spraying, although capable of producing porous films directly without the aid of pore formers, suffers from a number of characteristics which may limit its suitability to preparing highly active electrochemical

device electrodes. Since the process is thermal in nature, it has a tendency to destroy any micro-structure in the feed powder thereby limiting surface activity. Also, molten droplets can severly affect the actual electrolyte/electrode interface by increasing the localized temperature to a point beyond electrolyte stability. Plasma spraying has also been shown to be non-uniform and highly irregular resulting in random type films which are relatively thick thereby possibly limiting gas flow through the film.

For these reasons, it is felt that films formed by the direct application of electrode pastes produced in conjunction with low temperature pore formers and prepared by repeatable and controlled techniques such as screen-printing or tape casting, offer the best approach in forming thin films with good morphological and electrocatalytic properties.

5. RECOMMENDATIONS

The following recommendations are a result of the studies conducted in this program and highlight the areas to which this research can currently be applied, as well as serve as suggestions for further development that could increase the scope of these physical characterization techniques.

5.1 Evaluation of Candidate Electrode Materials

The goal of this program has been to identify and develop characterization techniques which can be applied to thin film electrodes for evaluating their physical morphology. The purpose was to subsequently employ these techniques to quantify those parameters which are strongly related to the electrochemical behavior of the electrode and use these methods to pre-qualify candidate electrode materials from a physical point of view.

Each of the techniques examined was shown to have some merit, although a few techniques are believed to be more applicable than others. The properties studied in this program, however, have not been assessed with regard to their influence on electrochemical properties and it is felt that

this correlation would provide a better opportunity to select and/or refine the most plausible characterization techniques. It is therefore suggested that a number of studies be initiated in cooperation with the Ceramics Section of CANMET.

5.1.1 Film Preparation

Due to the variability encountered in the plasma sprayed films and the lack of information generated on the platinum paste and perovskite structures, it is recommended that additional work be conducted on preparing porous thin films suitable for electrode applications in a reproducible manner. Screen-printing was found to be a highly repeatable technique for producing thin films of a controlled size and if perovskite powders and/or platinum particles can be suspended in a low-temperature binder/pore former mixture, this approach may result in consistent thin film morphologies.

Possible alterations to this method would be those considered in ORF's original proposal to CANMET (i.e. sol-gel preparation) or tape casting applications. In each case, the techniques developed in this study should be employed to ensure good film reproducibility.

5.1.2. Electrochemical Behavior

A study on the interdependence of physical parameters (e.g. porosity, pore size, three-phase line) on actual electrochemical behavior of electrode materials should be initiated. The following steps are recommended;

1) Select a suitable electrode material (possibly after successful completion of Section 5.1.1.) and prepare test cells;

2) measure any physical properties possible in a non-destructive manner (i.e. gas adsorption, profilometry)

3) determine the operational behavior of the test cell, isolating the electrochemical performance of the individual electrodes (to be done at CANMET);

4) remeasure electrode properties non-destructively noting any significant changes;

5) measure the complete range of morphological descriptors using a destructive technique such as image analysis;

6) repeat steps 1-5 with electrodes of varying morphologies (i.e. changes to pore former composition, curing temperatures to establish relationship between pore structure and electrochemical behavior.

5.1.3 Electrode Life Studies

Assuming one were able to successfully complete Section 5.1.1, thereby ensuring the reproducibility of electrode materials, a study should be conducted on the change in morphological parameters with operational life. Obviously, any characterization techniques which are destructive in nature, will necessitate a multitude of test cells to be run for various periods of time (and possibly various operational conditions) while examining any deviations in the porous structure of the electrode with increased usage. This information can be employed to monitor the changes in cell performance as well as providing estimates as to the stability and lifetime expected with particular electrode materials/configurations/conditions.

5.2 Characterization Technique Development

During the course of this program, conventional characterization techniques have been assessed and refined. Some of these have included modifications to existing equipment while others involved preliminary feasibility studies. Due to the limited scope of this study, however, a

number of techniques which have been indentified are as yet lacking in the extensive experimentation necessary to "prove" the methods. For this reason, a further development effort in the following areas may provide additional capabilities which should increase the ability to measure thin film morphology.

1) Construction of an ultra-sensitive gas adsorption unit (UHV) for precision measurement of surface area on individual films with absolute areas down to 10 cm^2. This unit could also be employed for chemisorption studies for the determination of chemical reactivity with particular materials. (e.g. H_2 or O_2 with platinum, perovskite compositions, etc.)

2) Testing of the permeability of candidate electrodes supported on porous substrates (e.g. platinum paste on silver membranes). Also varying substrates to study any possible effects on developed film morphology.

3) Refine the impregnation/polishing/etching procedure to be employed with profilometry to evaluate pore/particle dimensions of the bulk film.

4) Continue earlier attempts at developing impedance porosimetry by studying the effects of temperature, pressure, and materials composition on impedance measurements of films.

5) Investigate the practicality of employing Wood's metal porosimetry for introducing molten Wood's metal into the pores of thin film material at high pressures, then cooling and solidifying the metal in the pores for subsequent cross-sectional analysis of pore size and shape via image analyses.

6) Development of a micro-sectioning/image forming technique (e.g. ion milling) to assist in the preparation of 3-D images using

reconstruction based on 2-D images (image analysis). This would permit a true evaluation of tortuosity and pore shape, both of which are believed to strongly influence electrochemical behavior.

5.3 Other Applications

The techniques investigated as part of this program have been applied primarily to the characterization of thin films suitable for electrode materials. In a more general nature, these methods could be employed to evaluate any porous film and as such have significant application possibilities in other areas. Some of these other applications may include the characterization of;

1) filter type materials used for the separation of various components from either liquid or gas including reverse osmosis and ultrafiltration membranes,

2) paper products which need controlled pore stucture for various printing operations,

3) corrosion products (e.g. oxides) formed on metals and other substrates,

4) paints and coatings (e.g. solar collector paints which need a porous/rough structure to trap incident radiation),

5) electroplated metals where porosity can lead to serious limitations in the coatings application,

6) thin interfaces where forming processes can affect pore structure (e.g. pressed ceramic surfaces vs bulk, slip cast mold interface), and

7) porous coatings for biomedical implants.

In summary, this program has provided an opportunity to identify instrumental techniques as well as to develop the required expertise which can now be employed to study the importance of thin film morphology to a variety of end-use applications, only one of which is the electrochemical behavior of electrodes. It is hoped that further study in this area will lead to a better definition of appropriate techniques suitable for the "routine" examination of porous thin film structures.

M.P. Haley
Project Scientist

for I.H. Joyce
Project Manager

REFERENCES

1. Canaday, J.D., Kuriakose, A.K., Ahmad, A., and Wheat, T.A., "Electrodes for Solid-State Electrolyte Fuel Cells - Electrode Morphology", CANMET Report ERP/MSL p 83-134 (1983)

2. Dryden, W.G., "Achieving Consistent Results with Thick Film", Solid State Technology, September (1971).

3. Heraeus Cermalloy Catalog "Thick Film and Capacitor Materials" (1983)

4. Fauchais, P, Vardelle, A., Vardelle, M., Coudert, J.F., and Lesinski, J., "Correlation of the Physical Properties of Sprayed Ceramic Coatings to the Temperature and Velocity of the Particles Travelling in Atmospheric Plasma Jets : Measurements, Modelling, and Comparison". Thin Solid Films, 121, pp 303-316 (1984)

5. Fauchais, P., Bourdin, E; Coudert, J.F., and McPherson, R., "High Pressure Plasmas and their Application to Ceramic Technology", Top. Curr. Chem., 107, p 62 (1983).

6. LeMont Scientific, 2011 Pine Hall Drive, Science Park, State College, PA 16801

7. Shors, E.C., White, E.W., and Edwards, R.M., "A Method for Quantitative Characterization of Porous Biomaterials using Automated Image Analysis", ASTM Symposium on Porous Implants for Hard Tissue Applications, Nashville, TN, Nov. (1985)

8. MacDonald, W.A., Wheat, T.A., and Quon, H.H., "A Method for the Rapid Mounting and Polishing of Ceramic Materials for Microstructural Examinations", J. Mat Science Letters, 13, p 905 (1978)

9. Spurr Low-Viscosity Embedding Media available from Polysciences, Inc., Warrington, PA 18976-2590

10. "Rough Surface" ed. Thomas, T.R., Longman Inc, New York (1982)

11. Rank-Taylor Hobson equipment distributed in Canada by Alexander Tools Ltd., 215 Carlingview Drive, Unit #304, Rexdale, Ontario M9W 5X8

12. Grove, D.M., "Permeability and Flow Studies", Chap. IV in Porous Carbon Solids, ed. Bond, R.L., Academic Press, New York (1967)

13. Dees, P.J., Tjan, T.G., and Polderman, J., "Determination of Pore Diameter by Permeability Measurements", Powder Tech, 27, p 29 (1980)

14. Washburn, E.W., "A Method of Determining the Distribution of Pore Sizes in a Porous Material", Nat. Acad. Sciences, 7, p 115 (1921)

15. Lowell, S., and Shields, J.E., "Influence of Contact Angle on Hysteresis in Mercury Porosimetry", J. Colloid. Interface Science, 80, p 192 (1981)

16. Svata, M., "Determination of Pore Size and Shape Distribution for Porosimetric Hysteresis Curves", Powder Tech., 5, p 345, (1971)

17. Lowell, S., "Continuous Scan Mercury Porosimetry and the Pore Potential as a Factor in Porosimetry Hysteresis", Powder Tech., 25, p 37 (1980)

18. Micromeretics equipment distributed in Canada by Technical Marketing Associates, 6620 Kitimat Rd, Unit 6, Mississauga, Ontario, L5N 2B8

19. Cox, B., "A Porosimeter for Determining the Sizes of Flaws in Zirconium or other Insulating Films In-Situ", J. Nuclear Materials, 27, p 1 (1968)

20. Gregg, S.J., and Sing, K.S.W., "Adsorption, Surface Area, and Porosity", Academic, New York (1967)

21. Brunauer, S., Emmett, P.H. and Teller, E., J. Amer. Chem. Soc., 60, p 309 (1938)

22. Engelhard Corporation, Speciality Chemicals Division, 1 West Central Avenue, East Newark, New Jersey 07029

23. Metco, Inc., 1101 Prospect Avenue, Westbury, Long Island, New York, 11590

24. Mandelbrot, B.B., "Fractals: Form, Chance and Dimension", W.H. Freeman, San Francisco (1977)

25. Avnir, D., and Farin, D., "Surface Geometric Irregularity of Particulate Materials: The Fractal Approach", J. Coll. Interface Science, 103, pp 112-23 (1985)

26. Niemeyer, L., Pietronero, L., and Wiesmann, H.J., "Fractal Dimension of Dielectric Breakdown", Phys. Rev. Letters, 52, p 1033 (1984)

27. Kaye, B.H., "Fractal Geometry and the Characterization of Rock Fragments", presented at the International Conference on Fragmentation, Form, and Flow in Fractured Media held in Neve Ilan, Israel, Jan 6-9 (1986)

28. Patterson, L., "Dispersion and Fingering in Miscible and Immiscible Fluids within a Porous Medium", Powder Tech, 36, p 71 (1983)

29 Kaye, B.H., "Specification of the Ruggedness and/or Texture of a Fine Particle Profile by its Fractal Dimension", Powder Tech., 21, p 1 (1978)

30. Flook, A.G., "The Use of Dilation Logic on the Quantimet to Achieve Fractal Dimension Characterization of Textured and Structural Profiles", Powder Tech., 21, p 295 (1978)

31. Kaye, B.H., Clark, G.C. Leblanc, J.E., and Trotier, R.A., "Image Analysis Procedures for Characterizing the Fractal Dimensions of Fineparticles", in preparation.

32. Compliments of Dr. G. Murphy, Dept of Engineering Physics, Technical University of Nova Scotia, P.O. Box 1000, Halifax, Nova Scotia B3J 2X4

33. Osmonics, Inc., 5951 Clearwater Drive, Minnetonka, Minnesota 55343

34. CRC Handbook of Chemistry and Physics, ed. Weast, R.C., ed 56th edition, CRC Press, Cleveland, Ohio (1975)

APPENDIX A

Surface Texture Parameters Generated by
the Talysurf 6 Profilometer

R_a, R_q, W_a, W_q

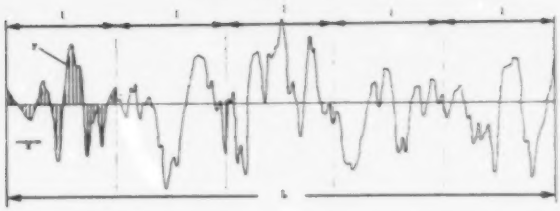

l_1 . . . l_5 are consecutive and equal sampling lengths (l the sampling length corresponds to filter cut-off length)

The assessment length L* is defined as the length of profile used for the measurement of surface roughness parameters (usually containing several sampling lengths, five consecutive sampling lengths are taken as standard)

R_a R_a is the universally recognised, and most used, international parameter of roughness. It is the arithmetic mean of the departures of the roughness profile from the mean line.

$$R_a = \frac{1}{L}\int_0^L |y(x)|\,dx$$

R_q R_q is the rms parameter corresponding to R_a

$$R_q = \sqrt{\frac{1}{L}\int_0^L y^2(x)\,dx}$$

W_a and W_q are the corresponding parameters from the waviness profile.

*The 'assessment length' is called 'traverse measuring length' or 'evaluation length' in ISO terminology

R_z (ISO)

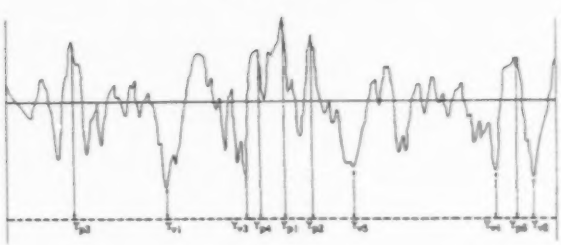

R_z Also known as the ISO 10 point height parameter, is measured on the unfiltered profile only and is numerically the average height difference between the five highest peaks and the five lowest valleys within the traverse length.

$$R_z\,(ISO) = \frac{(Y_{p1} + Y_{p2} + Y_{p3} + Y_{p4} + Y_{p5}) - (Y_{v1} + Y_{v2} + Y_{v3} + Y_{v4} + Y_{v5})}{5}$$

$$= \frac{1}{5}\left(\sum_{i=1}^{i=5} Y_{pi} - \sum_{i=1}^{i=5} Y_{vi}\right)$$

R_v, R_p, R_{pm}, R_t, W_v, W_p, W_t

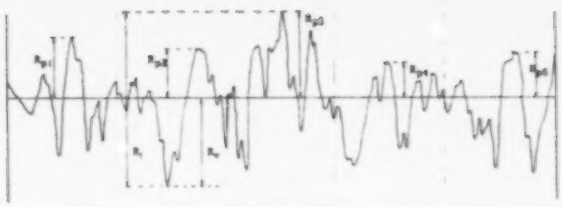

R_v R_v is the maximum depth of the profile below the mean line within the assessment length

R_p R_p is the maximum height of the profile above the mean line within the assessment length

R_{pm} R_{pm} is the mean of R_p values obtained for each sampling length of an assessment

Where n = the number of cut-offs, then

$$R_{pm} = \frac{1}{n} \sum_{i=1}^{i=n} R_{pi}$$

R_t $R_t = R_p + R_v$ and is the maximum peak to valley height of the profile in the assessment length

W_v, W_p and **W_t** are the corresponding parameters from the waviness profile

R_{sk}, R_{ku}

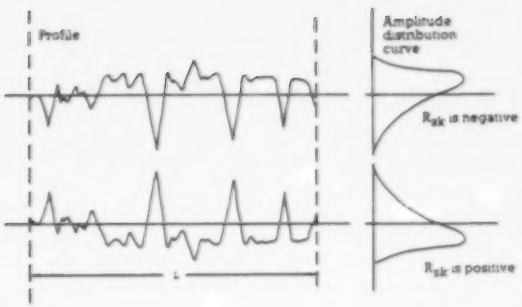

R_{sk} R_{sk} – Skewness – is the measure of the symmetry of the profile about the mean line. It will distinguish between asymmetrical profiles of the same R_a or R_q

Where n = number of data points in the profile, then

$$R_{sk} = \frac{1}{nR_q^3} \sum_{i=1}^{i=n} (Y_i)^3$$

R_{ku} R_{ku} – Kurtosis – is a measure of the sharpness of the surface profile

Where n = number of data points in the profile, then

$$R_{ku} = \frac{1}{nR_q^4} \sum_{i=1}^{i=n} (Y_i)^4$$

R_{ti}, R_y, R_{tm} (R_zDIN)

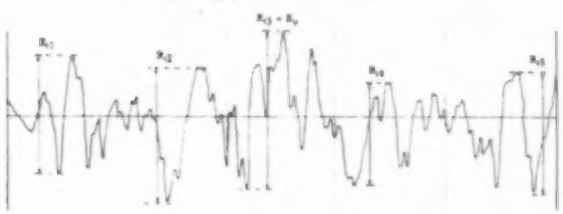

R_{ti} R_{ti} is the maximum peak-to-valley height of the profile in one sampling length

R_y R_y is the largest R_{ti} value within the assessment length

R_{tm} R_{tm} is the mean of all the R_{ti} values obtained within the assessment length. It is the equivalent of R_zDIN

Where n = number of cut-offs, then

$$R_z\,(DIN) = R_{tm} = \frac{R_{t1} + R_{t2} + R_{t3} + R_{t4} + R_{t5}}{5} = \frac{1}{n} \sum_{i=1}^{i=n} R_{ti}$$

R_{3y}, R_{3z}

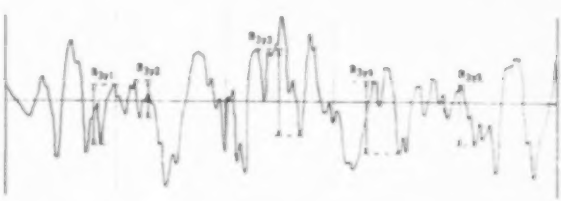

R_{3y} The deviation from the third highest peak to the third lowest valley in each sample length is found. R_{3y} is then the largest of these values

R_{3z} R_{3z} is the vertical mean from the third highest peak to the third lowest valley in a sample length over the assessment length

Where n = number of cut-offs, then

$$R_{3z} = \frac{1}{n} \sum_{i=1}^{i=n} R_{3yi} = \frac{R_{3y1} + R_{3y2} + \quad R_{3yn}}{n}$$

Spacing Parameters

HSC, P_c

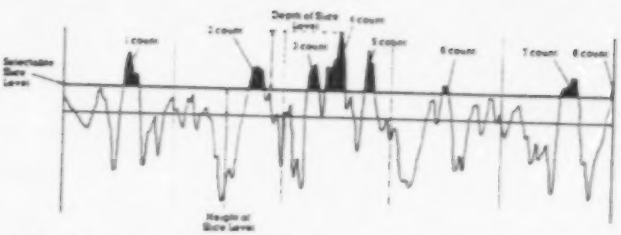

HSC The high spot count is the number of complete profile peaks (within assessment length) projecting above the mean line, or a line parallel with the mean line. This line can be set at a selected depth below the highest peak or a selected distance above or below the mean line

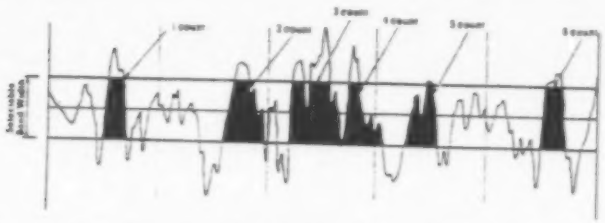

P_c The peak count is the number of local peaks which project through a selectable band centred about the mean line. The count is determined only over the assessment length though the results are given in peaks per cm (or per inch). The peak count obtained from assessment lengths of less than 1 cm (or 1 inch) is obtained by using a multiplication factor. The parameter should therefore be measured over the greatest assessment length possible

$$P_c = \frac{\text{No. of counts}}{\text{Assessment length (cm)}} = \text{Peaks/cm}$$

S, S_m

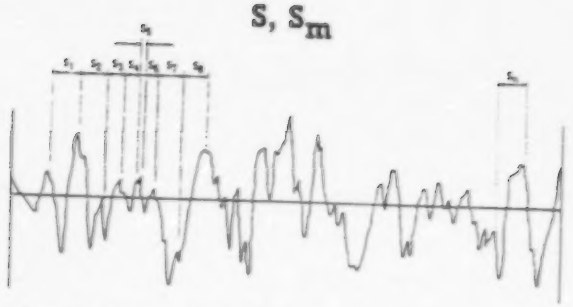

S S is the mean spacing of adjacent local peaks, measured over the assessment length. (A local peak is the highest part of the profile measured between two adjacent minima, and is only included if the distance between the peak and its preceding minima is at least 1% of the P - V of the profile.)

Where n = number of peak spacings then

$$S = \frac{1}{n}\sum_{i=1}^{i=n} S_i = \frac{S1 + S2 + S3 \ldots + S_n}{n}$$

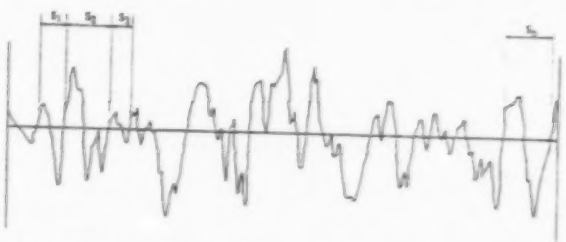

S_m S_m is the mean spacing between profile peaks at the mean line, measured over the assessment length. (A profile peak is the highest point of the profile between an upwards and downwards crossing of the mean line.)

Where n = number of peak spacings then

$$S_m = \frac{1}{n}\sum_{i=1}^{i=n} S_i = \frac{S1 + S2 + S3 \ldots + S_n}{n}$$

Δ_q, λ_q

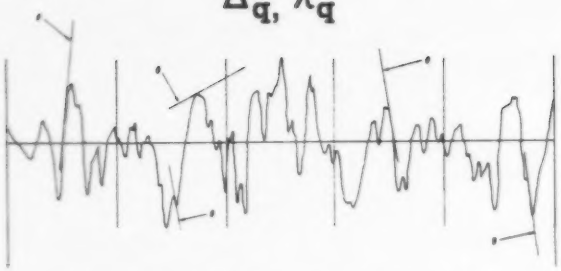

Δ_q is the rms slope of the profile throughout the assessment length

$$\Delta_q = \sqrt{\frac{1}{L}\int_0^L (\theta(x) - \hat{\theta})^2 \, dx}$$

$$\hat{\theta} = \frac{1}{L}\int_0^L \theta(x)\, dx$$

Where θ is the slope of the profile at any given point

$$\theta(x) = y'(x)$$

λ_q Average wavelength, λ_q (rms), is a measure of the spacings between local peaks and valleys, taking into account their relative amplitudes and individual spatial frequencies. Being a hybrid parameter, determined from both amplitude and spacing information, it is, for some applications, more useful than a parameter based solely on amplitude or spacing

$$\lambda_q = \frac{2\pi R_q}{\Delta_q}$$

Bearing Ratio t_p

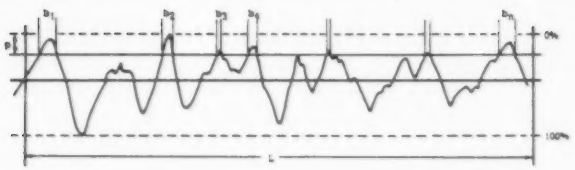

Bearing ratio t_p is the length of bearing surface (expressed as a percentage of the assessment length L), at a depth p below the highest peak.

t_p (%) is the ratio at the depth p

$$t_p = \frac{b_1 + b_2 + b_3 + b_4 \quad b_n}{L} \times 100 = \frac{100}{L} \sum_{i=1}^{i=n} b_i$$

The printout shows t_p% for each of the levels as for HSC.

The bearing ratio (or Abbott-Firestone) curve below, shows how the ratio varies with level

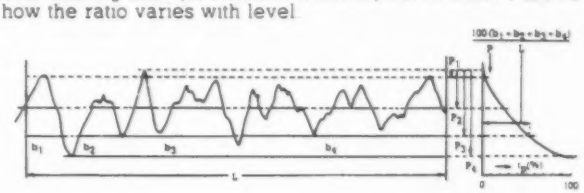

```
 BEGIN
 FOR C:=1 TO NUM DO
    BEGIN
    WRITE('STEP SIZE ',SIZE[C]:6:3);
    COUNT:=0;
    NPTY:=HT(SPTX);
    NPTX:=SPTX;
    CHECK:=SIZE[C]*1000;
    S:=CHECK*XF;
    B:=0;
    WHILE (NPTX+CHECK)<1000 DO
       BEGIN
       FLAG:=TRUE;
       WHILE (FLAG) AND (B<CHECK) DO
          BEGIN
          BX:=B*XF;
          ADD:=SQRT((S*S)-(BX*BX));
          HTB:=NPTY+ADD;
          IF HTB<HT(NPTX+TRUNC(B)) THEN
             BEGIN
             NPTX:=NPTX+TRUNC(B);
             NPTY:=HTB;
             B:=-1;
             FLAG:=FALSE
             END;
          B:=B+1
          END;
       WHILE FLAG DO
          BEGIN
          B:=B*XF;
          ADD:=SQRT((S*S)-(BX*BX));
          HTB:=NPTY-ADD;
          IF HTB<=HT(NPTX+TRUNC(B)) THEN
             BEGIN
             NPTX:=NPTX+TRUNC(B);
             NPTY:=HTB;
             FLAG:=FALSE
             END;
          B:=B-1
          END;
       IF B=-1 THEN
          B:=1
       ELSE
          B:=0;
       COUNT:=COUNT+1;
       WRITE('.')
       END;
    WRITELN;
    LEN[C]:=COUNT*SIZE[C]
    END
 END; (* STEP *)

 PROCEDURE DATAOUT; (* OUTPUT RESULTS *)

 BEGIN
 WRITELN;
 WRITELN;
 WRITELN('    STEP SIZE          LENGTH ESTIMATE ');
 FOR C:=1 TO NUM DO
    BEGIN
    WRITELN(SIZE[C]:12:3,LEN[C]:19:3)
    END
 END; (* DATAOUT *)


 BEGIN
```

```
PROGRAM FRACFRAC; (* CALCULATES THE FRACTAL VALUE OF A SURFACE PLOT *)
                 (* PROFILOMETERY DATA GENERATED BY THE TALYSURF 6 *)
USES
   TRANSCEND;

VAR
   XF,YF,NPTY :REAL;
   C,COUNT,NUM,SPTX,NPTX : INTEGER;
   LEN,SIZE :ARRAY[1..10] OF REAL;
   FNAME:STRING[20];
   PROF:ARRAY[1..1000] OF INTEGER;


PROCEDURE DATAIN;

VAR
   F:TEXT;

BEGIN
WRITE('ENTER PROFILE DATA FILE NAME (VOL:FNAME.TEXT)...');
READLN(FNAME);
RESET(F,FNAME);
WRITE('ENTER THE NUMBER OF POINTS TO READ...');
READLN(NUM);
FOR C:=1 TO NUM DO
   BEGIN
   IF (C MOD 10)=0 THEN
      READLN(F,PROF[C])
   ELSE
      READ(F,PROF[C])
   END;
CLOSE(F,LOCK);
WRITE('ENTER X SCALE FACTOR...');
READLN(XF);
WRITE('ENTER Y SCALE FACTOR...');
READLN(YF);
WRITE('ENTER STARTING POINT (1..500) ...');
READLN(SPTX)
END;

PROCEDURE STEPLENGTH;

BEGIN
WRITE('ENTER THE NUMBER OF SURFACE ESTIMATES...');
READLN(NUM);
FOR C:=1 TO NUM DO
   BEGIN
   WRITE('ENTER STEP SIZE (0.001..1) ..',C:2,'  ');
   READLN(SIZE[C])
   END
END;  (* STEPLENGTH *)

FUNCTION HT(POINT:INTEGER):REAL;

BEGIN
HT:=PROF[POINT]*YF;
END; (* HT *)

PROCEDURE STEP;

VAR
   FLAG:BOOLEAN;
   B,CHECK :REAL;
   BX,S,ADD,HTB :REAL;
```

```
UNITAIN;
STEPLENGTH;
STEP;
DATAOUT
END. (* PROFRAC *)
```

Appendix B

Pascal Program (Apple IIe) for the Numerical Solution of a Fractal Descriptor based upon a Talysurf 6 Profilometer Output (1000 points)

FILM COMPOSITION

Technique	Platinum Paste (A-4338)	Sprayed Nickel			Silver Membrane	
Image Analysis						
Particle diameter (μm)	2	50 - 70			3 - 5	
Pore diameter (μm)	3 - 5	10 - 20			1 - 4	
Porosity (%)	65 - 72	15 - 20			20 - 48	
Three Phase Line (cm/cm^2)	5500	360 - 450			3400 - 6400	
Profilometry						
Film Thickness (μm)	10 - 30	Not measured			40 - 70	
Fractal dimension	Not measured	∿1.6			Not measured	
Gas Permeability	Not measured					
Gas flow/pressure slope (ℓ/min. psi)	Not measurable					
Single pass	-	0.12 - 0.18			∿0.20	
Double pass	-	0.011 - 0.022			-	
Triple pass	-	0.010 - 0.011			-	
Mercury Porosimetry						
Pore area (m^2/g)	Not measurable	0.08			Not measurable	
Pore diameter (μm)	" "	0.2 - 0.8			" "	
Porosity (%)	" "	4 - 16			" "	
Gas adsorption						
Surface area (m^2/g)	Not measurable	Ni		0.05 - 0.08	0.11	0.16
		$C^{o}_{0.6}Ni_{0.3}(316SS)_{0.1}O_{3-x}$		0.065		
		$Ni_{0.39}Al_{0.59}Mo_{0.02}O_{3-x}$		0.375		
		$La_{0.8}Sr_{0.2}Co_{0.8}Ni_{0.2}O_{3-x}$		0.3		

ONTARIO **RESEARCH**
FOUNDATION

Energy

energy conservation programs and analyses, thermal insulation design and evaluation, waste heat recovery, building energy systems and monitoring, heat storage systems and materials, thermoelectric generation, combustion technology, burner development, heat transfer analysis, solar systems monitoring, National Solar Test Facility, solar technology, wind power, coal, lignite and oil sands processing, alternate fuel utilization, battery and fuel cell technology, peat processing and utilization, fenestration measurements, heat pump development and test facilities, residential heating systems, air to air heat exchange test facility, photovoltaic devices, . . .

Environment

ambient air quality assessment, environmental impact assessments, long-range transport of atmospheric pollutants, precipitation chemistry, particulate characterization studies, emission inventories, source sampling, odour emission and control, asbestos measurement and control, occupational health and safety studies, diesel emission control technology, air pollution control, pesticide residues, trace metal analysis, trace organic analysis, radionuclide analysis, mutagenic testing, noise and vibration analysis, radiation measurements, particulate identification and measurement, water surveys, water purification, industrial and municipal wastewater treatment, membrane separation techniques, wet oxidation, solid waste treatment and recovery, hazardous waste treatment and disposal, indoor air quality assessments, priority pollutant analysis, landfill technology, . . .

Materials

building materials, plastics, composites, metals, glass and ceramics, wood and wood composites, biomaterials, adhesives and printing inks, fibres, yarns, fabrics and geotextiles, leather, organic and inorganic chemicals, specification development, quality assurance, mechanical, chemical and thermal properties, test method development, failure analysis, fire and flammability, glass-metal seals, metal and alloy powders, metallography, materials characterization, materials characterization by optical and electron microscopy and X-ray microanalysis, photovoltaic materials, materials corrosion resource centre, corrosion properties and control, bacterial corrosion, coatings and sealants, rubber technology, X-ray analysis, cement and concrete, soils and aggregates, gypsum, body armour testing, footwear, paper-making materials, roofing and waterproofing, waste material stabilization and solidification, . . .

Products & Processes

clothing, footwear and industrial textile products, knitting technology, thin and thick film systems, microelectronics development, fibre optics, instrumentation, bioengineering, ultrasonic and fluid shear devices, microwave drying, transportation and equipment testing, mathematical stress and vibration analysis, product, equipment and machinery design & development, fuel emulsification, organic analysis and characterization, chemistry of foodstuffs, pulp and paper processes, ceramics processing, metallurgical process development, powder metal technology, packaging applications, technical and economic evaluations, industrial engineering applications, process control, enzyme analysis, electrical testing, radioactive surveys, industrial microbiology, biotechnology, technical and management skills development seminars, paper products, absorbent consumer products, detergent and cosmetic formulation, metal chemical analysis, flash hydropyrolysis of coal, electroplating, . . .

Resources

mineral processing, hydro and pyrometallurgical processing of ferrous and non-ferrous ores, coal evaluation, coal ash utilization and product development, asbestos processing and applications, non-metallic minerals/industrial minerals processing and utilization, uranium processing, forest utilization, utilization of forest and agricultural wastes, utilization of industrial, mining and domestic wastes, energy and chemicals from biomass, in-plant waste reduction, mineralogical services, mining and metallurgical waste disposal, . . .

ONTARIO RESEARCH FOUNDATION • SHERIDAN PARK, MISSISSAUGA, ONTARIO, CANADA L5K 1B3 • (416) 822-4111 • TELEX 06-982311